The University Of Sheffield.

Voltage gated Na^+ channels and spontaneous action potential activity in cochlear hair cells during development

Submitted to the University of Sheffield for the degree of

Doctor of Philosophy

February 2012

Tobias Eckrich

University of Sheffield, Department of Biomedical Science

Table of Content

List of Figures

Chapter One: Introduction

Chapter Two: Methods

Chapter Three: Results I - Spontaneous Action Potential Activity

Chapter Four: Discussion I - Spontaneous Action Potential Activity

Chapter Five: Results II - Biophysics of the sodium current

List of Tables

Abstract

Inner hair cells (IHCs) are the true sensory cells for sound. They receive acoustic stimuli and transduce them into graded receptor potentials that lead to the excitation of afferent nerve fibres, which transmit the sound information to the brain where the impression of sound arises.

Before hearing onset IHCs transiently generate spontaneous calcium action potentials without the input of sound (Marcotti *et al.*, 2003a). This activity is thought to orchestrate important developmental processes such as the refinement of synaptic connections and/or intrinsic IHC development such as that of ion channels and synaptic proteins (Kros *et al.*, 1998). Various membrane currents influence IHC action potentials, including a transiently expressed tetrodotoxin sensitive sodium current (Marcotti *et al.*, 2003b). In this thesis, electrophysiological recordings from rat IHCs were performed as a function of postnatal development and cochlear region in order to characterise the frequency and pattern of the spontaneous activity as well as the biophysical properties of the sodium current. By using *in situ* hybridisation it was attempted to reveal the molecular identity of the Na^+ channel α subunits expressed in immature IHCs.

Electrophysiological recordings revealed that rat IHCs spontaneously generate action potentials until the end of the first postnatal week. Thereafter, action potentials could still be triggered using depolarising current injections until just before the onset of hearing. A rapidly activating and inactivating sodium current was observed in all immature IHCs investigated. This sodium current showed high temperature dependence and both its size and kinetics changed as a function of development and IHC position along the cochlea.

Altogether, these results deepen our knowledge about the characteristics of the spontaneous action potential activity and reveal that the sodium current is active at physiological cell membrane potentials and involved in action potential generation.

Declaration

I declare, that this thesis is the result of my own work except where the work of others is cited, either explicitly or via the list of references.

No part of this work has been submitted for a degree, diploma or other qualification at any other university.

Tobias Eckrich

February 2012

Acknowledgements

I would like to thank my supervisors Walter Marcotti and Matthew Holley for their support over the past years. I'd also like to thank my advisors Liz Smythe and Liz Seward for their guidance and assistance with my work. Many thanks also to my lab colleague Stuart Johnson, for his kind assistance in writing and translating and especially Tooba Alizadeh for creating such a nice lab atmosphere.

Besonders Steffi möchte ich für ihre Ratschläge und Hilfe danken und für die emotionale Unterstützung während der letzten Jahre. Vielen Dank auch für Deine große Geduld, besonders während der Zeit des Zusammenschreibens oder wenn meine Versuche mal nicht geklappt haben.

Ich möchte mich auch bei meiner Familie, besonders meinen Eltern und meinem Bruder, für die Unterstützung aus der Ferne bedanken. Die große Entfernung zu Euch hat mir gezeigt, dass "Heimat" nicht einfach nur ein Ort, sondern die Verbindung zu den Menschen ist, die diesen bevölkern.

Lastly, I would like to thank the many friends I made here in Sheffield. In particular Joe and Rich for “Thursdays breakfast” and the board game nights together with Lauren and Phil, which provided so much fun and a lot of distraction.

Abbreviations

4AP	**4 Amminopyridine (K^+ channel blocker)**
ACh	**Acetylcholine**
ATP	**Adenosine-5'-triphosphate**
BT	**Body temperature (on average 35.5°C)**
BK channel	**Large conductance voltage and calcium activated potsassium channel (carrying $I_{K,f}$ or I_{BK})**
Ca^{2+} channel	**Calcium channel**
C_m	**Cell membrane capacitance**
E	**Embryonic day**
ECS	**Extracellular solution mimicking perilymph**
EPSC	**Excitatory postsynaptic current**
I	**Current**
I_{Ca}	**Calcium current**
I_{K1}	**Inward rectifier potassium current**
$I_{K,f}$ or I_{BK}	**Large conductance voltage and calcium activated potassium current (carried by BK channels)**
$I_{K,n}$	**Negatively activating potassium current**
$I_{K,s}$	**Delayed rectifying potassium current; at corresponding developmental time points also termed as $I_{K,emb}$ (embryonal) or $I_{K,neo}$ (neonathal)**
I_m	**Ionic current flowing across a cell membrane**
"Inactivation"	**Voltage clamp protocol; was used to determine the steady state inactivation of the Na^+ channel**
I_{out}	**Current output at the operational amplifier**
IPSP	**Inhibitory postsynaptic potential**
I_{Na}	**Voltage activated sodium current**
ISI	**Interspike interval**
I_{SK}	**Small conductance calcium activated potassium current (carried by SK channels)**
IHC	**Inner hair cell**
K^+ channel	**Potassium channel**
mV	**millivolt**

nA	**nanoAmpere**
Na^+ channel	**Voltage gated Na^+ channel**
Na_V	**Voltage gated Na^+ channel (usually followed by a number between 1.1 and 1.9, which depicts the α subunit)**
"Nacvc"	**Voltage clamp protocol; was used to determine the current to voltage relation of the Na^+ channel**
NMDG	**N-methyl-D-glucamine (Na^+ ion substitute; impermeable to Na^+ channel)**
OA	**Operational amplifier**
OHC	**Outer hair cell**
pA	**picoAmpere**
PBS	**Phosphate buffered saline**
P27	**Enzyme; cyclin dependent kinase inhibitor**
P2X	**Cation permeable purinergic receptor**
P2Y	**G-protein coupled purinergic receptor**
Q_{10}	**Temperature coefficient; was used to determine the rate of peak sodium current increase due to a temperature increase of 10°C**
R	**Resistance**
"Recovery"	**Voltage clamp protocol; was used to determine the recovery from inactivation of the Na^+ channel**
$R_{Pipette}$	**Patch pipette resistance**
R_s	**access/series Resistance (in series with the $V_{pipette}$)**
RT	**Room temperature**
SEM	**Standard error of mean**
SK channel	**Small conductance calcium activated K^+ channel (carrying I_{SK})**
τ	**Time constant**
$\tau_{inactivation}$	**Time constant of sodium current inactivation**
TEA	**Tetraethylammonium (K^+ channel blocker)**
TTX	**Tetrodotoxin (Na^+ channel blocker)**
t_{peak}	**Time to reach the peak sodium current from the start of a voltage step**
$t_{50\% peak}$	**Time to reach the half maximal sodium current from the start of a voltage step**
V	**Voltage**
V_{Cell}	**Membrane potential of a cell**
$V_{Command}$	**Potential applied by the operational amplifier**

V_{half}	**Potential at which half maximal activation or inactivation occurred**
V_{hold}	**Holding potential**
V_{m}	**Membrane potential of an IHC**
$V_{Pipette}$	**Potential at the patch pipette**
V_{Rest}	**Resting membrane potential**
V_{Rev}	**Reversal potential**
$V_{Threshold}$	**Membrane potential at which an IHC started to generate action potentials**

1. Introduction

The following introduction aims at giving an overview on the morphology, function and development of the auditory system with focus on the inner ear and inner hair cells (IHCs) in particular. It then deals with the role and function of spontaneous electric activity found during development. In the last part the structure and function of voltage gated sodium channels is discussed.

1.1. The Mammalian Auditory System

Throughout evolution the auditory system became an important sense for all land living vertebrates. It plays a crucial role in communication within and between species as it facilitates the perception of sound over a wide operational range with extraordinary sensitivity. Humans for example are able to perceive sound over a frequency range of 20 Hz up to about 20 kHz (Schwander *et al.*, 2010). The frequency detection range is specific to species and across the animal kingdom many extremes have evolved. Bats or dolphins for example are able to detect frequencies well above 100 kHz and use sound for echolocation purposes (Vater & Kössl, 2010). Another extreme is found in African elephants, which are able to perceive and use infrasound as long distance communication signals (Garstang, 2004). Very astonishingly the auditory system can detect sound induced vibrations of only 0.3 nm at threshold (Patuzzi & Sellick, 1983). But auditory clues are not solely used for communication. Species such as the barn owl (*Tyto alba*) have specialised hearing enabling them to hunt in absolute darkness by locating their prey with an accuracy of 1° in both vertical and horizontal planes using the interaural pressure and time differences arising between their ears (Payne, 1971). Humans are able to detect time differences of under 20 µs to localise sound (Hudspeth, 1997). In order to function with such extreme precision and be able to create an accurate impression of sound within the brain it is crucial that the physical properties of sound are encoded into electric signals with minimal loss of information.

1.1.1. Macroscopic Structure of the Mammalian Ear

The mammalian auditory system can be divided into three major compartments: the outer, middle and inner ear (Figure 1). The outer ear is formed by the auricle and the external auditory canal, which together act like a "collecting horn" both directing and increasing incoming sound pressure onto the tympanum (Geisler, 1998). The form of each pinna is slightly differing among individuals and creates specific interference patterns that help localisation of sound sources (Heldmaier & Neuweiler, 2003).

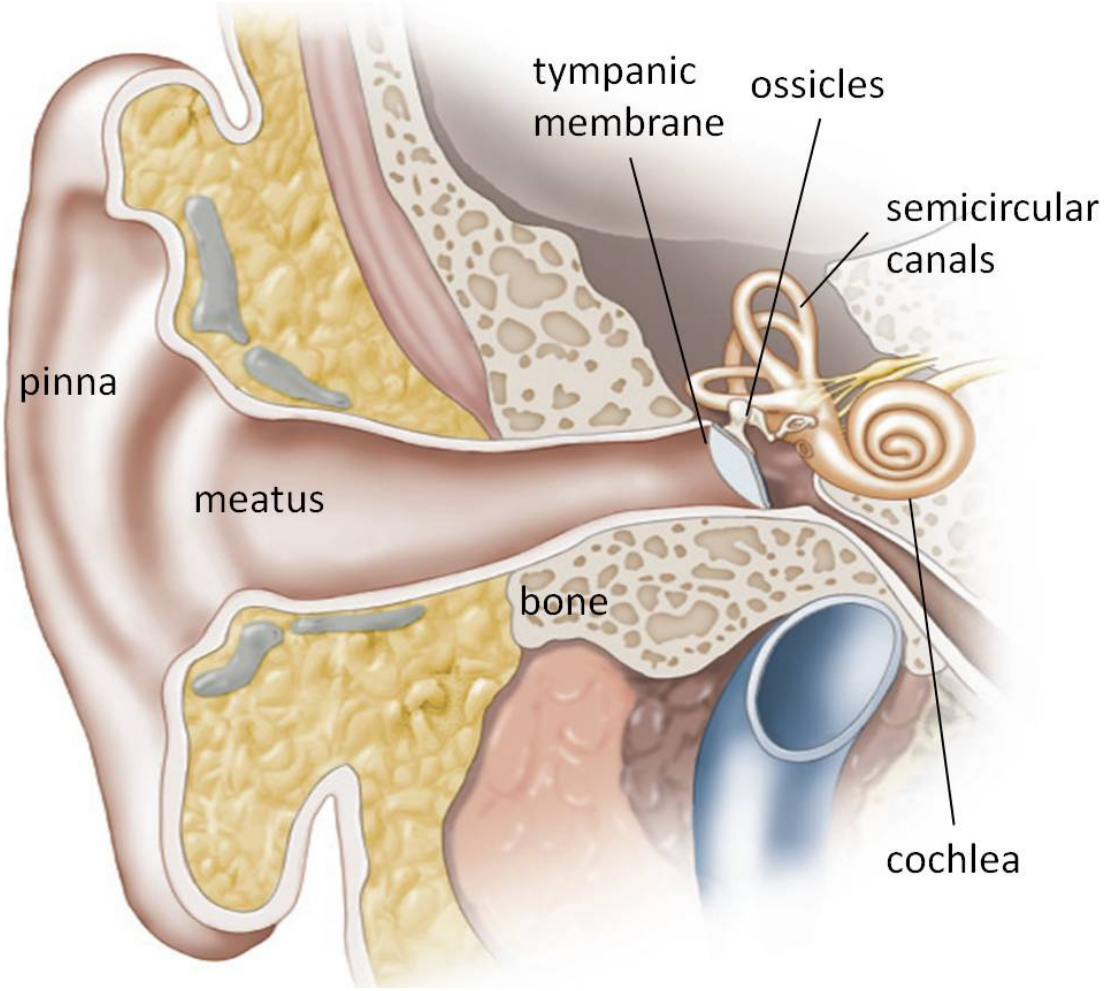

Figure 1: Schematic drawing of the human peripheral auditory system. The outer ear is formed by the pinna and the ear canal (meatus), which both channel sound onto the tympanum. The middle ear consists of the three ossicles (malleus, incus and stapes) and work together with the tympanum as an impedance transformer. The inner ear comprises of the vestibule with the semicircular canals and the cochlea. The latter inherits the sensory cells for sound. (Modified and reprinted with permission from Wolfe *et al.*, 2008: Sensation and Perception 2nd Ed, Sinauer Associates, Inc Publishers, Sunderland, MA).

Land living vertebrates face a tremendous challenge. Their sensory cells are embedded in a sensory epithelium that resides in fluid filled chambers of the inner ear. However, sound emitted from a source usually travels through air, a much "thinner" medium. Somehow the auditory system needs to overcome the impedance difference between the much "thinner" medium air and the “thicker” medium water, which would usually lead to a reflection of 99.9 % of the energy of a sound stimulus (Heldmaier & Neuweiler, 2003). This challenge is managed by the middle ear, which is formed by the tympanum and the three smallest bones (malleus, incus and stapes) of the human body. Sound channeled onto the tympanum causes a vibration that is conducted and slightly increased by the ossicles in a lever-like fashion (Jorgensen & Kanneworff, 1998). The stapes, which connects the middle ear to the inner ear at the oval window, transmits this vibration into pressure waves in the fluid filled cochlea. This complex structural and mechanical coupling of membranes and bones from the middle ear to the inner ear acts as an impedance transformer ensuring that the energy of sound is efficiently transferred from air into the fluid filled cochlea (Heldmaier & Neuweiler, 2003). Within the cochlea sensory cells reside that sense the sound induced vibrations and transduce them into an electrical signal.

The coiled structure of the mammalian cochlea resembles that of a snails shell. In humans it has an average outer length of about 42 mm making almost three coils (Erixon *et al.*, 2009; Marinkovic *et al.*, 2011). The mammalian cochlea is partitioned into three compartments called scala tympani, scala vestibuli and scala media, which is also referred to as the cochlear duct (Figure 2). These three compartments are separated from each other by tight membranes, which do not allow ionic diffusions across them. The Reissner's membrane, a thin, two cell layered epithelium, separates the scala vestibuli from the scala media. The reticular lamina restricts ion flow between scala media and scala tympani and is formed by tight junctions between hair cells and supporting cells (Raphael & Altschuler, 2003). To the lateral side of the scala media is the stria vascularis, a three layered cell membrane that is crucial for generating the high potassium concentration in the endolymph.

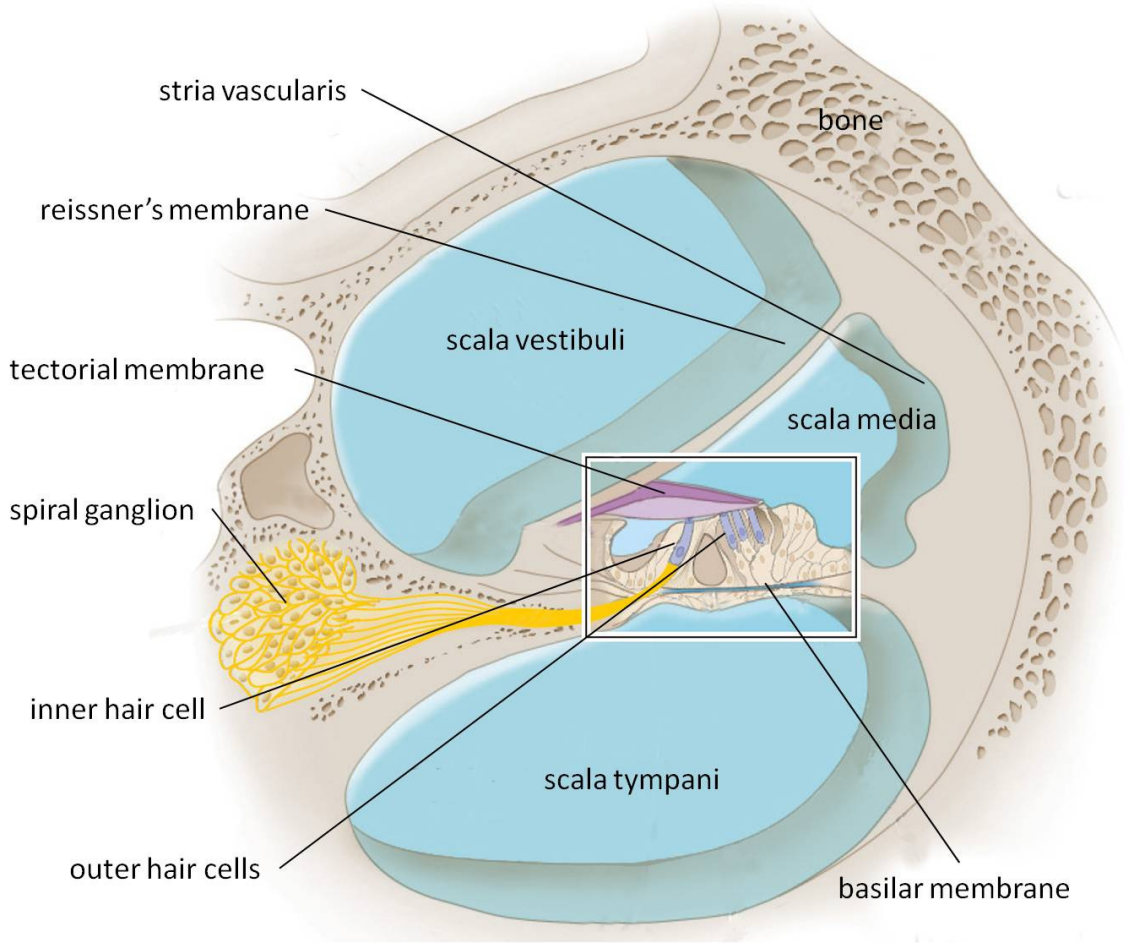

Figure 2: Schematic drawing of a cross section of the mammalian cochlea. Three fluid-filled compartments form the coiled structure of the cochlea. The scala vestibuli and scala tympani are filled with a sodium rich extra-cellular like solution called perilymph. The cochlear duct, also referred to as the scala media, is filled with a potassium rich solution called endolymph. Within the cochlear duct resides the sound stimulus receiving machinery, called the organ of Corti (highlighted by rectangular box), which sits on top of the basilar membrane and consists of supporting cells, sensory cells and the tectorial membrane. It is essential for normal cochlear function that the sensory cell bodies are bathed in perilymph, while only their stereociliary bundles reside in endolymph. This ensures the driving force for ions to enter the cell, thereby creating a receptor potential, when sound vibrations stimulate the sensory cells. The stria vascularis on the lateral side is important for the potassium homeostasis of the endolymph. (Modified and reprinted with permission from Wolfe *et al.*, 2008: Sensation and Perception 2nd Ed, Sinauer Associates, Inc Publishers, Sunderland, MA).

The sound detecting apparatus, the organ of Corti is situated on top of the basilar membrane (Figure 3). While the scala vestibuli and scala tympani are filled with a sodium rich extracellular-like solution called perilymph, the scala media is filled with endolymph, a unique potassium rich solution (Smith *et al.*, 1954; Anniko & Wroblewski, 1986). The cell bodies of the sensory cells are bathed in perilymph, while their stereocilia protrude into the

endolymph. This compartmentalisation within the cochlea is crucial for normal hearing as it provides the driving force for sensory transduction (Hibino *et al.*, 2010). Disruption of the potassium homeostasis can lead to deafness and hair cell loss (Kubisch *et al.*, 1999; Wangemann, 2002).

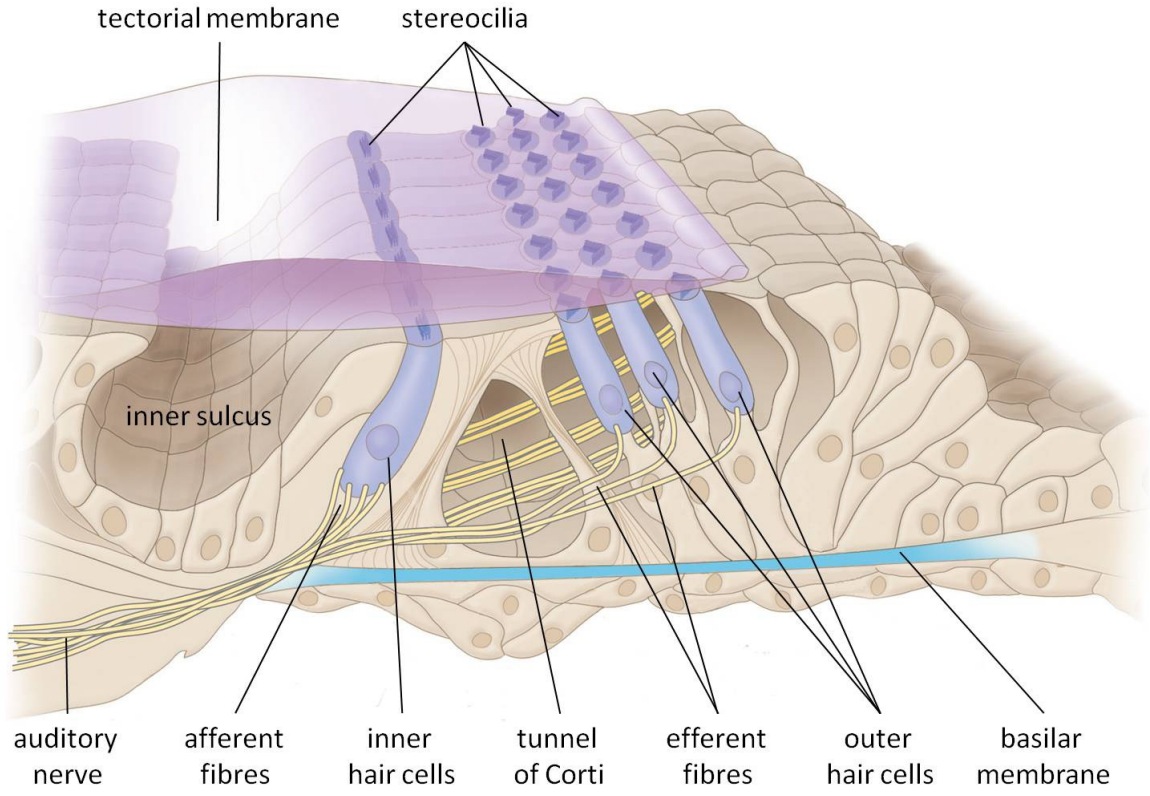

Figure 3: Drawing of the organ of Corti. One row of inner hair cells (IHCs) and three rows of outer hair cells (OHCs) are surrounded by several types of supporting cells providing structural support and being involved in physiological tasks, such as potassium homeostasis. Sound leads to the deflection of stereocilia of both IHCs and OHCs. Outer hair cells act by somatic electromotility as cochlear amplifier, whereas IHCs, mainly afferently innervated act as the true sensory cells that transmit acoustic stimuli to the brain. The tectorial membrane overlies the organ of Corti and acts as an inertial mass (Lukashkin *et al.*, 2010) deflecting the stereocilia of the OHCs due to sound vibrations. (Modified and reprinted with permission from Wolfe *et al.*, 2008: Sensation and Perception 2nd Ed, Sinauer Associates, Inc Publishers, Sunderland, MA).

The organ of Corti is a marvellous feat of biological engineering, inheriting morphological and physiological elements that are highly specialised to facilitate the transduction of sound from a physical stimulus into an electric signal. Its lower boundary is formed by the basilar membrane, an acellular structure consisting of matrix material and collagen fibres (Geisler,

1998). On top of the basilar membrane reside the cells of the organ of Corti. These comprise five different types of supporting cells, which are the Cells of Claudius, Hensen, Boetcher and Deiter and the Pillar cells. Supporting cells are involved in various functions, such as providing structural support and maintenance of the ionic homeostasis by recycling potassium from the perilymph back to the endolymph via the stria vascularis (Wangemann, 2002; Raphael & Altschuler, 2003). However, their function does not seem to be restricted to adult function since recent studies provide evidence for supporting cells being also involved in modulating the immature spontaneous activity that is thought to drive developmental programmes (Tritsch *et al.*, 2007; Johnson *et al.*, 2011b). Within the organ of Corti two types of sensory cells can be found: inner hair cells (IHCs) and outer hair cells (OHCs). Hair cells derive their name from the hair-like structures called stereocilia that project from their apical surface (Figure 4, left). Stereocilia are large microvilli protruding into the endolymphatic compartment of the organ of Corti (Figure 4) and they are very accurately organised like a staircase to form the hair bundle that normally consists of between two and four rows of stereocilia of different length. Stereocilia are inter-connected via extremely fine filamentous structures of about 150 – 200 nm in length. These filaments connecting the tip of the lower stereocilia with the lateral side of its taller neighbour are called tip links (Figure 4, right). Tip links are thought to be mechanically coupled to mechanoelectrical transducer ion channels present within the stereociliar membrane (Pickles *et al.*, 1984).

The tectorial membrane is a gelatinous structure, which extends from the spiral limbus (Figure 3) and overlies the sensory cells of the organ of Corti. It is mechanically coupled with the OHC stereocilia and is vital for the normal hearing function (Heldmaier & Neuweiler, 2003). Sound that enters the auditory system via the outer and middle ear causes vibrations in the cochlea. These vibrations lead to sheering movements between basilar and tectorial membranes, deflecting the hair cell stereocilia and ultimately leading to a receptor potential through the opening of mechanoelectric transducer channels. This receptor potential causes the opening of voltage gated calcium channels (Ca^{2+} channels) that are located in the basolateral membrane and ultimately to the influx of calcium into hair cells. Increases of intracellular calcium trigger the release of the neurotransmitter glutamate (Fuchs *et al.*, 2003) from the hair cells into the synaptic cleft. This neurotransmitter release

activates auditory afferent nerve fibres, which are responsible to relay sound information in the form of action potentials to the brain, where the impression of sound arises (Geisler, 1998).

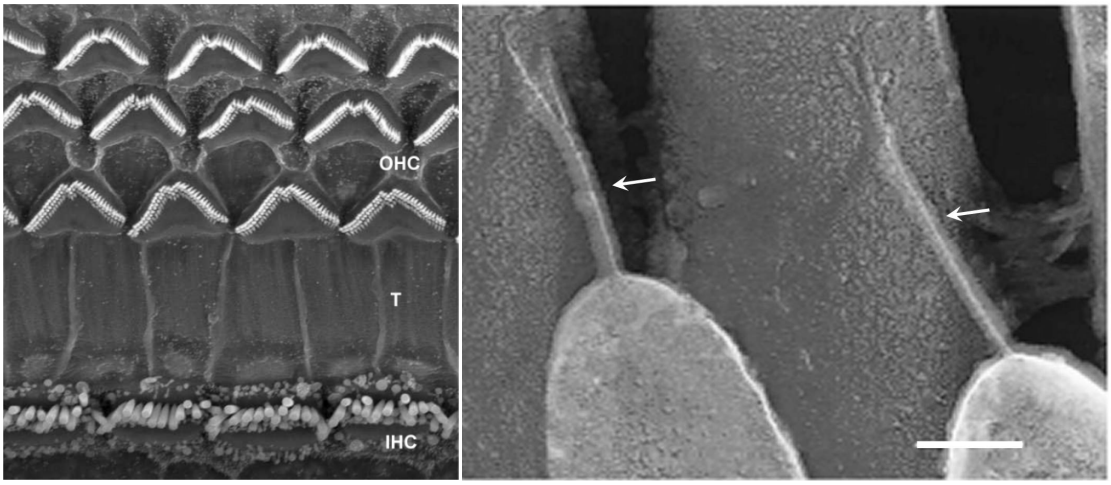

Figure 4: Anatomy of hair cell stereocilia. Left: electron micrograph showing the OHC and IHC apical surface where the stereocilia project into the endolymphatic solution. IHCs and OHCs are separated by the tunnel (T) of Corti (Picture with kind permission from: Vreugde et al., 2002). Right: electron micrograph showing the thin filamentous structure of the tip links (indicated by arrows) connecting stereocilia from adjacent rows. The deflection of stereocilia stretches tip links, which pull open tension gated ion channels within the stereocilia leading to cation influx. This so called mechanoelectric transduction is vital to sound perception as it generates a receptor potential that ultimately leads to neurotransmitter release and the transmission of sound information to the brain (Picture modified from: Kachar et al., 2000; copyright permission with the courtesy of National Academy of Sciences, U.S.A.)

Within the spiral structure of the mammalian cochlea, hair cells are organised tonotopically so that the frequency at which they respond best, gradually changes with their position along the organ of Corti. Therefore, hair cells showing maximal responses to high frequency sounds are located towards the base, while cells detecting low frequency sounds are positioned towards the apex (Figure 5).

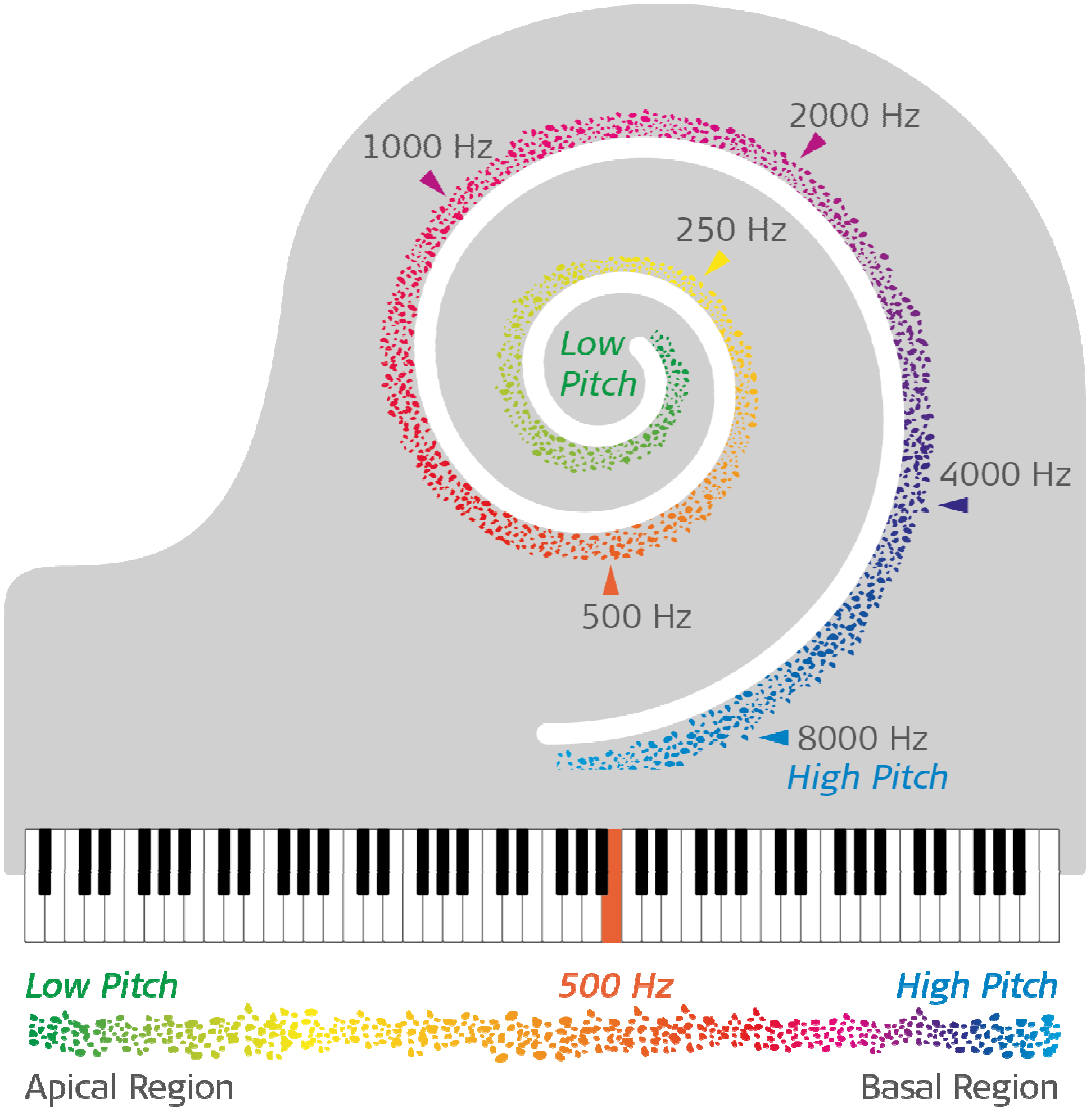

Figure 5: Tonotopic organisation of the human cochlea illustrated by comparison with the claviature of a piano. Maximum vibration by sound stimuli is distributed along the cochlea as a function of spatial localisation very much like the distribution of frequencies on the claviature of a piano. Higher frequencies are detected by hair cells towards the basal region (blue) and lower frequencies towards the apical (green) region (Photo kindly provided by: MED-EL, Innsbruck, Austria)

Several morphological gradients facilitate the tonotopic distribution of frequencies. These are briefly: the stiffness of the basilar membrane (von Bekesy, 1960) and the tectorial membrane (Richter *et al.*, 2007) decrease from cochlear base to apex. Furthermore, the length of stereocilia of both IHCs and OHCs increases from base to apex as well as the somata length of OHCs (Turner *et al.*, 1981; Vater & Kössl, 2010). The biophysical

properties of hair cells such as transduction (Jia *et al.*, 2007; Johnson *et al.*, 2011a), potassium currents (Johnson *et al.*, 2011a) and calcium currents (Johnson & Marcotti, 2008) also differ along the cochlea. These gradients lead to a gradual change in the mechanical resonance frequency. Thus sound is split by the organ of Corti into its frequency components in a spatial manner, which displays a striking feature of cochlear function. This tonotopic distribution is preserved from the auditory periphery through nuclei in the brainstem to the cortex in the form of neuronal maps (Heldmaier & Neuweiler, 2003; Mann & Kelley, 2011).

1.1.2. The Hair Cell's unique Physiology provides the Transduction of Sound

A pure sinusoidal tone that enters the cochlea leads to a pressure wave resulting in the vibration of the basilar membrane. This vibration rises in amplitude along the cochlea until it reaches its place of resonance in the basilar membrane (von Bekesy, 1960). At the place of resonance, the vibration of the basilar membrane is maximal and leads to a maximal deflection of the hair bundles so that they slide along each other stretching the tip links. Changes in tip-link tension are thought to modulate the open-probability of mechanoelectrical transducer channels (Howard & Hudspeth, 1987; Raphael & Altschuler, 2003) that are likely to be located at the tip of each stereocilium, except those in the tallest row (Beurg *et al.*, 2009; Furness *et al.*, 2010). Opening of the mechanoelectrical transducer channels results in an influx of cations from the endolymph. Due to endolymph composition, this cation current is carried mainly by potassium, but also by calcium, which is thought to modulate the mechanoelectrical transducer channel open probability (Eatock *et al.*, 1987; Schwander *et al.*, 2010). The influx of cations results in a graded receptor potential, which depends on the amplitude of stereocilia deflection (Hudspeth, 1989). It is sensed and modulated by voltage gated ion channels in the basolateral membrane.

Several voltage gated ionic currents orchestrate the physiological functions of a mature IHC. A calcium current, which is carried by L-type $Ca_V1.3$ voltage gated Ca^{2+} channels (Platzer *et al.*, 2000) that are expressed in close proximity to the synapse at the base of the IHC (Brandt *et al.*, 2005; Knirsch *et al.*, 2007), respond to the receptor potential with a calcium influx. This triggers the release of neurotransmitter by which the sound information is passed onto afferent nerve fibres (Beutner *et al.*, 2001). Two potassium currents are responsible for the repolarisation: the large conductance voltage and calcium activated K^+ current ($I_{K,f}$ or I_{BK}), which is carried by BK channels (Kros & Crawford, 1990; Kros *et al.*, 1998; Hafidi *et al.*, 2005) and the negatively activating potassium current ($I_{K,n}$) carried by the KCNQ4 channel (Oliver *et al.*, 2003; Engel *et al.*, 2006). BK channel activation is very fast, leading to a rapid repolarisation of the membrane potential (Kros & Crawford, 1990). One further type of potassium current is present in mature IHCs, the delayed (or classic) outward rectifier potassium current ($I_{K,s}$; Kros & Crawford, 1990; Marcotti *et al.*, 2003a). Together with $I_{K,n}$ it has the important function of keeping the resting membrane potential at a rather negative voltage of about -80 mV.

1.1.3. Inner and Outer Hair Cells possess different Functions

The mechanoelectrical transduction process and receptor potential modulation works generally for both IHCs and OHCs in the same manner. But it ultimately leads to different results reflecting the different function between IHCs, which relay sound information onto the auditory nerve and OHCs that are responsible for cochlear amplification.

In order to transmit mechanoelectrically transduced acoustic signals, IHCs have specialised synapses responsible for encoding precise and sustained release of neurotransmitter. These synapses are called ribbon synapses due to their electron-dense structure with a ribbon-like appearance (Sterling & Matthews, 2005; Moser *et al.*, 2006). Synaptic ribbons tether a large number of synaptic vesicles at the IHC active zones. These vesicles are loaded with glutamate (Fuchs *et al.*, 2003) that is released into the synaptic cleft following Ca^{2+} influx

through voltage gated Ca^{2+} channels (Platzer *et al.*, 2000), which are activated by IHC depolarisation. The release of glutamate excites adjacent afferent nerve fibres that transmit acoustic information such as sound frequency and intensity to brainstem nuclei in the form of action potentials (Hudspeth, 1989). In the adult mouse an IHC contains about 10 to 30 ribbon synapses, each connected to only one adjacent unbranched afferent nerve fibre (Liberman, 1980; Liberman *et al.*, 1990). The unique structure of ribbons and the large amount of vesicles attached and ready for exocytosis allows a very precise transmission of acoustic stimuli onto the afferent nerve fibres.

IHCs are the true sensory receptors of the mammalian cochlea, since 95 % of afferent nerve fibres in the cochlea contact them (Pujol *et al.*, 1998). Together they are responsible for relaying acoustic information to the central nervous system (Ryugo, 1992; Dannhof & Bruns, 1993). OHCs act in parallel to enhance the sensitivity and frequency selectivity of the cochlea by active mechanical amplification (Dallos & Fakler, 2002). The mechanical feedback mechanism arises from voltage dependent OHC somatic electromotility, mediated by the motor protein prestin (Dallos *et al.*, 2006). The basolateral wall of OHCs is densely packed with prestin, which changes its shape in response to variations in the membrane potential and this works as a direct voltage to force converter (Brownell *et al.*, 1985; Zheng *et al.*, 2000; Dallos *et al.*, 2006). A loss of prestin and hence electromotile function, results in a 40 – 60 dB increase in hearing threshold (Liberman *et al.*, 2002). OHCs are mainly innervated by efferent fibres descending from medially located superior olivary nuclei of the brainstem. Together with type II afferent spiral ganglion neurons they are thought to act as a negative feedback system that modulates the degree of mechanical amplification from the OHCs (Maison & Liberman, 2000; Raphael & Altschuler, 2003). Although the hypothesis of somatic amplification is generally accepted, recent findings have shown that calcium driven active hair-bundle motility could also contribute to cochlear amplification (Kennedy *et al.*, 2005; Fettiplace, 2006; Kennedy *et al.*, 2006).

1.2. Development of the Mammalian Auditory System

The auditory system detects sound stimuli and transduces them into electric signals in a highly specialised fashion. Following the transduction of sound by the hair cells into a neuronal impulse, the encoded acoustic information is processed at numerous levels in the central nervous system up to the auditory cortex. The epicentre of sound transduction is the IHC, of which humans have about 3500 per ear (Holley, 2005). This small number of cells can be subject to numerous harmful influences throughout life such as noise trauma or prescribed ototoxic drugs. Unlike lower vertebrates, such as birds and amphibians, mammalian hair cells are not able to regenerate (Corwin, 1992), which makes each individual hair cell indispensible for the auditory system of mammals. To date many important aspects of the auditory system, such as tonotopicity, structural design and physiology have been described in the literature. However, the processes involved in the development of the auditory system remain largely unknown. Deciphering the mechanisms underlying auditory development in general and those specific to the hair cells is an essential step to understand how the mature auditory system functions.

1.2.1. General Development of the Auditory System in Mice and Men

The morphological development of the human auditory system takes place mainly in the womb during the first five to six months of pregnancy (Hall, III, 2000). During this period of development hair cell differentiation and stereociliogenesis take place and synaptic connections between auditory nerve fibres and hair cells are made. The exact onset of hearing is not known but thought to occurs during the sixth month of pregnancy, when the morphological structure of the inner ear appears to be mature (Hall, III, 2000).

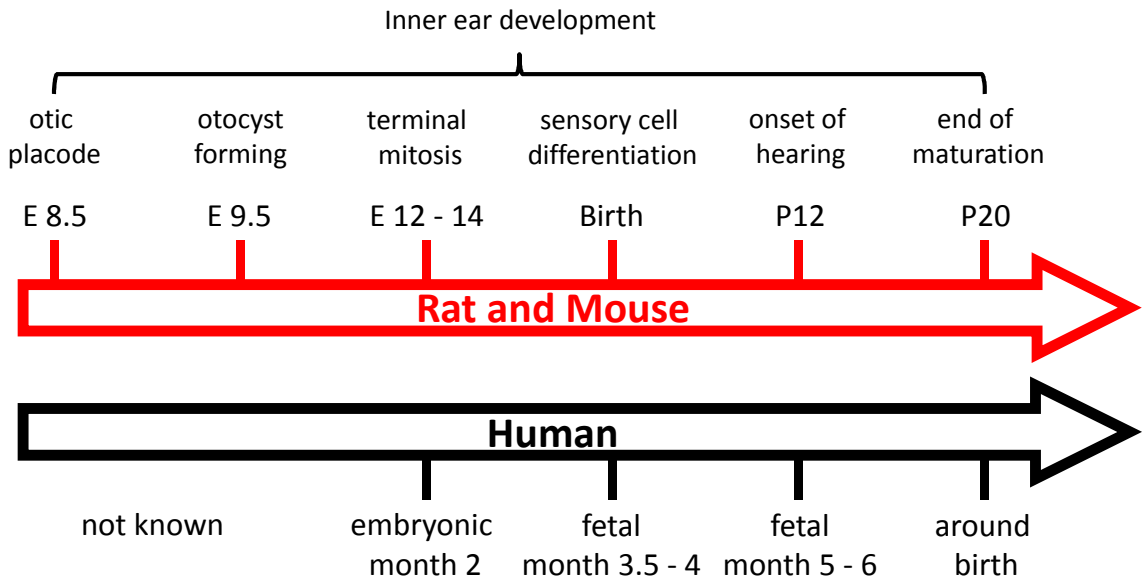

Figure 6: Main developmental stages of the mammalian auditory system of humans, rat and mouse with focus on the inner ear. The development of the auditory system in humans happens in substance before birth. Onset of hearing appears during the sixth month after conception. On the contrary rodents such as rats and mice are born deaf, which makes them a very interesting animal model for developmental auditory research.

The onset of hearing in many rodents, such as mice and rats is around postnatal day 12 (P12; Ehret, 1977; Blatchley *et al.*, 1987; Geal-Dor *et al.*, 1993) and unlike humans, they are born deaf. Hence, a large part of cochlear development takes place after birth making them an ideal animal model to study auditory development (Figure 6). At birth, the outer and middle ear of most rodents is still immature. The ear canal is still closed and acoustic stimuli cannot be channelled onto the tympanum. It has been shown in gerbils and other rodents that the ear canal does not open before the end of the first postnatal week (Marston & Chang, 1965; Forsythe, 2007). The transmission of sound stimuli by the middle ear is not functional before the end of the second postnatal week, because the ossicles are still cartilaginous and the middle ear cavity is filled with fluid (Huangfu & Saunders, 1983; Zimmer *et al.*, 1994). Therefore, the onset of the mature middle ear function closely coincides with the onset of hearing at around P12. A striking phenomenon is that by the onset of hearing the major development of the inner ear is nearly complete. Not only is the hair cell's synaptic machinery functional, but all the synaptic connections are in place and the IHCs, as well as the OHCs are highly specialised to respond appropriately to acoustic

stimuli. How is it possible for the sensory cells to mature to such a high degree of specialisation without the input of acoustic stimuli? And how are the cells able to select the appropriate synaptic connections in order to encode sound stimuli at the onset of hearing?

1.2.2. Formation of the Inner Ear

The development of the mouse inner ear begins around embryonic day 8.5 (E8.5), when cells of the neural ectoderm, close to the hindbrain, begin to form the otic placode, which is observed under the microscope as a bilateral thickening (Driver & Kelley, 2009). During the next 24 hours these cells invaginate and form a hollow sphere, referred to as the otocyst. All cells within the organ of Corti derive from progenitors within this early otocyst. However, before the sensory epithelium of the cochlea is formed, the otocyst has to traverse several morphological changes. These changes commence with the outgrowth of cells from the otocyst forming small pockets, which sprout and elongate to form the early vestibule and cochlea. Elongation and outgrowth is not finished until E18 whereupon the developing cochlea reaches its mature length and elaborate three dimensional structure (Morsli *et al.*, 1998).

Between embryonic day 12 and 14, cells of the cochlear epithelium reach terminal mitosis (Ruben, 1967), which marks an important step in cochlear development. Over the next two to three weeks the homogenous population of cells within the primordial cochlear epithelium has to differentiate into mechanosensory hair cells and several types of supporting cells. Cells of the organ of Corti develop with two distinct gradients (Chen *et al.*, 2002b; Eatock & Hurley, 2003; Lee *et al.*, 2006). Generally, cells at the base mature two days earlier than those in the apical coil. The second differentiation gradient occurs radially from the modiolar side of the cochlear with IHCs appearing earlier than OHCs. The exact mechanism underlying these gradients remains so far elusive. However, several molecular factors have been shown to be essential for cochlear development indicating that the precise control over the mitotic cell cycle and cell differentiation is essential for the normal development of cells within the auditory epithelium. For example, the enzyme P27,

a cyclin dependent kinase inhibitor is important for cells to enter their postmitotic life, since a knock out leads to supernumerary hair cells and supporting cells within the cochlea (Chen & Segil, 1999; Lee *et al.*, 2006). After the cells of the organ of Corti enter their postmitotic cell cycle, hair cells seem to be the first to become specified (Driver & Kelley, 2009). The transcriptional factor Math1 is up-regulated exclusively in a subpopulation of cells within the primordial organ of Corti that become the hair cells. The importance of Math1 for cell fate was shown in Math1 knockout mice in which the same subpopulation of cells underwent apoptosis instead of forming hair cells (Chen *et al.*, 2002b). The notch signalling pathway seems to play an important role in deciding the fate of supporting cells, which is consolidated by the fact that nearly all supporting cells develop as hair cells when this signalling pathway is impaired (Driver & Kelley, 2009). The interplay of many more signalling and transcription factors and their accurately timed up- and down-regulation determines cell fate within the undifferentiated and immature sensory epithelium of the inner ear. Many different transcription factors regulate the very complex developmental processes in inner ear development (Fekete & Wu, 2002; Bok *et al.*, 2007; Driver & Kelley, 2009; Chatterjee *et al.*, 2010).

One of the first morphological processes that uncovers hair cell differentiation using microscopy is the maturation of the hair bundle (Lenoir *et al.*, 1987). Stereociliogenesis starts a few days after terminal mitosis with the growth of a single kinocilium and can be further described as a three staged process. Initially, actin based microvilli grow and become differentiated into rows graded in height. Then, the immature hair bundle becomes reorganised and supernumerary stereocilia are removed. During the last step, stereocilia elongate to their final length, which depends on the cochlear region since stereocilia are longer towards the cochlear apex (Nayak *et al.*, 2007; Schwander *et al.*, 2010). Stereociliogenesis is complete at about the onset of hearing (Pujol *et al.*, 1998). However, hair bundle growth is not the only morphological change that occurs during the development of the organ of Corti. In fact, quite a few non-mitotic growth processes can be observed after terminal mitosis (Chen *et al.*, 2002b). Briefly, the basilar membrane grows in length, width and thickness, the latter two being dependent on cochlear region (Roth & Bruns, 1992b). Also OHC somata grow to form the gradient in cell length with basal OHCs being shorter than apical (Pujol *et al.*, 1998).

Another morphological change during development is the refinement of synaptic connections between nerve fibres and both inner and outer hair cells. At around the time of terminal mitosis, before hair cells can be distinguished from supporting cells, afferent spiral ganglion neurons spread into the embryonic cochlear epithelium making the first synaptic like contacts with the differentiating hair cells (Pujol *et al.*, 1998). Two types of afferent fibre, myelinated type I and unmyelinated type II spiral ganglion neurons can be distinguished from about the first postnatal week (Romand *et al.*, 1980; Schwartz *et al.*, 1983). The immature spiral ganglion neurons are highly branched making many synaptic contacts with both inner and outer hair cells (Figure 7). This pattern is very different to the adult configuration, where 90 - 95 % of afferent type I fibres contact IHCs exclusively. Furthermore, they undergo extensive pruning until each type I afferent makes a one to one contact with an IHC with 10 to 30 afferents contacting a single cell (Pujol *et al.*, 1998; Rubel & Fritzsch, 2002; Huang *et al.*, 2007). The remaining 5 - 10 % of afferents are unmyelinated type II fibres that contact the OHCs (Pujol *et al.*, 1998; Heldmaier & Neuweiler, 2003; Huang *et al.*, 2007). Their innervation pattern is distinctly different to afferents innervating IHCs since each fibre contacts multiple OHCs. By P6 the afferent innervation of IHCs has reached its adult-like state (Huang *et al.*, 2007).

Efferent fibres begin to invade the early sensory epithelium at the same time as the afferents, initially making direct contact to IHCs, before synaptic refinement takes place that reorganises efferent fibres. The adult efferent innervation is grossly characterised by projections from the medial olivary complex that directly innervate the OHCs and those from the ipsilateral superior olive that contact the spiral ganglion neurons below IHCs (Pujol *et al.*, 1998).

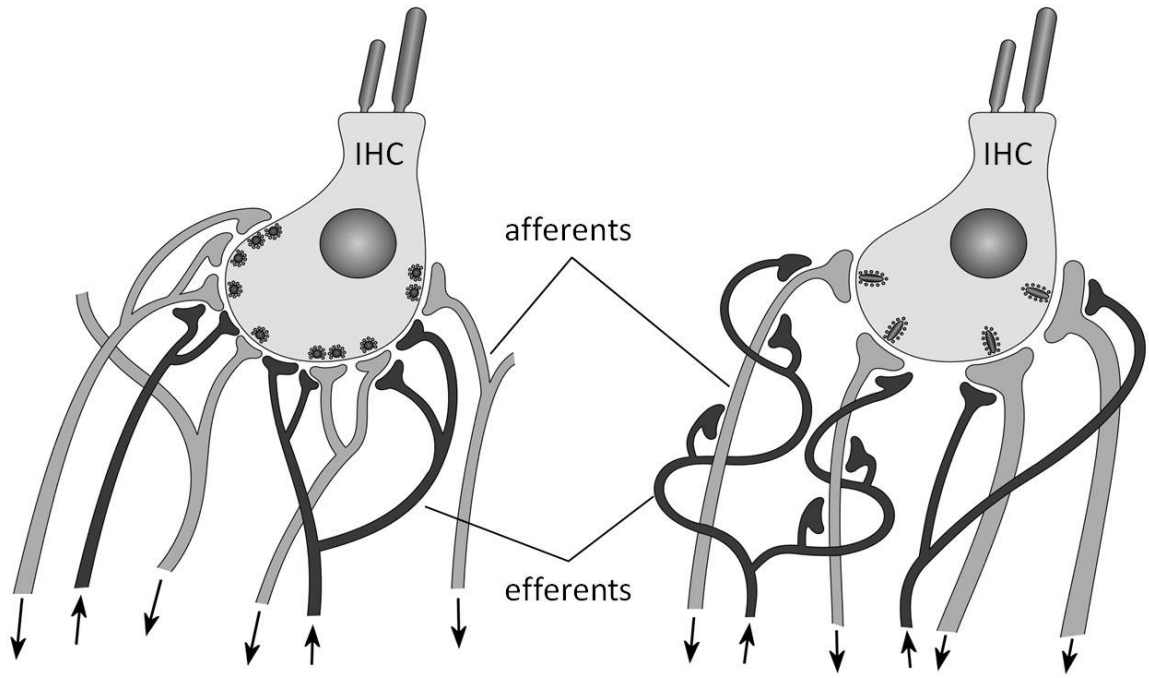

Figure 7: Refinement of the IHC nervous innervation pattern. Left: schematic diagram showing an immature IHC with highly branched afferent fibres (light grey) and efferent fibres (dark grey). Note that the efferent terminals make contacts with both the afferent fibres and the IHC. Right: Afferents are highly organised in adult IHCs with one to one synaptic connections while efferents only contact afferent fibres. Arrows beneath the nerve fibres depict the direction of information transfer (outgoing = afferent fibre; ingoing = efferent fibre; graphic with kind permission by S.L. Johnson).

1.2.3. Physiological Development of Inner Hair Cells

The maturation of the organ of Corti is also the result of major physiological changes within the hair cells. A defined set of ion channels, such as the mechanoelectrical transducer channel, voltage gated potassium channels (K^+ channels) and the voltage gated Ca^{2+} channel $Ca_V1.3$ translate acoustic stimuli into graded receptor potentials making mature IHCs highly specialised sound transducers. However, just three weeks earlier, the cells of the organ of Corti have just reached terminal mitosis and are not yet differentiated. The expression of ion channels in these immature IHCs is completely different to their

mature composition. While some ion channels are not yet expressed, others become eliminated at around the onset of hearing (Figure 8 and 9).

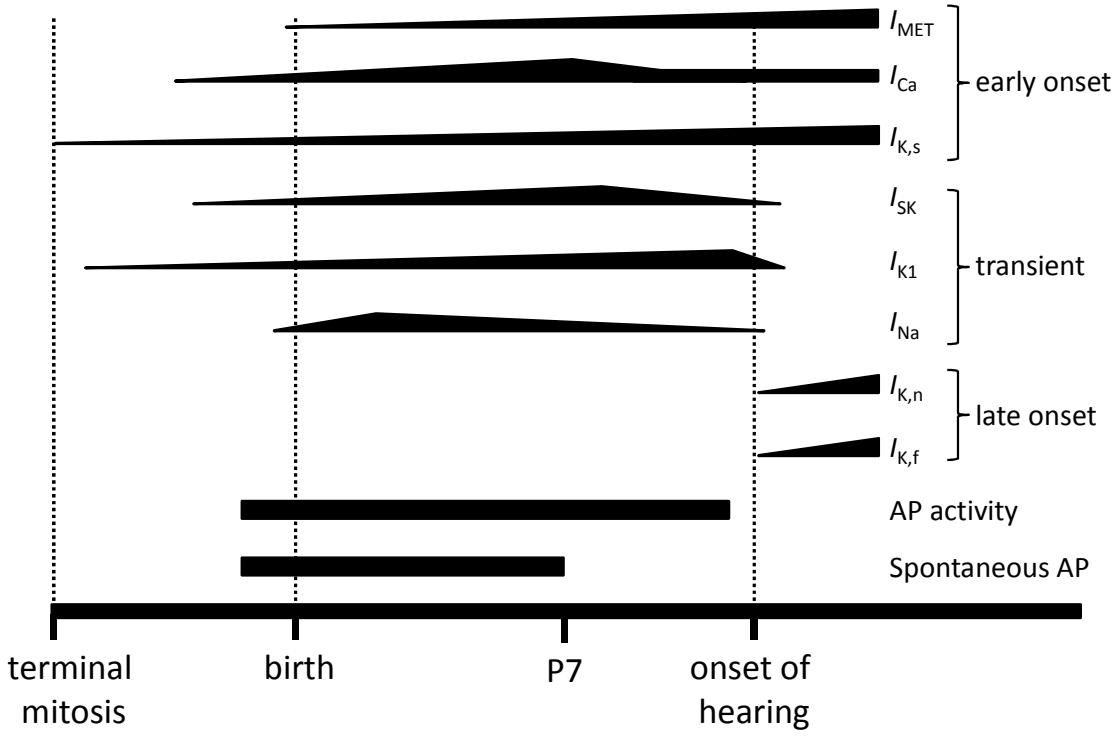

Figure 8: Changes in the expression pattern of ionic currents and excitability during mouse IHC development. I_{MET} = mechanoelectrical transducer current; I_{Ca} = calcium current; $I_{K,s}$ = delayed rectifier potassium current; I_{SK} = small conductance calcium activated potassium current; I_{K1} = inward potassium rectifier; I_{Na} = sodium current; $I_{K,n}$ = negatively activating potassium current; $I_{K,f}$ = calcium dependent large conductance potassium current; AP = action potential. (graphic re-drawn from Housley *et al.*, 2006; Marcotti, 2012).

After terminal mitosis IHCs begin to acquire voltage and ligand gated ion channels. These channels can be classified based on their expression pattern into three different groups: early onset, transient and late onset. Among the first ion channels to be expressed at around E14.5 is a slowly activating outward rectifier K^+ channel (Marcotti *et al.*, 2003a). The corresponding current has been classified as $I_{K,emb}$ before birth, $I_{K,neo}$ between birth and onset of hearing and $I_{K,s}$ after the onset of hearing. During early embryonic development IHCs are electrically quiescent and respond only slowly to current injection (Marcotti *et al.*, 2003a). The first signs of a functional mechanoelectrical transducer channel can be

observed as early as P0 in rats, which is shortly after the onset of hair bundle growth. However, the biophysical properties of the mechanolelectrical transducer current, such as current amplitude, speed of activation and adaptation are primitive compared to its mature state (Waguespack *et al.*, 2007). The third early onset current that can be observed in immature IHCs from E17 is the calcium current (I_{Ca}). The amplitude of I_{Ca} steadily increases until P6, where it peaks. After P6 the calcium current amplitude declines to reach its mature levels from around P12 (Beutner *et al.*, 2001; Johnson *et al.*, 2005).

Three ionic currents that have been described so far, are only transiently present in immature IHCs. The inward rectifier potassium current (I_{K1}) can be detected from about E15.5 until P12-14 (Marcotti *et al.*, 1999; Marcotti *et al.*, 2003a). The second transiently expressed ionic current, the small conductance calcium activated potassium current (I_{SK}) is up-regulated shortly after birth until just after the onset of hearing (Marcotti *et al.*, 2004). The third current, a sodium current (I_{Na}), which is carried by voltage gated Na^+ channels, is also present from around birth up to the onset of hearing whereupon it suddenly disappears (Marcotti *et al.*, 2003b). The early onset and transiently expressed ion channels allow IHCs to generate spontaneous action potentials from shortly before birth until the end of the first postnatal week (Kros *et al.*, 1998; Beutner & Moser, 2001). Action potential activity is not observed in mature IHCs since it would be detrimental to accurate sound encoding. Immature IHC action potentials depend on the presence of I_{Ca} since in the absence of extracellular calcium they are not observed (Marcotti *et al.*, 2003b). I_{Na} is expressed by the majority of mouse IHCs and is thought to modulate action potential generation by speeding up the depolarisation phase of the action potential waveform (Marcotti *et al.*, 2003b). While I_{Ca} and I_{Na} define action potential depolarisation I_{SK2}, I_{K1} and $I_{K,neo}$ are important for the repolarisation phase and for setting the resting membrane potential (Marcotti *et al.*, 2003a; Marcotti *et al.*, 2004).

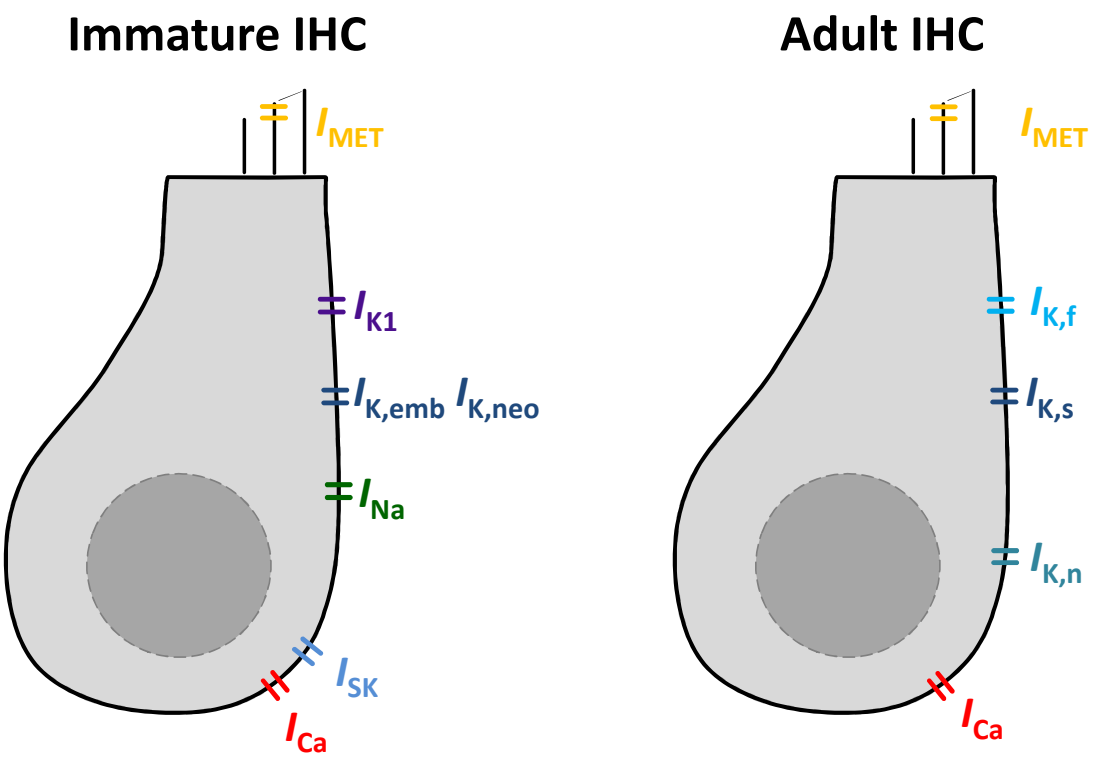

Figure 9: Comparison of ionic currents in immature (left) and adult (right) IHCs. Currents can be classified as early onset, to which the transducer current I_{MET}, the slowly activating delayed rectifier potassium current $I_{K,s}$ (in immature IHCs referred to as $I_{K,emb}$ or $I_{K,neo}$) and the calcium current I_{Ca} belong. The sodium current I_{Na}, the inward rectifier potassium current I_{K1} and the calcium activated potassium current I_{SK} are also present from an early time point, but downregulated at around or just after the onset of hearing. Late onset currents are the fast voltage and calcium activated potassium current $I_{K,f}$, and the negatively activating outward rectifying potassium current $I_{K,n}$, which both are upregulated from around the onset of hearing (Housley *et al.*, 2006).

The group of late onset ionic currents are closely related to the mature IHC function. This group consists of the voltage and calcium activated large conductance potassium current ($I_{K,f}$) and the negatively activating potassium current ($I_{K,n}$). Both are up regulated from around the onset of hearing. The appearance of $I_{K,n}$ causes the cells resting membrane potential to become more hyperpolarised (Oliver *et al.*, 2003). The rapid activation and the large amplitude of $I_{K,f}$ speeds up the cell membrane time constant preventing the generation of action potentials even at very depolarised levels. The mature composition of potassium currents together with I_{Ca} allow IHCs to respond to depolarisation via the mechanoelectrical transducer channel with graded receptor potentials (Kros *et al.*, 1998). A graded receptor

potential can be considered as an analogue signal with much higher resolution to acoustic signal strength compared to the digital all-or-nothing answer of an action potential.

Another crucial developmental change of IHCs is that of their synaptic machinery, which allows them to respond to sound stimuli with continuous and graded release of synaptic vesicles. From a morphological point of view this maturational change can be observed from the shape of their ribbon synapses. Immature IHCs display spherical ribbons (Figure 10), which during maturation change to be more ellipsoid (Sobkowicz *et al.*, 1982; Nouvian *et al.*, 2006). Physiologically the development of the synaptic machinery was investigated, for example, by studying the calcium dependent exocytosis. It was shown that the magnitude of the calcium induced exocytosis does not decline, while the calcium current amplitude decreases during the second postnatal week, indicating an increase in the calcium efficiency of exocytosis (Johnson *et al.*, 2005).

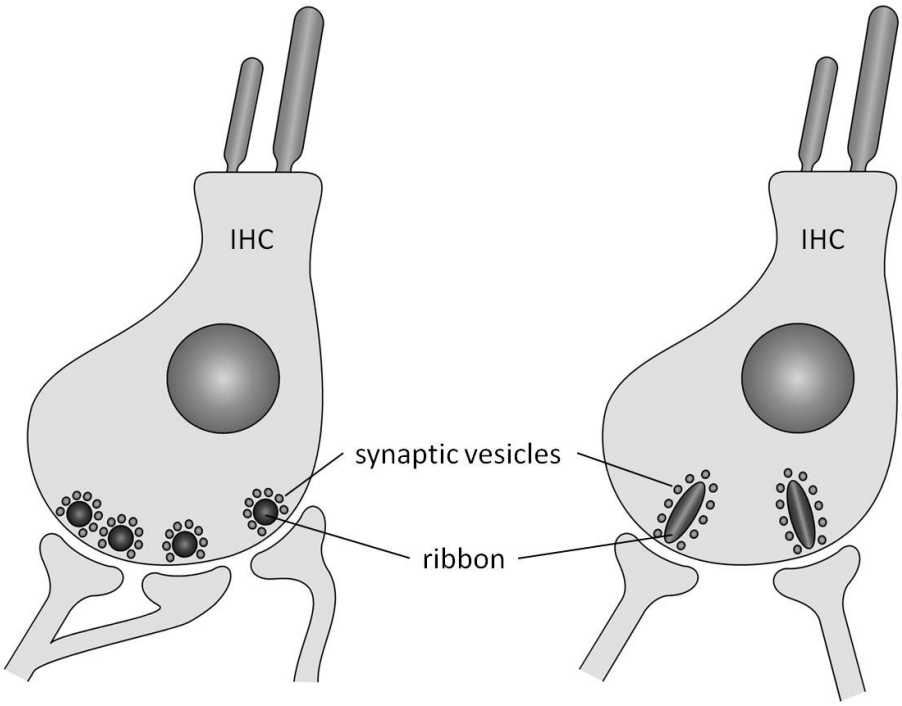

Figure 10: Schematic drawing of the morphological changes of the hair cell ribbon synapse during development. The ribbon is an electron dense structure, to which neurotransmitter filled vesicles are tethered. It is thought to act as a conveyer belt for rapid and sustained neurotransmitter release. During development the shape of the ribbon changes from spherical (left = immature) to ellipsoid (right = mature). Physiological changes comprise a more calcium efficient exocytosis (graphic with kind permission by S.L. Johnson).

Although substantial morphological and physiological reorganisation and neuronal refinements have been described to occur in the auditory system throughout development, we have very little knowledge about the programmes that induce, control or modulate these changes. The fact that spontaneous action potential activity occurs concomitantly with auditory development suggests that it might hold an instructive role on developmental programs.

1.3. The Role of Spontaneous Action Potential Activity during Development

Spontaneous electrical activity before the onset of adult function is not unique to the cochlea. In many neuronal systems such as the cortex, brainstem and spinal cord as well as in sensory systems such as the retina, spontaneous electrical activity occurs during development (Zhang & Poo, 2001; Blankenship & Feller, 2010). This early electrical activity is not restricted to mammals, since it is commonly observed across vertebrates, such as chicks or amphibians and in invertebrates such as ascidians (Jaffe & Cross, 1986; Moody & Bosma, 2005). The spontaneous activity displayed by these systems during development is not an immature, simplified version of the adult electrical activity. Quite the contrary, it is usually extremely specialised (Housley *et al.*, 2006), supporting the idea that these systems need specific electrical activity to drive developmental programmes (Moody & Bosma, 2005). This is reflected by the ion channel expression needed to generate and maintain repetitive action potential activity during maturation as well as the mechanisms that modulate it. It has been shown that manipulating or disrupting the properties of spontaneous action potential activity can have a substantial influence on the normal development of adult functionality (Meyer, 1983; Schmidt & Buzzard, 1993; Mostafapour *et al.*, 2000; Gnuegge *et al.*, 2001). One common characteristic of the different types of spontaneous activity is a rise of intracellular calcium concentration (Moody & Bosma, 2005) either by calcium entry through voltage gated ion channels or by calcium release from internal stores, accompanying the spontaneous electrical activity (Spitzer, 2002). This rise in intracellular calcium and especially its frequency and amplitude are believed to trigger or change the course of developmental programmes (Buonanno & Fields, 1999; Moody & Bosma, 2005). Aside from having intrinsic roles on gene expression (Hanson & Landmesser, 2004) it often occurs in developing systems during a phase of major plasticity, leading to the hypothesis that early spontaneous activity instructs synaptic or network refinements via, for example, long term potentiation or long term depression (Katz & Shatz, 1996; Spitzer, 2006; Blankenship & Feller, 2010). Due to the easy experimental access to the peripheral visual system, the pattern and function of spontaneous electrical activity has probably been best described in the retina.

1.3.1. Role of Spontaneous Action Potential Activity in the Developing Retina

The eye functions very much like a camera. Light passes through the cornea and lens, which both refract light and pass an inverted image to the retina. Retinal photoreceptors detect light quantity (measured in lux) and quality (wavelength) and transduce the light stimulus into electrical signals. These signals are passed via bipolar neurons, retinal ganglion cells and the central visual pathways to the visual cortex, where the neuronal impression of an image is formed (Land & Fernald, 1992; Heldmaier & Neuweiler, 2003).

The development of the visual system and the auditory system share several similarities, which comprise: 1) highly specialised receptor cells that generate a receptor potential. Both systems rely on the exocytosis of glutamate as neurotransmitter to transmit information on to adjacent ganglion neurons (Glowatzki and Fuchs, 2002; tom Dieck & Brandstätter, 2006); 2) major restructuration of synaptic connections and neuronal projections occur before the onset of function (Sengpiel & Kind, 2002); 3) both sensory systems rely on the spatial organisation of their neuronal networks, when computing sensory information. In the visual system this means that light information is computed by creating maps of visual space, so called retinotopic maps. Adjacent photoreceptors pass information onto neurons that project into adjacent neuronal areas in the brain (Heldmaier & Neuweiler, 2003). In the auditory system hair cells are spatially arranged very much like a claviature of a piano, which leads to adjacent frequencies exciting hair cells in close proximity. This tonotopic organisation is preserved within the brain. In both sensory systems a crude topographic map is initially formed that is then successively refined throughout development. This refinement is thought to be driven by spontaneous electric activity before physical stimuli excite sensory cells. Furthermore this spontaneous activity is calcium dependent and shows a specific pattern (Moody & Bosma, 2005).

The generation of spontaneous electrical activity appears in mice before the detection of visual stimuli from around birth until the opening of the eyes at around P13 to 14 (Blankenship & Feller, 2010). Depending on the type of neurotransmitter being released the electrical activity is defined into an early cholinergic and late glutamatergic stage (Firth *et al.*, 2005). Spontaneous activity in the retina is characterised as randomly occurring

electrical bursts spreading across the retina in a wave like manner. Calcium imaging has revealed that with spreading bursts, the intracellular calcium concentration transiently rises in retinal ganglion cells, hence the spontaneous electric activity is often referred to as calcium waves (Sernagor *et al.*, 2001). The calcium waves in general last a few seconds and occur at intervals of about one to two minutes after which the internal calcium concentration falls back to normal levels (Meister *et al.*, 1991). During calcium waves retinal ganglion cells generate action potential activity. This activity is highly correlated with distance between individual retinal ganglion cells, which leads to retinal ganglion cells in close proximity being more synchronous than those further apart (Maffei & Galli-Resta, 1990).

The spontaneous calcium waves found in the retina before the onset of vision have been hypothesised to have an instructive role at different levels of visual system development. Maffei and Galli-Resta (1990) suggested that spontaneous activity contributes to the neuronal connectivity in the retinal system by consolidating synaptic efficacy following the Hebbian theory: when a presynaptic cell excites an adjacent cell repeatedly and persistently, then growth changes or metabolic changes take place resulting in an increased synaptic efficiency – "Cell's that fire together, wire together" (Heldmaier & Neuweiler, 2003). And indeed it was shown that dendritic trees of retinal ganglion cells failed to segregate and mature to their elaborate adult morphology when retinal calcium waves were manipulated (Sernagor *et al.*, 2001). Furthermore, it was hypothesised that the electrical activity in the retina drives retinotopic mapping within the visual pathway (Shatz & Stryker, 1988; Maffei & Galli-Resta, 1990; Grubb & Thompson, 2004). Evidence proving this hypothesis was found by manipulating the early cholinergic spontaneous phase, which showed that the refinement of retinal ganglion cell axons projecting into the superior colliculus was dependent on calcium waves in the retina (McLaughlin *et al.*, 2003). Other studies showed the instructive role of calcium waves on the development of the neuronal network of the dorso-lateral geniculate nucleus (Katz & Shatz, 1996; Sengpiel & Kind, 2002). Altogether the research performed on the early electric activity during visual development indicates that spontaneous activity plays not only a crucial role in the refinement of single retinal ganglion cells, but also on neuronal networks forming in the visual pathway.

1.3.2. Spontaneous Activity in the Cochlea

The role of spontaneous activity in the auditory system is not as well understood as it is in the retina. This is probably due to the complex morphology and the lower accessibility of the auditory periphery, which makes manipulations more difficult. Nevertheless it is known that immature mammalian cochlear IHCs fire spontaneous action potentials before the onset of hearing (Kros *et al.*, 1998; Beutner & Moser, 2001; Marcotti *et al.*, 2003b; Brandt *et al.*, 2007). This activity is mainly dependent on the interplay of a calcium current and several potassium currents.

From a developmental point of view, it would be beneficial for the auditory system to have control over the spontaneous action potential activity, especially when the frequency and pattern of the spontaneous activity could have an instructive role on its development. The transient cholinergic innervations of the IHC and purinergic signalling are two mechanisms shown to control spontaneous activity in the cochlea (Glowatzki & Fuchs, 2000; Housley *et al.*, 2006; Tritsch *et al.*, 2007; Johnson *et al.*, 2011b). The modulation by acetylcholine is facilitated by efferent fibres descending from the superior olive. These fibres transiently innervate the basolateral membrane of IHCs during the same time when spontaneous action potentials are reported (Pujol *et al.*, 1998). Acetylcholine released by the efferent nerve fibres triggers calcium influx through heteromeric α9α10 acetylcholine receptors, which are transiently expressed in immature IHCs (Elgoyhen *et al.*, 2001; Maison *et al.*, 2002). This calcium influx triggers the activation of SK-channels leading to a hyperpolarisation of the IHC membrane potential (Glowatzki & Fuchs, 2000; Marcotti *et al.*, 2004). The action potential activity found in IHCs appears highly dependent on their position along the tonotopic axis of the cochlea (Johnson *et al.*, 2011b). Apical IHCs generate more obvious bursts of action potentials and with a lower frequency than basal IHCs, which showed a more sustained firing pattern. This difference in action potential generation in IHCs along the cochlea seems to be due to a difference in membrane potential between apical and basal IHCs, resulting from a more pronounced effect of acetylcholine in the apical coil of the cochlea (Johnson *et al.*, 2011b). This was shown by experimentally modulating the membrane potential via the block of the acetylcholine receptor using strychnine, which could prime apical IHCs to generate action potentials in a basal-like pattern.

The influence of adenosine-5'-triphosphate (ATP) on the spontaneous activity seems to be of a more complex nature. IHCs as well as supporting cells express both P2X and P2Y purinergic receptors (Nikolic *et al.*, 2003; Housley *et al.*, 2006; Huang *et al.*, 2006; Tritsch *et al.*, 2007; Ito & Dulon, 2010). Tritsch et al (2007) have shown that ATP is periodically released by supporting cells within the Koelliker's organ, a transient epithelial ridge adjacent to IHCs. This ATP release leads to slowly propagating calcium waves within the population of supporting cells. The nature of these calcium waves is not fully understood, but it was shown that the action of ATP is not limited to supporting cells. In fact, Tritsch & Bergles (2010) have shown that IHCs can only fire action potentials when sufficiently depolarised by ATP mediated inward currents. However, the authors of these studies used an extracellular solution that was rather atypical for IHCs (Johnson *et al.*, 2011b). This solution produced a more hyperpolarised membrane potential than that found with perilymph-like extracellular solution in which IHCs showed a membrane potential positive to -65 mV (Beutner & Moser, 2001; Johnson *et al.*, 2007). Using a perilymph like solution, IHCs are capable of spiking spontaneously indicating that ATP was not required to induce this activity. However, depending on the experimental concentration of ATP used, the induced calcium influx into IHCs via P2X receptors could have a dual effect (Johnson *et al.*, 2011b): 1) a low ATP concentration (3-300 nM)) causes IHC hyperpolarisation by activating nearby calcium activated SK2 channels; 2) higher ATP concentrations (30 nM to 100 µM) caused a depolarisation which overcomes the hyperpolarising effect of SK2 channels. ATP was shown to modulate the membrane potential of IHCs and by that the frequency and pattern of IHC action potential activity (Tritsch & Bergles, 2010; Johnson *et al.*, 2011b). Moreover, supporting cells release ATP in a defined spatiotemporal manner and its effect seems to be locally restricted to about 6-10 IHCs (Tritsch *et al.*, 2007). As a result, the spontaneous activity of a few IHCs in close proximity to each other should be altered in the same manner, creating a locally restricted modulatory effect on action potential activity. Thereby a mechanism could exist that locally synchronises the frequency or pattern of action potential activity (Tritsch & Bergles, 2010). This would display a process similar to the retina, where due to calcium waves a correlation between the closeness of retinal ganglion cells and the synchronised action potential generation is observed.

Despite the ongoing research on spontaneous action potential activity in the cochlea it remains unknown to what extent it is able to influence developmental programmes of the auditory system. However, some hypotheses for its probable role and function have been postulated. For example, it seems possible that similar to the retina action potentials of the auditory system might have an instructive role on the development of the neuronal circuitry of the auditory pathway. Evidence for this stems from the fact that a single action potential generated by the IHC can trigger the release of sufficient neurotransmitter to change the activity in the spiral ganglion neurons (Beutner & Moser, 2001; Glowatzki & Fuchs, 2002). Furthermore, the peripheral pattern and frequency of action potential activity seems to be conserved to some extent in higher nuclei of the auditory pathway (Tritsch *et al.*, 2010). When the activity of the auditory nerve was stifled, by a removal of the cochlea or by blocking the spiral ganglion activity, a significant loss of neurons in the nucleus cochlearis was observed (Tierney *et al.*, 1997; Mostafapour *et al.*, 2000). However, it could well be that the developmental role of spontaneous action potential activity in IHCs is not restricted to the refinement of synaptic circuitry. Periodic calcium influx mediated by $Ca_V1.3$ channels may also orchestrate changes in gene expression level within the IHC (Moody, 1998; Marcotti *et al*., 2003b).

1.4. Voltage Gated Sodium Channels

Voltage gated Na^+ channels play an essential role in neurons and most other excitable cells. They sense voltage fluctuations of the cell membrane potential, to which they respond with channel activation and sodium influx. This sodium influx further depolarises the cell and leads to a cascade-like opening of voltage gated Na^+ channels. In this way, they are responsible for cell excitability and play a critical role in the initiation and propagation of action potentials in most neurons (Wood & Baker, 2001). This chapter briefly describes the general phylogeny of voltage gated ion channels, before focussing on structure, function and expression pattern of voltage gated Na^+ channels.

1.4.1. Phylogeny and Genetics of Voltage Gated Sodium Channels

The evolution of voltage gated Na^+ channels dates back into the early metazoan era and seems to coincide with the occurrence of specialised neurons (Hille, 1992; Yu & Catterall, 2003). Within the phylogenetically older group of protozoans only voltage gated K^+ and Ca^{2+} channels, but not Na^+ channels are found, which led to the hypothesis that the evolutionary younger Na^+ channels might have evolved from voltage gated K^+ channels via gene duplications (Goldin, 2002). By this the structure of voltage gated K^+ channels, which are formed by protein tetramers of single domain subunits, would have been transformed into a single protein carrying four domains that forms the functional Na^+ channel (Yu *et al.*, 2005). Together with cyclic nucleotide channels, these three classes of voltage gated ion channels form one phylogenetic superfamily (Terlau & Stuhmer, 1998; Yu *et al.*, 2005).

Voltage gated Na^+ channels consist of a single α subunit usually accompanied by accessory β subunits. So far nine genes encoding for functional α and four for β subunits have been described, with a tenth gene encoding for an α subunit that was identified but not found to be functionally expressed (Goldin *et al.*, 2000; Patino & Isom, 2010). The gene sequence

for α subunits is highly conserved throughout evolution. Among mammals, voltage gated Na^+ channels display great homology with over 75 % identical amino acid sequence. The stability found in the gene sequence over evolution as well as throughout the animal kingdom highlights their critical role and functional importance. Due to the similar amino acid sequence of all known and functionally expressed voltage gated Na^+ channels, all were classified into the same distinct voltage gated Na^+ channel family Na_V1 (Figure 11; Goldin, 2002). It contains 9 isoforms ($Na_V1.1$ - $Na_V1.9$) of which $Na_V1.1$, $Na_V1.2$, $Na_V1.3$ and $Na_V1.7$ are located on human chromosome 2 (Goldin *et al.*, 2000; Catterall *et al.*, 2003). Together with $Na_V1.4$ and $Na_V1.6$ these channels display high nanomolar sensitivity to the common Na^+ channel blocker tetrodotoxin, hence they are also classified as tetrodotoxin sensitive voltage gated Na^+ channels (Catterall *et al.*, 2005). The genes for $Na_V1.4$ and $Na_V1.6$ are located on human chromosome 17 and 12, respectively. The second phylogenetically close related group of Na^+ channels comprises of isoform $Na_V1.5$, $Na_V1.8$ and $Na_V1.9$, which are all mapped on human chromosome 3. These isoforms are only blocked by higher tetrodotoxin concentrations in the micromolar range (Yu *et al.*, 2005). The different sensitivity to tetrodotoxin is related to differences in amino acid residues within the outer pore of the channel (Fozzard & Lipkind, 2010).

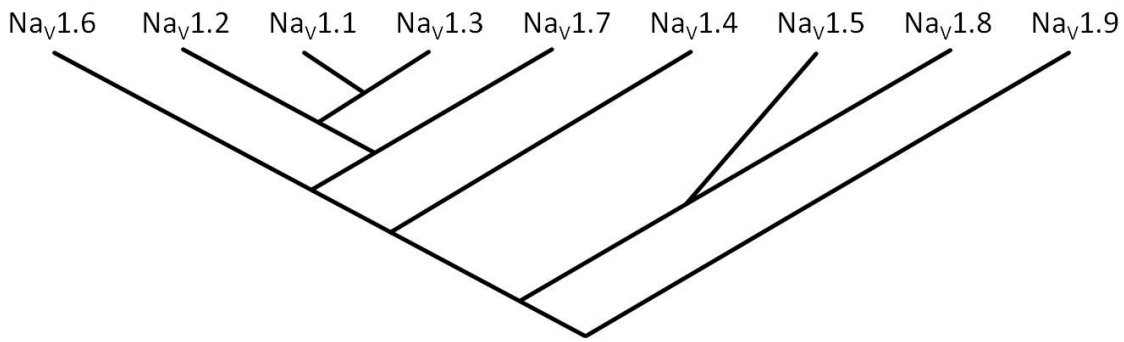

Figure 11: Phylogenetic tree of voltage gated Na^+ channel isoforms. The genes encoding for the isoforms can be found on human chromosome 2 ($Na_V1.1$–1.3 and $Na_V1.7$), 3 ($Na_V1.5$, $Na_V1.8$ and $Na_V1.9$), 12 ($Na_V1.6$) and 17 ($Na_V1.4$; Goldin, 2002; Catterall *et al.*, 2005).

1.4.2. Molecular Ultrastructure of the Voltage Gated Sodium Channel α Subunit

Voltage gated Na^+ channels are integral cell membrane proteins that form a Na^+ selective pore with voltage dependent properties. Their molecular structure comprises a single α subunit that forms the ion conductive aqueous pore (Catterall, 1992). In expression systems, the α subunit has been shown to be sufficient to provide the essential channel properties, such as voltage dependence, ion selectivity and rapid inactivation. Nevertheless, the α subunit is generally accompanied by accessory β subunits. These have been shown to be involved not only in conductive processes altering the kinetics and voltage dependence of the α subunit, but also in non-conductive processes such as cell-cell adhesion (Brackenbury & Isom, 2011).

The α subunit is a relatively large protein of approximately 260 kDa, which was discovered by using photoreactive neurotoxins and photolabelling (Beneski & Catterall, 1980). The primary amino acid sequence folds into 4 homologous domains (I-IV), each of which contain 6 transmembrane segments (Figure 12). These transmembrane segments are formed by alpha helices, which are connected by re-entrant loops extrinsic of the lipid bilayer of the cell membrane. The largest re-entrant loops on the extracellular side are found between transmembrane segments 5 and 6 of each domain, which are associated with forming the outer pore of the Na^+ channel. The largest re-entrant loops on the intracellular side provide the connection of the four domains with each other (Yu & Catterall, 2003). Both the carboxyl- and amino-terminal tail of the amino acid sequence are on the intracellular side of the cell membrane.

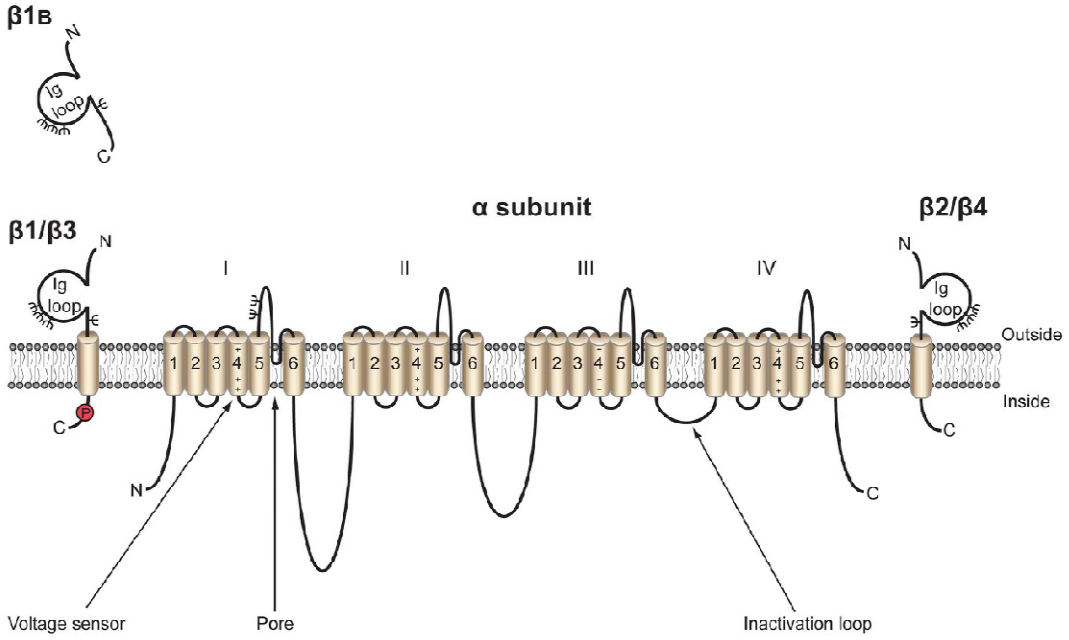

Figure 12: Primary structure of the α and β subunit of the voltage gated sodium channel with highlighted functional regions. The α subunit provides the aqueous pore with the important channel properties. The β subunits modulate channel properties by covalently or non-covalently binding to the α subunit. Roman figures depict the four domains and arabic numbers depict the six transmembrane segments. (Further explanation see text; figure as originally published in Brackenbury and Isom, 2011).

The three dimensional structure of the voltage gated Na^+ channel under helium-cooled cryo-electron microscopy appears as a bell shaped molecule with several cavities (Sato *et al.*, 2001). To form that shape, the transmembrane segments of the four domains are thought to cluster together, with the transmembrane segment 6 forming the aqueous pore on the inside of the channel molecule (Yu & Catterall, 2003). Several neurotoxin interaction sides have been reported within the ion channel structure. For example, common Na^+ channel blockers, such as tetrodotoxin or saxitoxin, react with amino acid residues in the outer pore region acting like a plug that leads to complete channel block (Catterall *et al.*, 2003).

1.4.3. Functional Properties of the Voltage Gated Sodium Channel

The early work performed by Hodgkin and colleagues (Hodgkin *et al.*, 1952) on Na^+ channels in the squid axon led to the discovery of three key functions for these channels: 1) voltage dependent activation; 2) rapid inactivation; 3) ion selectivity. In order to be able to respond to voltage changes of the cell membrane, a voltage sensor must be present in the channel. The most feasible solution for a voltage sensor to act rapidly to changes in the electrical field would be to rely on electrical charged amino acids. In case of the Na^+ channel, positively charged amino acid residues within transmembrane segment 4 were found to be responsible for sensing voltage changes. In the closed state of the channel these charges are in a locked position within the transmembrane electric field. However, upon depolarisation these charges are moved towards the outside of the cell membrane (Armstrong, 1981; Catterall *et al.*, 2003). It was shown that the whole transmembrane segment 4 moves towards the extracellular side (Yang *et al.*, 1996), a process probably best described by the sliding helix model (Catterall, 1986). This movement leads to a conformational change of the channel structure ultimately resulting in the pore opening.

In order to achieve ion selectivity a channel needs a selectivity filter, which only allows the preferred ion to pass. Generally this filter works by restricting size and charge. In the case of the Na^+ channel the narrowest part of the channel pore is about 3 to 5 Å wide (Hille, 1992; Payandeh *et al.*, 2011). Two amino acids in analogous positions in the re-entrant loop between segments 5 and 6 in all four domains form the selectivity filter of the Na^+ channel. These 8 amino acids form an outer ring comprised of the amino acids EEDD (E = glutamic acid, D = aspartic acid) and an inner ring comprised of DEKA (K = lysine, A = alanine; Yu & Catterall, 2003). Mutations exchanging amino acids within these rings have been shown to significantly affect the ion selectivity of the channel (Schlief *et al.*, 1996). When for example DEKA was changed to EEEE this caused the selectivity filter to change from sodium to calcium (Heinemann *et al.*, 1992).

Upon prolonged depolarisation the Na^+ channel inactivates rapidly. Gene sequencing has revealed an evolutionary highly conserved region between domain III and IV forming a hairpin-like loop on the intracellular side. Studies have shown that manipulating this loop influences the inactivation process (Vassilev *et al.*, 1988; Stuhmer *et al.*, 1989). The commonly accepted theory of channel inactivation is that this re-entrant loop between

domain III and IV folds into the Na^+ channel pore from the intracellular side and blocks the Na^+ ion movement (Terlau & Stuhmer, 1998; Catterall, 2000). The physiological importance of channel inactivation is highlighted by mutations that impair it. Several mutations within the gene sequence encoding for the loop region between domain III and IV have been identified in the human to cause diseases, for example the temperature induced muscle stiffness paramyotonia congenital or hyperkalemic periodic paralysis, where mutations cause hyperactive Na^+ channels (Ptacek *et al.*, 1991; McClatchey *et al.*, 1992).

1.4.4. Structure and Function of Sodium Channel β Subunits

Sodium channel α subunits are generally associated with one or two accessory β subunits (Hanlon & Wallace, 2002). To date four transmembrane β subunits, β1 to β4 with their four encoding genes have been described. Like α subunits, β subunits are highly expressed in most excitable tissues within the central and peripheral nervous system, as well as in cardiac and skeletal muscle cells (Patino & Isom, 2010). Interestingly they are also expressed in a variety of non excitable cells, such as stem cells, glia, vascular endothelial cells and carcinoma cells (Chioni *et al.*, 2009; Brackenbury & Isom, 2011).

Structurally β subunits consist of a single alpha helical transmembrane segment anchoring them to the cell membrane, with a large immunoglobuline like domain on the extracellular side and a short intracellular domain (Catterall, 1992). They are linked by either disulfide bridges (β2 and β4) or bound non-covalently (β1 and β3) to the Na^+ channel α subunit. β subunits interact on both intra- and extracellular side with the α subunit (Patino & Isom, 2010).

The functional role of β subunits is very complex and depends on a variety of factors, such as the animal model, tissue and expression level (Brackenbury & Isom, 2011). Due to this variety and complexity only key roles shall be mentioned here: β subunits have been shown to interact with the α subunit to modulate its conductive properties. This was, for example, shown by comparing the biophysical properties of the sodium current provided by the α

subunit with or without the β subunit in an expression system. This experiment revealed that β1 and β2 increased the peak sodium current and speed up the inactivation kinetics of the α subunit (Isom *et al.*, 1994; Isom *et al.*, 1995). But the role of β subunits is not limited to the modulatory role on α subunits (Patino & Isom, 2010). They seem to be also important in cell-cell adhesion and neuronal migration and have been shown to increase the amount of functional Na^+ channels at the cell surface (Chen *et al.*, 2002a).

1.4.5. Tissue specific Expression of Sodium Channel Isoforms

Sodium channel α subunits show specific expression patterns as a function of developmental stage and tissue localisation (Goldin, 1999). $Na_V1.1$, $Na_V1.2$, $Na_V1.3$ and $Na_V1.6$ are classified as the voltage gated Na^+ channels of the central nervous system, since they are highly expressed in central neurons. Their expression pattern has mainly been studied in rodents and found to differ significantly throughout development. $Na_V1.3$ expression peaks in early embryonic development and is down-regulated after birth. During adulthood it is usually no longer detected (Beckh *et al.*, 1989). The expression of $Na_V1.6$ peaks during early development, but this isoform is still most abundantly expressed in the adult rat brain (Felts *et al.*, 1997). Both $Na_V1.1$ and $Na_V1.2$ are up-regulated during development and are expressed at the highest levels in adulthood (Beckh *et al.*, 1989). The isoforms of the central nervous system also show very complex expression patterns among different tissues or even among different anatomical structures of a single neuron (Goldin, 1999). For example, in the spiral ganglion neurons that contact the inner and outer hair cells $Na_V1.6$ is restricted to the nodes of Ranvier and the unmyelinated segment of the neuron within close proximity to the hair cells. No sign of $Na_V1.2$ was found in the spiral ganglion cells. Very interestingly $Na_V1.6$ was not present in the efferents, whereas $Na_V1.2$ was highly expressed (Hossain *et al.*, 2005).

$Na_V1.7$, $Na_V1.8$ and $Na_V1.9$ are the most abundant Na^+ channels in the peripheral nervous system, although their expression can be accompanied by low levels of $Na_V1.1$ (Beckh, 1990) and $Na_V1.6$ (Dietrich *et al.*, 1998). $Na_V1.7$ is the only one of these three Na^+ channels

that shows high sensitivity to tetrodotoxin in the nanomolar range (Catterall *et al.*, 2005). Due to its abundant expression in the cell membrane of axons it is thought to allow action potential propagation (Toledo-Aral *et al.*, 1997). The role of $Na_V1.8$ and $Na_V1.9$ seems to be closely related to pain perception (Akopian *et al.*, 1999; Yu & Catterall, 2003).
The expression of $Na_V1.4$ and $Na_V1.5$ is mainly restricted to heart and skeletal muscle and largely absent from neuronal tissues (Goldin, 1999). $Na_V1.4$ is blocked by nanomolar concentrations of tetrodotoxin, whereas $Na_V1.5$ is blocked only by micromolar concentrations (Kallen *et al.*, 1990). Their function is to facilitate muscle contraction by initiating action potential depolarisation.

1.4.6. Voltage Gated Sodium Channels in Hair Cells

Information about Na^+channel expression and function in hair cells of the vertebrate inner ear is to date fairly sparse. Both avian (Masetto *et al.*, 2003) and mammalian vestibular hair cells (Rusch & Eatock, 1997; Li *et al.*, 2010) express voltage gated Na^+ channels. Their physiological role is puzzling, since they are largely inactivated at the presumed cell resting membrane potential (Rusch & Eatock, 1997; Wooltorton *et al.*, 2007). Even less is known about voltage gated Na^+ channels and their role within cochlear hair cells. The first evidence for the presence of a voltage activated sodium current in cochlear hair cells came from the alligator (Evans & Fuchs, 1987). The authors of this work reported that a tetrodotoxin sensitive sodium current was present in about a quarter of tall hair cells, which displayed fast activation and rapid inactivation kinetics upon membrane depolarisation. It was hypothesised that this conductance contributes to action potential activity generated by hair cells of the alligator. Indeed about 15 years later it was shown that a tetrodotoxin sensitive sodium current expressed in immature IHCs of the mouse is essential for speeding up the rising phase of spontaneous action potentials (Marcotti *et al.*, 2003b). The expression of a Na^+ conductance is not restricted to IHCs, as it was also found in 97 % of developing OHCs of the rat (Oliver *et al.*, 1997) and in 10 % of adult guinea pig OHCs (Witt *et al.*, 1994). However, in OHCs the sodium current appears largely inactivated at

rest, thus questioning its possible functional role in these cells (Witt *et al.*, 1994; Oliver *et al.*, 1997). Although Na^+ channels have been reported to be expressed in hair cells, very little is known about their role and function.

1.5. Aims of the Thesis

1.5.1. Characterisation of the Spontaneous Action Potential Activity in Immature Rat Inner Hair Cells

At the time when this project began there was very little evidence about the pattern and frequency of the spontaneous action potentials in IHCs. To allow the spontaneous action potential activity to fulfil their earlier proposed developmental roles in neuronal refinement, instruction of tonotopic organisation or orchestration of IHC gene expression, it was hypothesised that the spontaneous activity might differ as a function of age during postnatal development. Furthermore, the pattern of spontaneous activity might instruct topographic organisations by inheriting a location specific electric activity. To test the above hypotheses, current-clamp recordings of spontaneous or induced calcium action potentials were performed from IHCs at different stages of immature development (P0-P12) and positioned at different locations along the rat cochlea (at about 20 % and 90 % from the base). Initially, action potential activity was recorded under current-clamp mode using long lasting recordings, complemented with long lasting cell recordings in cell attached mode.

1.5.2. Characterisation of the Rat Inner Hair Cell Sodium Current

The aim of this part of the study was to comprehensively characterise the size and kinetics of the voltage dependent sodium current of immature rat IHCs as a function of postnatal development and cochlear region.

Sodium currents were previously reported in IHCs (Marcotti *et al.*, 2003b) and vertebrate hair cells (Evans & Fuchs, 1987; Oliver *et al.*, 1997; Masetto *et al.*, 2003; Wooltorton *et al.*, 2007). But still, very little is known about their physiological role and expression pattern in

IHCs as a function of postnatal development and cochlear region. Following the observation that many base to apex gradients exist along the cochlea, both at morphological (Roth & Bruns, 1992a; Pujol *et al.*, 1998) and physiological level (Engel *et al.*, 2006; Johnson *et al.*, 2008; Johnson *et al.*, 2011a), it was hypothesised that some of the biophysical properties of the sodium current might be specific to a cochlea region. To test this hypothesis voltage clamp recordings on immature rat IHCs from P0 onwards were performed as a function of cochlear region (again from positions around 20% and 90% from the base). Voltage clamp protocols were applied to IHCs in order to measure the current responses for offline analysis. The isolated sodium current was obtained by subtracting the current recorded during the superfusion of the common Na^+ channel blocker tetrodotoxin or the Na^+ channel impermeable cation N-Methyl-D-glucamine from the total current.

1.5.3. Molecular Identity of the Na^+ Channel α Subunit expressed in Immature Rat IHCs

It has been previously shown that vertebrate hair cells might express several isoforms of voltage gated Na^+ channels (Mechaly *et al.*, 2005; Wooltorton *et al.*, 2007). In IHCs the current is sensitive to nanomolar concentrations of tetrodotoxin (Marcotti *et al.*, 2003b), suggesting that only tetrodotoxin sensitive Na^+ channels are likely to be present in these cells. To date five tetrodotoxin sensitive Na^+ channel α-subunits are found to be expressed within neuronal tissues. These isoforms are: $Na_v1.1$, $Na_v1.2$, $Na_v1.3$, $Na_v1.6$, $Na_v1.7$. *In situ* hybridisation experiments using digoxigenin labelled RNA probes against these five isoforms were planned in order to consolidate these preliminary findings.

2. Materials and Methods

2.1. Electrophysiology

The following chapter describes the theoretical background of patch clamp experiments, animal procedures, experimental set-up and the experimental procedures necessary to record from IHCs. It is then complemented with a detailed data analysis description.

2.1.1. Patch Clamp Technique in General

For all excitable cells the current flowing through voltage gated ion channels is of vital importance. The early work done by Cole and Curtis as well as Hodgkin and Huxley in the early fifties of the last century led to the discovery of how to study the electrical activity of excitable cells (Numberger & Draguhn, 1996). Since the initial work on the squid axon using intracellular recordings with sharp pipettes (Hodgkin *et al.*, 1952), many different microelectrode techniques and recording configurations have been developed (Halliwell *et al.*, 1994). The major part of this thesis was performed by using one of these microelectrode configurations, the whole-cell patch clamp. Generally speaking, the patch clamp technique uses a fine microelectrode, which is used to gain access to the interior of a cell. The cell's voltage can then be controlled by the electric circuits of the patch clamp set-up connected via the headstage to the microelectrode (Figure 13). The "heart" of the set-up is the patch clamp amplifier, which consists of various electric circuits that allow to control and measure the electrical activities of cells. In general the amplifier has two main modes to control a cell: voltage clamp and current clamp. In voltage clamp mode, the voltage of the cell is controlled so that current flowing across the cell membrane can be measured.

Current clamp mode allows to measure the membrane potential of the cell in resting condition or during current injection.

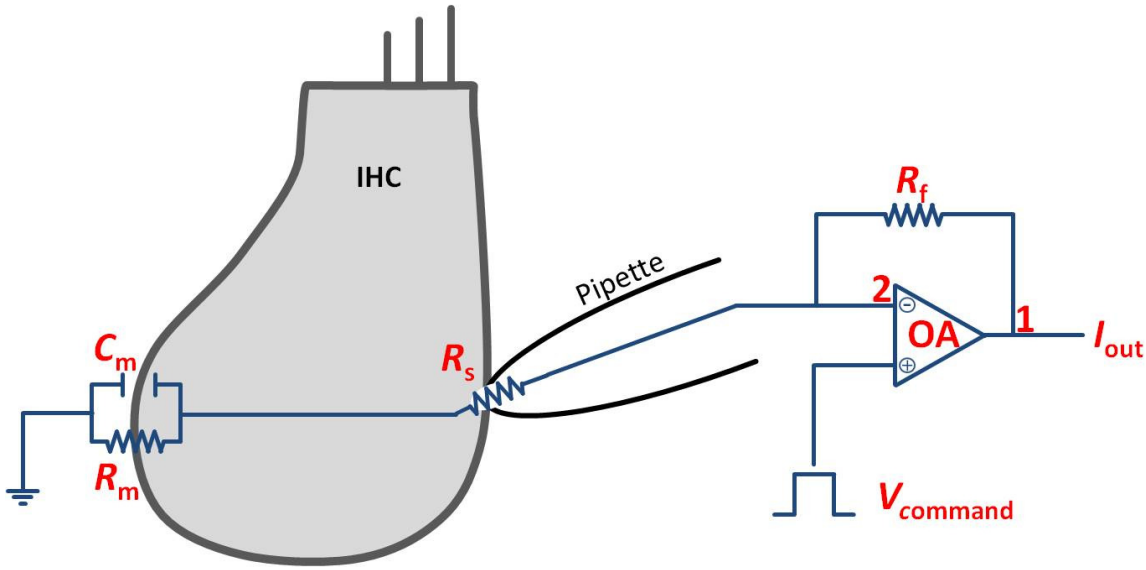

Figure 13: Diagram showing a simplified electric circuit of an IHC connected to the essential circuit elements of an amplifier. The cell membrane consists of a capacitor C_m and a resistor R_m which is variable as it changes when a change in current through ion channels occurs. The access to the cell is gained by a patch pipette and restricted by a resistance R_s. The simplified circuit on the right inherits a few key characteristics: The operational amplifier (OA) delivers a voltage at the output (1), which is proportional to the difference between the OA inputs (2) but highly amplified. Both inputs of the OA have a very high resistance in the order of 10^{12} Ω so that the voltage can be measured without current flowing. $V_{command}$ = voltage applied by the OA. R_f = a resistor build in parallel to 1 and 2 within the circuit board, I_{out} = current being measured by the amplifier.

There are three crucial characteristics of the whole cell voltage clamp circuit: 1) the operational amplifier (OA) delivers a voltage at the output, which is proportional but highly amplified to the voltage at its inputs; 2) both inputs of the OA measure voltage. Due to a very high access resistance in the order of 10^{12} Ω no current flows across the OA; 3) at the resistor R_f a voltage is applied, which is proportional to any current difference between the input and output of the OA. In whole cell voltage clamp configuration, the aim is to keep the membrane potential (V_{cell}) constant, which ideally is equal to the potential applied by the OA ($V_{command}$) at the tip of the patch pipette ($V_{pipette}$). A current flowing through the cell membrane would normally cause a potential difference between $V_{command}$ and $V_{pipette}$.

However, due to the circuit elements a compensating current will flow across R_f until $V_{command}$ and $V_{pipette}$ are equal. This compensating current, which is proportional to the current flowing across the cell membrane, will be measured at the current output (I_{out}).

The cells access resistance R_s is in series with the $V_{pipette}$ and proportional to the pipette resistance $R_{pipette}$. R_s should ideally be kept as close to zero as possible since it will otherwise lead to a slight deviation of V_{cell} from $V_{command}$. When R_s differs from zero it causes an artificial representation of the recordings in three ways: 1) V_{cell} will deviate from $V_{command}$ when an ionic current is flowing through the cell membrane (I_m) with the magnitude of $R_s * I_m$. 2) If a voltage step is applied to the cell, the actual membrane potential of the cell will change with a time constant of $\tau = R_s * C_m$. 3) Furthermore, and very important when measuring very fast activating currents, the R_s together with the cell membrane capacitance (C_m) build a RC filter. This leads to current flowing through the cell membrane being filtered with a -3 dB corner frequency of $2\pi * R_s * C_m$. A few steps can be undertaken in order to minimise these three R_s errors. The $R_{pipette}$ should be kept as small as possible by using pipettes with a rather big opening diameter. Most OA come with a built-in R_s compensation circuit that adds a certain amount of voltage to the $V_{command}$ in order to reduce R_s to only a fraction of its initial value.

2.1.2. Animal Housing

For this study Wistar rats belonging to the species *Rattus norvegicus* were used. Animals were obtained from Harlan (Harlan Laboratories, UK) in 2006 and since then have been bred by the Biological Services of the University of Sheffield. All animals were kept under the same laboratory conditions with a 12 h light and dark cycle with water and food ad libidum. They were fed with 2018 Teklad Global 18% Protein Rodent Diet (Harlan Laboratories, UK). Room temperature and humidity were computer controlled and kept constantly at 21˚C and 50 %, respectively. Animals were checked daily, usually early in the

morning and afternoon for a new litter to ensure high precision of the time of birth. The day of birth is referred to as P0. For this study, animals between P0 and P12 were studied.

2.1.3. Animal Procedures and Tissue Preparation

Immature rats were sacrificed by cervical dislocation in accordance with UK Home Office regulations. After decapitation, the temporal bones containing the inner ear were kept in ice cold extracellular solution (normal ECS, see Table 1 for more details). One cochlea was immediately dissected to obtain the isolated organ of Corti, while the other cochlea was stored in ice cold solution for up to 30 minutes for later use if required. The dissection was performed on a cool pad stored at -20˚C under times 11 to 128 magnification using a Leica MZ 16 microscope (Leica Microsystems, Milton Keynes, UK). Depending on the animal age, the bone or cartilage and the tectorial membrane covering the organ of Corti were removed using fine forceps. Then, both the intact apical and basal turns of the organ of Corti were acutely dissected out, transferred to an experimental chamber made by the University workshop (Figure 14) and immobilised under a nylon mesh, which was fixed to a small steel ring.

The position of IHCs along the cochlea was determined by measuring their fractional distance from the extreme end of the base. Apical IHCs were considered those of a fractional distance of 0.83 to 0.95, which corresponds to a frequency range of 1.5 to 5 kHz in the adult animal. Basal IHCs had a fractional distance of 0.15 to 0.30 corresponding to a frequency range of 25 to 40 kHz in the adult animal (von Bekesy, 1960; Mueller, 1991).

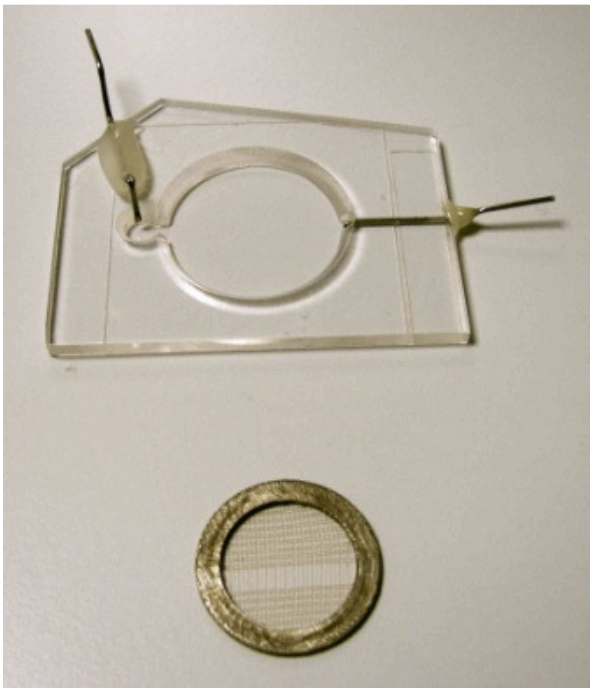

Figure 14: Experimental chamber with steel ring and nylon mesh.

2.1.4. Experimental Set-Up

The experimental chamber (Figure 14) containing the immobilised organ of Corti was transferred onto the stage of an upright microscope equipped with a HCX Apo X63/0.90 W objective (Leica DM LFS, Leica Microsystems, Milton Keynes, UK) or an Olympus BX51WI equipped with a LUMPlan N X60/1.00 W objective (Olympus Imaging & Audio Ltd, Essex, UK). In order to gain access to IHCs positioned along the coiled organ of Corti, the microscope stage was modified so it could be rotated by 360°. Microscope, pipette holders and headstage of the amplifier were attached to an antivibration table (TMC, MA, USA) to reduce mechanical vibrations that could prevent seal formation[1] or lead to a loss of

[1] Patching a cell briefly comprises the following steps: A patch pipette is filled with solution and driven under positive pressure close to the cell of interest. Under very faint positive pressure, the pipette is driven against the cell membrane up to the point, where a small dimple can be observed under visual control. Then the positive pressure is removed and a gentle suction is applied under the utmost care. Seal formation then generally occurs within seconds and can be acknowledged by a seal resistance in the range of giga ohm.

seal (Figure 15). A Faraday cage, which was equipped with a front curtain containing a thin copper mesh surrounded the antivibration table to reduce electrical noise from the environment.

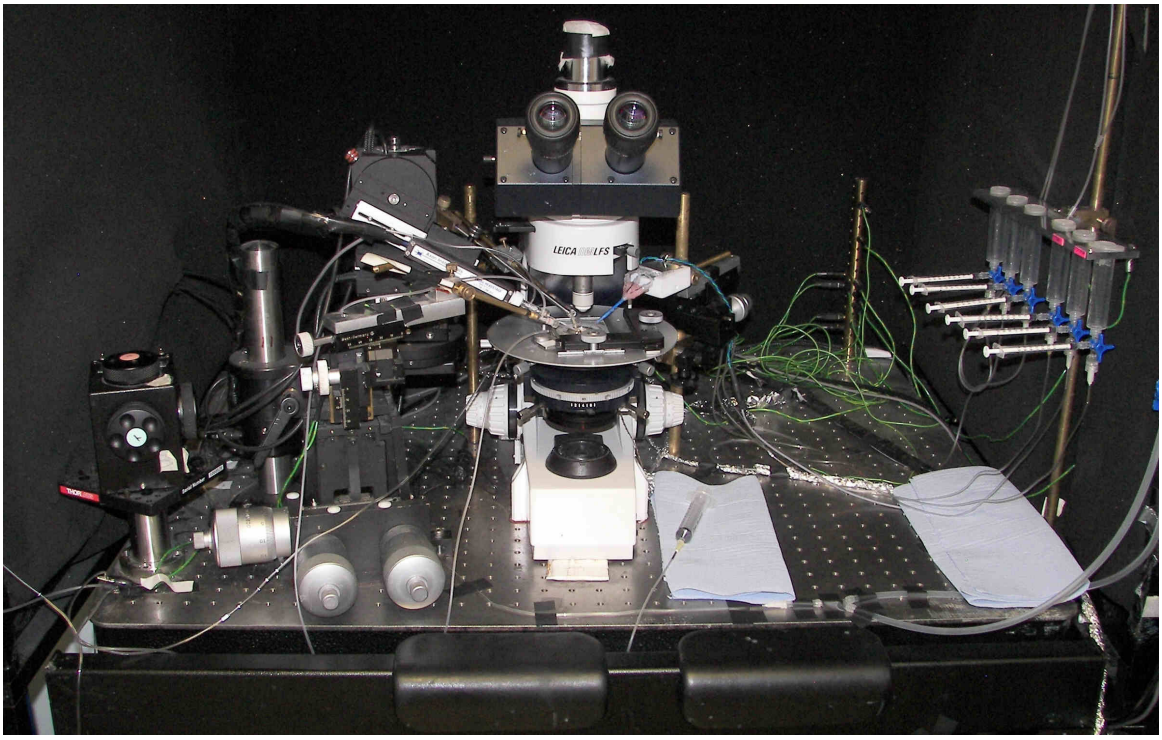

Figure 15: Experimental set-up showing the microscope, pipette holders and gravity perfusion system (barrels on the right) fixed on top of an antivibration table. A Faraday cage is surrounding the equipment in order to reduce electric noise.

A cartridge pump (Masterflex, L/S model 7519-20) was connected to the experimental chamber in order to continuously superfuse the organ of Corti with normal extracellular solution at a speed of 30 ml / h. To reduce any possible electrical noise from this pump, a small capacitor of 64 µF was connected between the ground and the stainless steel influx pipe of the experimental chamber. The organ of Corti was observed under Nomarski differential interference contrast optics. Before patching an IHC, surrounding supporting

---

Whole cell configuration is obtained by a very brief slightly stronger suction that breaks the membrane under the patch.

cells were partially removed using a suction pipette with an opening diameter of 5 to 7 µm, which was filled with the same extracellular solution used for the superfusion. Only cells with a healthy appearance, such as intact stereocilia, lack of Brownian movement, smooth surface and absence of vacuoles, were patched.

Most of the experiments performed for this thesis required fast exchanges of extracellular solutions containing drugs. In order to facilitate a fast solution exchange in the order of a few seconds, a local gravity controlled perfusion system was used (Figure 16). This system consisted of five barrels, which each could be filled separately with different extracellular solutions, depending on the type and aim of the experiment. These barrels were connected via small PVC tubes to a perfusion tip that was placed in close vicinity to the patched IHC without touching or damaging the tissue.

Figure 16: Gravity perfusion system with barrels that contain different extracellular solutions (left). From these barrels small PVC tubes ran through a heating element into a plastic tip (right) that was placed in close proximity to the patched IHC.

Experiments have shown that this system provides a fast exchange of solution surrounding the patched IHC in the order of a few seconds. To make sure all solutions had the same flow speed, the barrels were always filled to the same height, the pressure by gravity was kept constant by not changing the height of the barrels and the PVC tubes all had the same inner diameter.

2.1.5. Temperature Control System

In order to study ion channel activity in IHCs as close as possible to physiological conditions almost all experiments were done near body temperature at 34-37˚C. Therefore the solution within the experimental chamber was warmed up by a temperature control unit. Six small resistors fixed underneath the microscope stage served as heat producing elements. With a potentiometer built in the temperature control unit, the voltage at the resistors and by that the heat produced by the resistors could be adjusted. A thermocouple, which was in contact with the solution in the experimental chamber, was used as a feedback system to automatically adjust any change in the set temperature. To prevent a temperature drop by the local perfusion a second heating element consisting of four flat resistors was interconnected between the barrels and the perfusion tip (Figure 16 right). Since there was no thermocouple built in this second system, it was given at least 30 min to preheat to reach the desired temperature before an experiment. Prior to first use, both temperature systems were calibrated using a voltmeter at which a thermocouple was attached. This sensor was small enough to be placed at the exact position in the experimental chamber, where the tissue later would lay. The temperature system was calibrated to a temperature between 34-37˚C.

2.1.6. Solutions

For all solutions, purified water was obtained from a water purifying system (Purelab ELGA, Marlow, UK). All glassware and spatula were thoroughly rinsed prior to use. The pH was measured and adjusted to 7.28 for intracellular solutions and 7.48 for extracellular solutions using a pH meter (pH211 or Hi 2211, HANNA Instruments, Leighton Buzzard, UK). The pH meter was calibrated with standard solutions pH 4 and 7 at least every 2 weeks. Osmolarity was checked using an osmometer (The Advanced^{TM} MicroOsmometer 3300, Advanced Instruments Inc, Norwood, Massachusett, USA) and was 293 mmol kg^{-1} for pipette filling and 306 mmol kg^{-1} for extracellular solution. The osmometer was

calibrated at least once a year or anytime discrepancies were detected. Normal extracellular solution was always made fresh and stored at -20°C for a maximum of two weeks. To ensure better patching conditions most of the solutions used for the experiments were filtered with 0.22 µm syringe filters. Three different classes of solutions were made:

1) Extracellular solution for dissection and continuous bath perfusion, which will be referred to as "normal extracellular solution" (normal ECS). This solution was the standard extracellular solution in which the tissue was bathed during all procedures. The ionic composition and concentrations of ECS (Table 1) mimicked that of the perilymph (Bosher & Warren, 1971). Amino acids and vitamins from concentrate (Invitrogen, Life Technologies Ltd, Paisley, UK) were added, pH was adjusted using NaOH.

2) Extracellular solutions used for local IHC perfusion. These solutions were used to apply or washout chemicals locally to IHCs in order to block or isolate specific ionic currents. Initially, solutions containing the K^+ channel blockers tetraethylammonium (TEA) and 4-amminopyridine (4-AP) were used. They were termed "TEA-4AP" and "TEA-4AP-NMDG" (Table 1). However, under these conditions IHCs deteriorated rapidly preventing long lasting recordings. For this reason, solutions termed "E" and "E-NMDG" were used for the sodium current isolation; the latter contained N-methyl-D-glucamine as sodium substitute. These solutions were very similar to normal ECS (Table 1), pH was adjusted using NaOH. A Ca^{2+} free solution "0-Ca" was used to test the influence of Ca^{2+} on the spontaneous action potential activity. pH was adjusted with NaOH.

3) Intracellular solution used for pipette filling (Table 2). Depending on the type of experiments, pipettes were filled with different solutions. KCl based solution was mainly used for characterising the spontaneous action potential activity and did not contain any ion channel blockers. PH was adjusted using KOH, the liquid junction potential[2] was -4 mV. CsGlutamate based solution was used to minimise the contamination of the sodium current from the potassium currents expressed in IHCs. pH was adjusted using CsOH, liquid junction potential was -11 mV.

[2] When two solutions of different ionic concentrations are in contact with each other, diffusion of ions from the higher into the lower concentrated solution will occur. The speed of diffusion will depend on charge and size of a specific ion. Differences in speed of diffusion will create a difference in potential, which is called the "liquid junction potential". This needs to be corrected for, when performing patch clamp experiments.
For example, the liquid junction potential between normal ECS and CsGlutamate based solution was measured four times: -11.7, -11.4, -9.3, -11.4. From these values the mean liquid junction potential (11.0 ± 0.6, $n = 4$) was calculated.

Table 1: Extracellular solutions used for dissection, superfusion and local perfusion. All concentrations are given in mM.

	Normal ECS	E	E NMDG	TEA-4AP	TEA-4AP NMDG	0-Ca
NaCl	135	146		105		146
$CaCl_2$	1.3	1.3	1.3			
KCl	5.8	5.8	5.8			5.8
$MgCl_2$	0.9	0.9	0.9	3.9	3.9	2.2
Hepes	10	10	10	10	10	10
Glucose	5.6	5.6	5.6	5.6	5.6	5.6
NaH_2PO_4	0.7					
NaPyruvate	2					
CsCl				5.8	5.8	
TEA-Cl				30	30	
4-AP				15	15	
NMDG			146-148		105	

Table 2: Intracellular solution for pipette filling. All concentrations in mM.

	KCl	CsGlut
KCl	131	
Phosphocreatine	10	10
$MgCl_2$	3	3
Na_2ATP	5	5
Hepes	5	5
KOH-EGTA	1	
EGTA-CsOH		1
L-Glutamic Acid		110
CsCl		20

The liquid junction potential was measured as previously described (Neher, 1992). Briefly, the reference electrode (ground) was filled with 3 M KCl solution. Both pipette and bath were filled with the intracellular solution and under current clamp mode of the amplifier the voltage offset was set to zero. Next, the bath solution was exchanged with normal ECS and the voltage offset in current clamp was determined as the liquid junction potential. This

process was repeated three to four times and the liquid junction potential was averaged across these three measurements. All liquid junction potentials were determined at the same temperature at which the recordings were performed.

2.1.7. Patch Pipettes

Patch pipettes were usually prepared on the day of use or the late afternoon on the previous day to reduce dust particles settling on the tip, which would prevent seal formation. For current clamp or cell attached recordings mainly soda glass capillaries with a 1.5 mm outer diameter and 1.2 mm inner diameter (Harvard Apparatus LTD, Edenbridge, UK) were used. Capilliaries were cut to the right length and the sharp edges were fire polished using a Bunsen burner. They were then oven-baked for 2 - 3 hours at 200 - 230˚C to remove any dust particles. Soda glass capillaries were pulled using a Narishige PP-83 puller (Narishige Scientific, Tokyo, Japan). For most of the voltage clamp experiments quartz glass capillaries with 1.0 mm outer and 0.7 mm inner diameter (Intracel LTD, Herts, England) were pulled using a laser operated micropipette puller (P-2000. Sutter Instruments Co., Novato, USA). Pipette resistances ranged between 2 and 4.5 MΩ. The shank of all pipettes was coated with wax (Coconut flavor, Mr Zoggs SexWax, CA, USA) prior to use in order to reduce the capacitive transient. Usually small transients did occur due to small changes in the amount of solution in the bath (Figure 32). The use of quartz glass pipettes for voltage clamp experiments showed a significant advantage over soda glass, as the capacitive transients were generally smaller (not shown).

2.1.8. Voltage Clamp Protocols

The biophysical characterisation of the sodium current was mainly achieved by using three different voltage step protocols. They were designed using Clampex10.2 (Molecular Devices LLC, Silicon Valley, USA). For all three voltage clamp protocols the holding potential (V_{hold}) was set to -81 mV, which also includes the liquid junction potential of -11 mV characteristic of the Cs-glutamate solution. The current to voltage relation (*I-V*) curve for the sodium current was obtained using a voltage step protocol named "Nacvc" (Figure 17). This protocol consisted of 10 ms long voltage steps from V_{hold} up to -1 mV in nominal 5 mV increments, preceded by a 80 ms conditioning step to -110 mV to remove channel inactivation. An initial 5 mV voltage step with a duration of 10 ms from V_{hold} to -76 mV was used to calculate the linear leak conductance, which was corrected during offline analysis. The interval between consecutive sweeps was 0.25 s making the whole protocol duration, depending on sweep number, between 4 and 5 seconds.

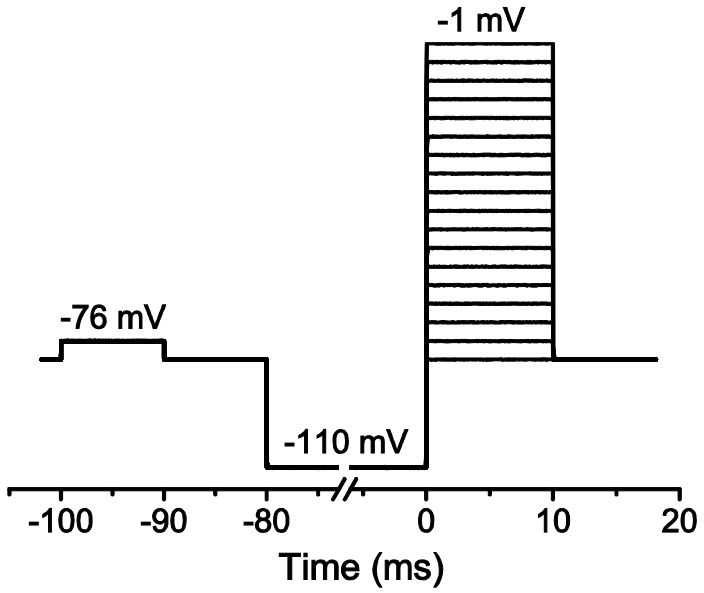

Figure 17: Whole cell voltage clamp protocol "Nacvc" was used to study the *I-V* relation as well as kinetics of the sodium current activation and inactivation.

The second protocol, termed “Inactivation”, was run to measure the steady state inactivation of I_{Na} (Figure 18). Therefor IHCs were depolarised for 10 ms from V_{hold} to -21 mV (close to the maximal peak I_{Na}) following a series of 50 ms conditioning steps to a range of voltages from -131 mV to -1 mV in 5 mV nominal increments. The linear leak conductance was obtained as for the Nacvc protocol.

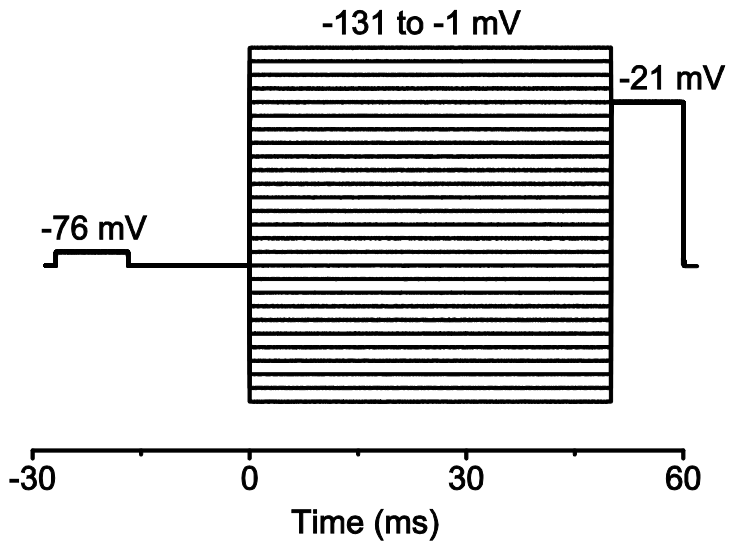

Figure 18: Whole cell voltage clamp protocol "Inactivation" used to determine the steady state inactivation.

A third protocol named "Recovery" (Figure 19) was used to investigate the recovery from inactivation of the sodium current. Starting from V_{hold}, the time of recovery was determined by hyperpolarising IHCs to -131 mV for 100 ms before a 10 ms depolarising step to -21 mV (step 1). This initial voltage step was followed by a second step (step 2) of similar duration and amplitude but varying the interstep interval in 2 ms or 5 ms increments or in an exponential fashion (in ms: 0.1, 0.2, 0.3, 0.5, 0.7, 1, 1.5, 2, 2.5, 3, 3.5, 4, 5, 6, 7, 9, 11, 13, 15, 17, 19) depending on the temperature at which the recordings were made. The currents obtained from the second step were normalised to the current recorded during the first step.

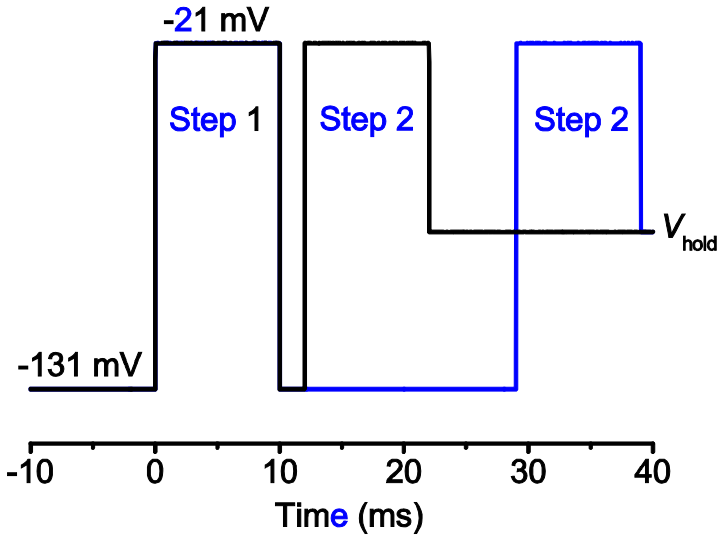

Figure 19: Whole cell voltage clamp protocol "Recovery" was a two voltage step protocol used for investigating the recovery from inactivation. The interstimulus time was progressively increased from sweep to sweep. Two example sweeps with 2 ms (black) and 19 ms (blue) interstep time are shown.

2.1.9. Data Acquisition

For electric recordings both the Optopatch (Cairn Research Ltd, UK) and the Axopatch 200B (Molecular Devices, USA) patch clamp amplifier were used. The Optopatch incorporates a true current clamp built-in circuit and was used for nearly all current clamp recordings. The Axopatch 200B was used for whole cell voltage clamp and cell attached voltage clamp recordings and for a few current clamp recordings. Data acquisition was done using pClamp software (Axon Instruments, Union City, CA, USA) and a Digidata 1320A data acquisition board (Molecular Devices, CA, USA). In current clamp mode of the amplifier the sampling rate was 5 kHz and data were filtered at 2 kHz. In whole cell voltage clamp, data were sampled at 100 kHz and filtered at 10 kHz. In cell attached voltage clamp recordings filtering was set to 1 kHz and sampling rate to 10 kHz. Data were stored on a personal computer for offline analysis using Origin8.0 (OriginLab, Northhampton, MA, USA), Clampex10.2 and Clampfit10.2 (Molecular Devices LLC, Silicon Valley, USA) and Mini Analysis Software (Synaptosoft, Decatur, GA, USA).

2.1.10. Data Analysis I – Current Clamp Recordings

In this part of the project the main focus was to characterise the spontaneous action potential activity of immature IHCs. Therefore current clamp recordings were performed directly after obtaining the whole cell configuration. IHC voltage responses were monitored using a continuous protocol. The absence of current injection allowed testing for the presence of spontaneous action potential activity. When IHCs did not show any spontaneous activity, depolarising current injections of 10 pA, 20 pA or 100 pA increments were applied. Current clamp recordings were complemented by the voltage step protocol "Nacvc" to test for the presence of the sodium current.

In cells that were spontaneously active, the continuous recording was analysed. The IHCs resting membrane potential (V_{rest}) was determined by averaging data points over a period when the resting voltage was stable. V_{rest} very often correlated with the spike threshold ($V_{threshold}$), which was the membrane potential at which the first action potential occurred (Figure 20). In whole cell current clamp recordings, IHCs generally tend to slowly depolarise over time leading to an increase in action potential frequency. In order to compare IHCs from different ages and frequency positions along the cochlea, only the initial part of the recordings was used for the analysis. Precautions were taken to objectively analyse this initial part depending on the following parameters: 1) the resting membrane potential did not depolarise by more than 2.1 mV from the action potential threshold (with an average of 1.6 ± 0.14 mV, n = 9); 2) no fast deterioration of the action potential amplitude was seen.

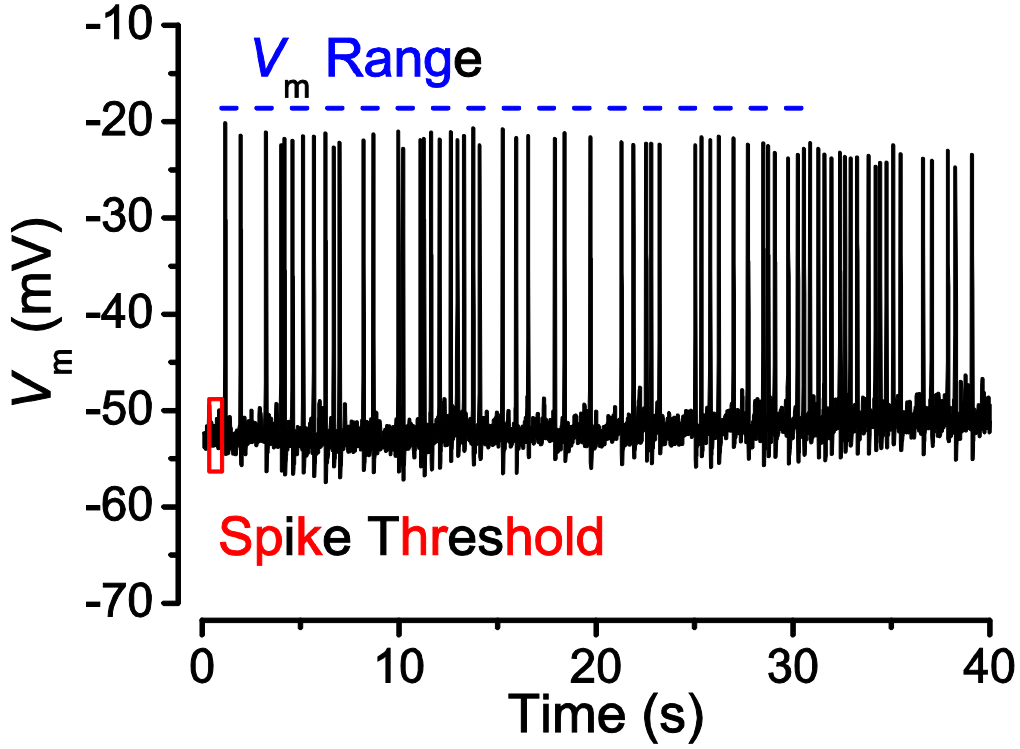

Figure 20: Example of a continuous recording from a spontaneously active IHC. The $V_{threshold}$ was taken closest to the first AP (indicated by the box). V_{rest} in this cell was equal to $V_{threshold}$. The action potential activity was analysed from the first spike up to the point, where the membrane potential depolarised by maximum 2.1 mV from the $V_{threshold}$. (indicated by the blue dashed line)

2.1.11. Data Analysis II – Voltage Clamp Recordings

In order to analyse the biophysical properties of the sodium current expressed in IHCs, it was essential to work on an isolated current. Immature IHCs express a large variety of ion channels, inward rectifying calcium and potassium, as well as several outward rectifying potassium currents (Platzer *et al.*, 2000; Marcotti *et al.*, 2003a; Kros, 2007). One possible approach, which was used in this thesis was to abolish sodium currents from the total current and then isolate it by subtraction from a control recording containing all currents (Standen *et al.*, 1994). In order to abolish the sodium current one can either use specific Na^+ channel blockers such as tetrodotoxin (Catterall, 1980) or substitute sodium in the

extracellular solution with the impermeable ion N-Methyl-D-glucamine ($NMDG^+$; Wooltorton *et al.*, 2007). Therefore, recordings were performed in the presence (E or TEA-4AP: see solutions, table 1) and absence (E-NMDG or TEA-4AP-NMDG) of sodium in the bath solution. To reduce possible contaminations from other currents, the solutions were designed to minimise the potassium currents. This was achieved by using Cs^+, which is a common K^+ channel blocker, as the main cation in the pipette filling solution (Standen *et al.*, 1994). Particular care was taken to make sure that R_s and C_m did not significantly change during the recordings in order to avoid an artefactual representation of the isolated sodium current.

The inactivation time constant ($\tau_{inactivation}$) of the sodium current was obtained by fitting the decaying current immediately after its peak with the following single exponential function:

$$\text{Equation 1:} \quad I_{Na} = A \exp((-x/\tau_{inactivation}) + y0)$$

where A is the current amplitude, x is the time and y0 is the offset of the trace. The range, at which the sodium current was fitted, was between the time point when the current declined to 90 % of the peak amplitude and 3 sec for body temperature and 5 sec for room temperature from the beginning of the voltage step (Figure 21). Time constants were obtained for voltage steps between nominal -10 mV and -50 mV. Because the actual membrane potential depends on the residual uncompensated R_s and the amplitude of total current, the final values for $\tau_{inactivation}$ were obtained by fitting the values from eqn. 1 for each IHC and extrapolate the $\tau_{inactivation}$ at fixed membrane potentials (in mV for P2 and P4: -40, -35, -30, -25, -20, -15 and for P0: -40, -30, -20, -15, -10).

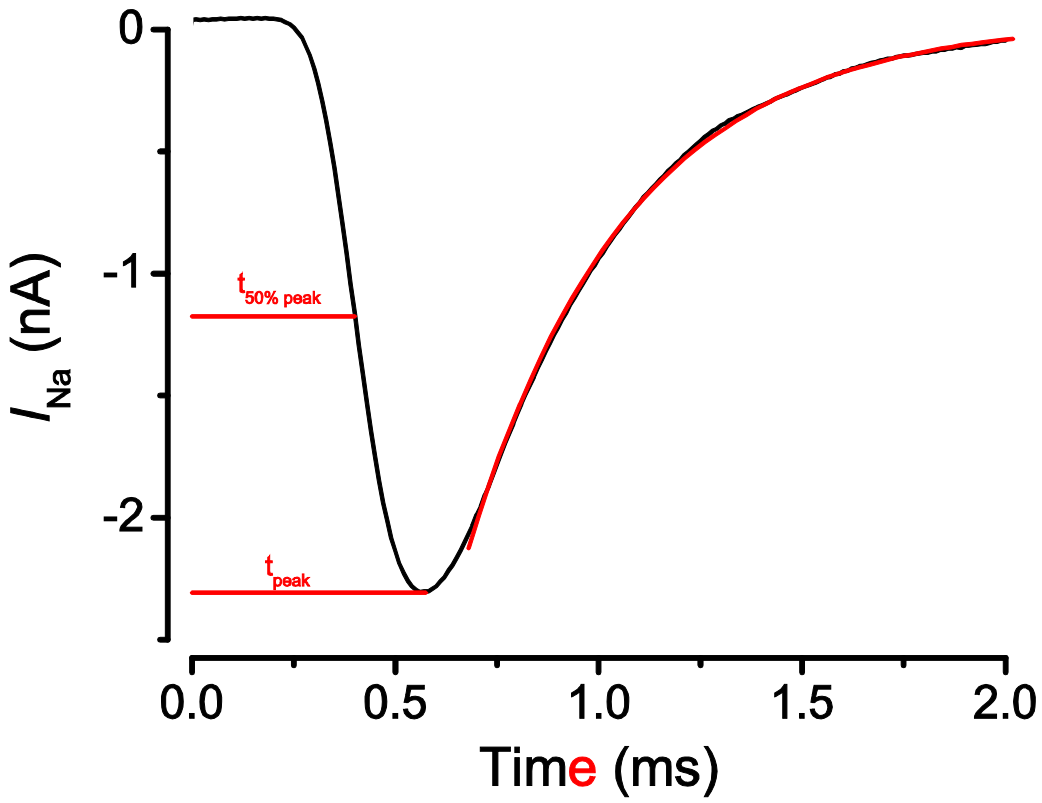

Figure 21: Analysis of a single step of the "Nacvc" protocol. The inactivation time constant was calculated from a fit between 90 % current after peak up to until 3 ms (body temperature) or 5ms (room temperature) after the voltage step started. $t_{50\% peak}$ and t_{peak} were analysed by measuring the time to peak and time to half peak from the onset of the voltage step. For clarity only the first 2 ms of the recording are shown. 0 ms indicates the start of the voltage step.

The speed of activation of the sodium current was measured by determining the time to peak (t_{peak}) and time to half-maximal activation ($t_{50\%\text{-}peak}$; Figure 21). Values were taken for depolarising voltage steps between nominal -10 mV to -45 mV. As described above, the membrane potential for the same voltage step slightly differed among cells due to the residual R_s. For statistical comparison values were grouped into 5 mV consecutive steps, with a bin size of +2.49 and -2.5 mV.

2.1.12. Statistical Analysis

Depending on the type of data two tailed Student's t-test or, for multiple comparison two way ANOVA followed by a Bonferroni posthoc test were used, unless otherwise stated. All averaged data in this thesis are shown with standard error (SEM).

2.2. *In Situ* Hybridisation

The molecular identity of the Na^+ channel expressed in rat IHCs is currently unknown. *In situ* hybridisation experiments were performed in order to determine which α subunits are expressed in immature IHCs. RNA probes for α subunit isoforms $Na_V1.1$, $Na_V1.2$, $Na_V1.3$, $Na_V1.6$ and $Na_V1.7$ were generated from vector DNA and used on cryosections from the immature rat cochleae to detect mRNA.

2.2.1. *In Situ* Hybridisation in general

In situ hybridisation is a method for detecting mRNA in tissue. It gives a snapshot of the expression of a specific gene at a certain time, which makes it a useful tool for developmental studies. The *in situ* hybridisation performed for this study uses colorimetric detection of mRNA in the cytoplasm. This mRNA needs to be specifically targeted with a RNA probe and following binding, the mRNA - RNA probe complex needs to be made visible. Specific probes for a certain mRNA can be complementary RNA strands, cDNA, double stranded DNA or oligonucleotides. Labelling can be performed by either a radiometric or chemical reaction, depending on the type of probe. Usually the detection of mRNA is visualised in the fixed tissue of interest (hence "*in situ*") and the *in situ* hybridisation itself comprises of three main steps: 1) hybridisation of mRNA with the RNA probe 2) several washing steps 3) colorimetric detection. *In situ* hybridisation is mainly performed on thin tissue sections of 10-20 µm, but is also possible on whole mounts.

For this study *in situ* hybridisation experiments were performed on cryosections from immature rat cochleae at the age of P3, which corresponds to the age range when the size of the sodium current is close to its maximum. Vectors containing the nucleotide sequence for generating RNA probes against $Na_V1.1$, $Na_V1.2$, $Na_V1.3$, $Na_V1.6$ and $Na_V1.7$ and the information for making RNA probes were obtained from Fukuoka *et al*., (2008).

2.2.2. RNA Probe Design and Vector Beneficiation

RNA probes were designed by Fukuoka *et al*., (2008) from dorsal root ganglion cells for $Na_V1.1$-1.3, $Na_V1.6$ and $Na_V1.7$. Briefly, Fukuoka Labs have extracted RNA from dorsal root ganglia and have transcribed it into cDNA by reverse transcriptase. cDNA containing the RNA probe sequence was then specifically amplified by using defined primers. Next, they have isolated the cDNA containing the probe sequence by gel electrophoresis and have cloned each probe sequence into pGEM T Easy Vectors (Figure 22; Promega, Southampton, UK). This vector contains a SP6 and T7 RNA polymerase promoter region and several restriction enzyme sites flanking a cloning site. The RNA probe sequence for each of the α subunits was cloned into this cloning site. The vector also contains an ampicillin resistance information which can be utilised to certify vector uptake by E-coli.

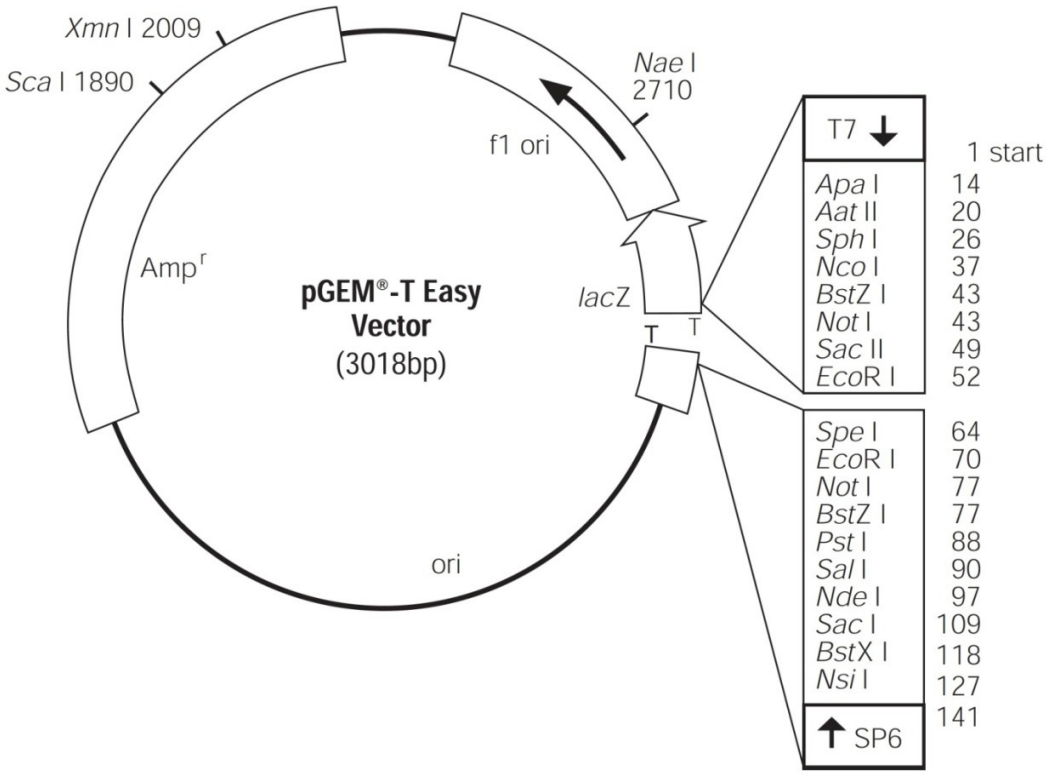

Figure 22: pGEM®-T Easy Vector. It contains a SP6 and T7 RNA polymerase promoter region as well as restriction sites that are recognised by Sal I and Sac II (amongst others) flanking a cloning site. Per vector one probe sequence for one of the Na_V α subunits was cloned into this site by Fukuoka *et al.* (2008). Amp^r is a sequence for ampicillin resistance that can be utilised to judge vector uptake by E-coli. Reproduced with permission from Promega Corporation.

About 60 µg of dried vector DNA for each RNA probe was sent to our lab (kindly provided by Fukuoka Labs, Department of Anatomy and Neuroscience, Hyogo College of Medicine, Hyogo, Japan) on filter paper and was reconstituted in purified water. Vectors were then introduced into electro competent E-coli cells (Invitrogen) using a small electric pulse supplied by a micropulser (MicroPulser – program "Eco1", Bio-Rad Laboratories GmbH, München, Germany). These bacteria were then streaked out onto agar plates containing ampicillin.

Due to the ampicillin resistance information of the pGEM vector only those bacteria could grow on the agar plate that had taken up the vector. After overnight growth, a single colony was picked using an Eppendorf pipette tip. This tip was briefly dipped into an aliquot of a PCR mix and a PCR was done. PCR parameters were: Initial 95°C for 3 min followed by 33 cycles of 95°C for 15 s (denaturation of DNA), 57°C for 15 s (annealing of primers) and 72°C for 45 s (elongation); the protocol was completed after a final elongation step of 72°C for 5 min. The PCR product was sent for sequencing (Eurofins MWG Synthesis GmbH, Ebersberg, Germany) to verify that no mutation had occurred within the RNA probe sequences. The Eppendorf pipette tip that still contained the majority of the bacterial colony was placed into a 5 ml standard lysogeny broth (LB) medium (Merck KGAA, Darmstadt, Germany) to allow the bacteria to grow over night. Thereby the concentration of vector DNA was also increased. Streaks within the LB medium indicated sufficient bacterial growth. As next step a QIAprep Miniprep (Quiagen) was performed on the bacterial culture in order to purify the vector DNA from the medium. Briefly, the MiniPrep comprised of the following main steps: 1) Centrifugation of the bacterial medium. 2) Use of three different buffer solutions to first resuspend the bacterial pellet, followed by lysis of the bacteria and finally precipitation of the DNA. 3) Several processing steps of centrifuging and washing lead to purified vector DNA in 10 mM Tris-HCl, with a pH of 8.5. This vector beneficiation leads to an increased DNA concentration sufficient for RNA probe synthesis. To ensure probe specificity the vector DNA was again sequenced after the Miniprep to make sure that no mutations occurred during bacterial growth.

2.2.3. RNA Probe Synthesis from Vector DNA

RNA probes were synthesised from the vectors and labelled with digoxigenin via *in vitro* transcription. For each target mRNA two probes were made. One probe containing the complementary nucleotide sequence is referred to as "antisense" probe. The other probe contained the same nucleotide sequence as the target mRNA and is referred to as "sense" probe. Only the antisense probe has the potential to bind to the target mRNA and produce a specific stain. The sense probe served as negative control and was run in each *in situ* hybridisation experiment to determine the general background staining arising from an unspecific stain. The generation of both sense and antisense RNA probes from one vector was possible because each Na_V gene sequence was inserted into the pGEM T-Easy vector in between polymerase transcription initiation sides and restriction enzyme cutting sequences (Figure 22). Depending on the orientation (5' to 3') of the Na_V gene inserted into the vector it was possible to produce either the antisense or sense probe with the T7 or SP6 promoter primers and the Sal I or Sac II restriction enzymes, respectively (Table 3).

Table 3: Promoter primer with respective restriction enzyme for synthesising either antisense or sense RNA probe.

Na_V Gene	Antisense RNA Probe		Sense RNA Probe	
Na_V 1.1	SP6	Sac II	T7	Sal I
Na_V 1.2	T7	Sal I	SP6	Sac II
Na_V 1.3	T7	Sal I	SP6	Sac II
Na_V 1.6	SP6	Sac II	T7	Sal I
Na_V 1.7	SP6	Sac II	T7	Sal I

The first step of the probe synthesis was the linearisation of the vector by the restriction enzyme cutting behind the Na_V gene sequence. This crucial step ensures that the polymerase, which starts to synthesise the probe from the other side, falls off the DNA strand behind the desired probe sequence. This ensures that the RNA probe only consists of the Na_V gene sequence, as without the restriction enzyme the polymerase would generate a RNA probe containing also pGEM T-Easy vector sequences. The linearisation of the vectors was done in an overnight digestion at 37°C in a linearisation mix consisting of

about 3 µg vector DNA, 1 µl restriction enzyme and 2 µl restriction enzyme buffer. Purified water was added until the volume of the mix was 20 µl. Following the digest, the DNA was extracted by phenol chloroform extraction, which consists of several washing steps with chloroform, phenol and isopentyl alcohol in order to remove enzymes resulting in the purified and linearised DNA. Next, the DNA is precipitated using ethanol at -70°C and further purified by an ethanol wash. The final DNA beneficiation removes the ethanol and possible chloroform contamination by air drying the DNA. Before probe synthesis, the DNA is re-suspended in DEPC treated water to limit contamination by RNAses. The final step of probe synthesis is the *in vitro* transcription. Therefor a mix containing, 2 µl digoxigenin labeling mix[3], 2 µl transcription buffer, 2 µl RNA-polymerase (T7 or SP6), 1 µg probe DNA and DEPC treated water added to reach a final volume of 20 µl was prepared and incubated at 37°C for 2 h. During these two hours the RNA polymerase synthesised digoxigenin labeled RNA probes. Another ethanol wash and precipitation of RNA at -80°C and re-suspension in DEPC treated water ensured the removal of redundant polymerase and buffer. In order to avoid RNA contamination and degradation, these steps were done with ice cold ethanol and under the utmost care. Finally, the re-suspended RNA probe was divided into 10 µl aliquots and stored at -80°C.

2.2.4. Preparation of Cryosections

Immature P3 rats were culled, their skull was cut in half in rostrocaudal direction and immediately fixed in 2 % paraformaldehyde in phosphate buffered saline (PBS; Oxoid LTD, Basingstoke, Hampshire, UK) for 2 h at 4°C. Following the fixation, the tissue was placed in increasing concentrations of sucrose. Sucrose concentration in PBS was 10 % and 20 %, each for 2 h and 30 % overnight (all sucrose steps were done at 4ºC). The next day the specimen was removed from the sucrose and carefully placed on a soft tissue in order to

[3] The digoxigenin labeling mix contains Uracil molecules, to which a digoxigenin molecule is covalently bound. These are built into the RNA strand during the RNA probe synthesis. During the *in situ* hybridisation protocol the digoxigenin is then targeted by antibodies (antibody-phosphatase), which is a required step for the labeling reaction (Mülhardt, 2008).

remove excess sucrose. It was then positioned in a small plastic chamber filled with embedding compound (Cryo-M-BED, Bright lnstrument Co Ltd, Huntingdon, UK). Special care was taken to always place the tissue in the same orientation. The chamber was then put into isopentane, which was cooled down by liquid nitrogen. The sudden temperature drop ensured that the tissue was still in the same orientation, when the embedding compound began to freeze into a solid block. This block was stored at -80°C.

In order to cut cryosections, the block was fixed in a cryostat with a microtome (Bright OTF 5000 and 5040 Microtome, Bright lnstrument Co Ltd, Huntingdon, UK; Figure 23). After that it was given enough time to slowly reach the temperature of the cryostat.

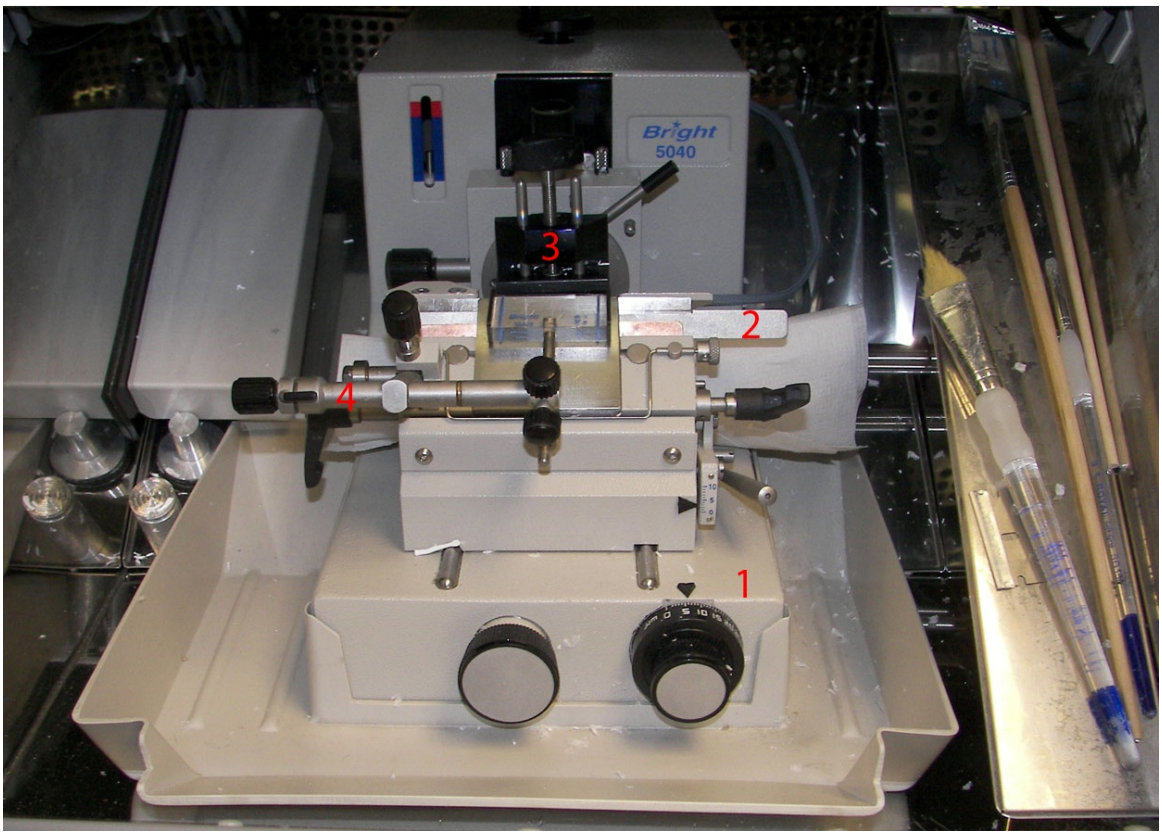

Figure 23: Microtome inside the cryostat. 1) Control screw setting the section thickness. 2) Blade holder. 3) Specimen holder. 4) Several screws and levers for setting blade angle, section angle etc.

Each time new cryosections were cut, a new blade was mounted in the microtome to limit contamination of slides with ribonucleases. After cutting the cochlea in the sagittal plane of the animal, cryosections were captured on an objective slide (Superfrost Plus, Gerhard Menzel GmbH, Braunschweig, Germany) and stored at -20°C. For *in situ* hybridisation experiments only cochleae from P3 were used.

2.2.5. Solutions used for *In Situ* Hybridisation

Before the RNA probes could be used on the cryosections, several solutions had to be prepared. Therefor all glassware was thoroughly rinsed and autoclaved prior to use and depending on solution the freshly made solution was autoclaved prior to use. Solutions for *in situ* hybridisation were made using the same purified water as for the electrophysiological solutions. The pH was adjusted with either HCl or NaOH.

2x Standard Saline Citrate (SSC)

300 mM NaCl and 30 mM Na-citrate. The pH was adjusted to 7. Prior to use this solution was autoclaved and diluted to 0.1x with autoclaved and purified water.

Tris-HCl

100 mM Tris-HCl and 150 mM NaCl. The pH was adjusted to 7.5. Prior to use this solution was autoclaved and 0.5 ml Tween20 was added per litre of solution.

Blocking Reagent

10 g of blocking reagent (Roche Diagnostics Ltd, Burgess Hill, UK) was diluted in 100 ml maleic acid solution, which consisted of 100 mM maleic acid, 150 mM NaCl at a pH of 7. It was then heated up in a microwave for even dissolving. The autoclaved blocking solution was stored in 1 ml aliquots at -20°C. Prior to use 30 µl Triton X-100 and 9 ml Tris-HCl (pH 7.0) were added to the blocking solution.

Antibody-phosphatase buffer

100 mM Tris-HCl and 100 mM NaCl. The pH was adjusted to 9.5. Prior to use this solution was autoclaved and 5 mM MgCl were added. The purpose of this solution is to create a slightly alkaline medium, which is needed for the substrate to work.

Substrate

Prior to use 35 µl BCIP (Sigma B-8503) and 34 µl NBT (Sigma N-6876) were added to 10 ml of antibody phosphate buffer. BCIP and NBT are chemicals used for the colorimetric detection of antibody phosphatase labelled molecules. When both are added to an alkaline buffer solution in presence of antibody phosphatase, they precipitate in form of a purple product.

Mowiol (Sigma-Aldrich Company Ltd., Gillingham, UK)

12 g Mowiol were added to 30 ml purified water. While stirring 60 ml Tris-HCl buffer (200 mM, pH 8.5) was added. Overnight incubation following 45 min at 90°C in a shaking water bath secured sufficient dilution results. After slowly cooling down to 50°C, 23.8 ml Glycerin were added and centrifuged for 15 min at 5000 g. The supernatant was distributed into 1 ml aliquots and stored at -20°C.

2.2.6. *In Situ* Hybridisation Protocol

The protocol for *in situ* hybridisation on fixed sections from P3 rat cochleae required between two and three days of work. On day one the tissue was prepared for overnight hybridisation at with the RNA probe. Day two consisted of several washing steps and antibody phosphatase treatment. Depending on the staining, the labelling reaction could be stopped on day two or three.

A sterile working space was crucial throughout the majority of the protocol in order to prevent contamination of the cryosections. Therefore, gloves were used for all procedures and all surfaces as well as fine tools were cleaned with 70 % ethanol. Cryosections were removed from -20°C and left on a bench until they reached room temperature. RNA probes were diluted 1:50 in hybridisation buffer (Amersham, Buckinghamshire, UK). To remove any excess proteins from prior RNA synthesis or early contamination, RNA probes were heated to 65°C and then immediately put on ice for 5 min to limit probe degradation. Every objective slide containing the cochlea sections was then treated with 50 µl RNA probe and carefully covered with a cover slip. Then the objective slides were incubated overnight in a hybridisation oven at -55°C. The signal to noise ratio was determined by comparing the nonspecific staining of the cryosections treated with the sense probe with the specific staining from those treated with the antisense probe. Ideally, no stain should occur in cryosections treated with the sense probe. To achieve this, a possible nonspecific staining from the sense probe can be reduced by increasing RNA probe dilution or hybridisation temperature.

After overnight hybridisation the objective slides with the cryosections were taken out of the oven and put carefully into 0.1x SSC. At room temperature the cover slips were removed and the objective slides were washed twice for 30 min at hybridisation temperature. Performing this step at hybridisation temperature secured removal of unbound RNA probes or probes bound to wrong targets. A last 10 min wash in Tris-HCl was done to change the pH and to prepare the sections for the antibody phosphatase treatment. Then 500-700 µl blocking reagent was put on top of each objective slide and the cryosections were incubated at room temperature for 30 min. Afterwards 50 µl anti digoxigenin-antibody-phosphatase 1:750 diluted in blocking solution (polyclonal antibody against digoxigenin; Roche Diagnostics Ltd, Burgess Hill, UK) per objective slide were used and

the cryosections were covered with a cover slip. Another incubation of 30 min at RT followed. During this time the anti-digoxigenin-antibody phosphatase bound to the digoxigenin labelled RNA probe. The cover slips were removed again and the objective slide was washed in Tris-HCl twice for 15 min to remove the excess anti digoxigenin antibody-phosphatase. The slides were rinsed once with antibody-phosphatase buffer before a field was drawn around the cryosections with a water repellent pen (Dako Delimiting Pen, Dako UK Ltd, Ely, UK). 500-800 µl of substrate was added and the objective slides were incubated at RT in a humid chamber to prevent the substrate from drying out. From now onwards the slides were checked for purple staining from the precipitated antibody RNA complex until the staining was found to be sufficient or until a weak staining could be observed in the sense probe. Then, the labelling reaction was stopped by washing the slides two to three times for 30 to 60 min in purified water. The cryosections were air dried and Mowiol (Sigma Aldrich Company Ltd., Gillingham, UK) and a cover slip were used to secure them. They were stored at -20˚C.

Pictures were taken on an Axioskop 2 MOT microscope with the following objectives 5x (Plan Neofluar, 5x / 0.15) 10x (Plan Neofluar, 10x / 0.30) and 20x (Plan Neofluar, 20x / 0.50; Carl Zeiss Ltd, Welwyn Garden City, UK). Background correction was done with Velocity (Velocity Software GmbH, Mannheim, Germany). Picture of antisense and sense probes were always treated in the same manner to not accidentally skew staining intensities.

3. Spontaneous Action Potential Activity in Inner Hair Cells

Chapter three solely deals with the action potential activity of immature IHCs. First, the results obtained during the course of this thesis are shown. Afterwards, they are discussed in conjunction with the currently available literature in order to understand their role and function, as well as their underlying ionic machinery.

3.1. Results I - Spontaneous Action Potential Activity in Rat Inner Hair Cells

The aim of this first result chapter is to describe the action potential activity recorded from rat IHCs between P2 and P12. Using mainly current clamp recordings, IHCs were spontaneously active during the first postnatal week. During the second postnatal week IHCs were still able to generate action potentials, when sufficiently depolarised. Upon the onset of hearing at around P12 IHCs were no longer able to generate repetitive action potentials. Action potentials in IHCs were dependent on extracellular calcium and their frequency, pattern and spiking threshold differed significantly between the apical and basal region of the cochlea.

3.1.1. IHCs are Spontaneously Active

To test whether action potentials in IHCs from the apical and basal coil occur spontaneously, current clamp recordings were performed. After obtaining whole cell configuration the patch clamp amplifier was set to current clamp mode and a continuous recording was started in order to monitor the IHC voltage responses. Because the main aim of these recordings was to test spontaneous activity, no current was injected into the cell (Figure 24). Voltage responses were recorded from 61 apical and 44 basal IHCs. Cells from both apical and basal coil displayed repetitive spontaneous action potentials. The width of an action potential recorded in whole cell current clamp mode revealed relatively broad action potentials (Figure 25).

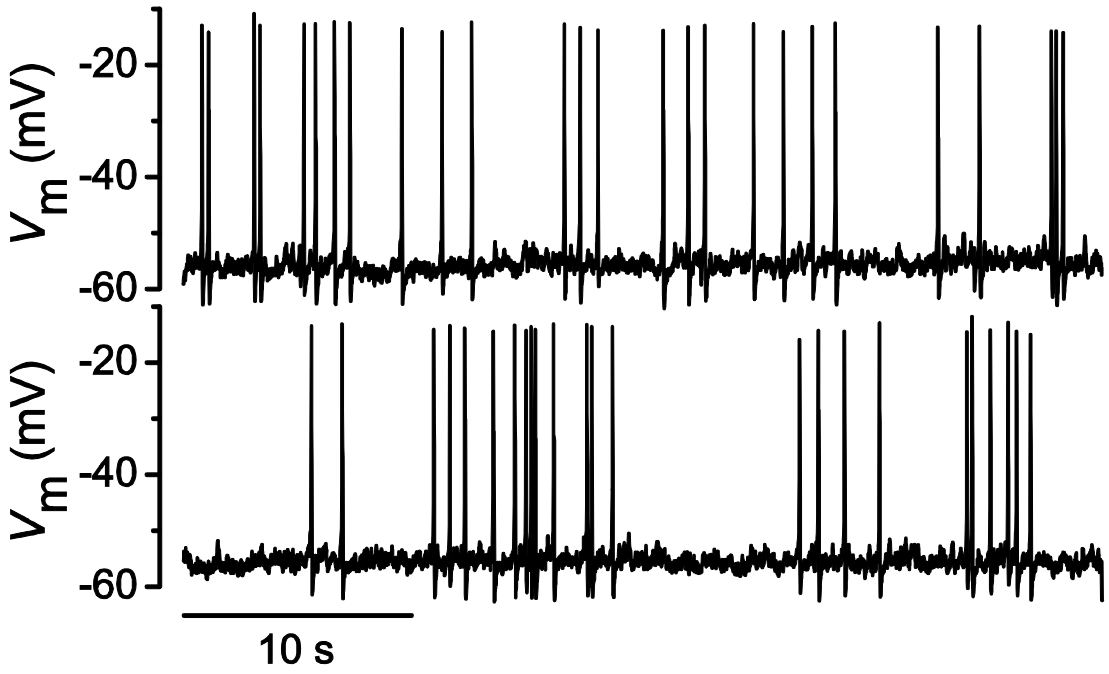

Figure 24: Continuous current clamp recording from a P3 basal IHC showing spontaneous action potential activity. The length of the recording shown is 40 s out of a total recording length of 10 min. Recording conditions were: C_m = 6.0 pF, R_s = 4.2 MΩ and g_{leak} = 3.0 nS.

In 3 apical and 3 basal IHCs during the continuous recording 0-Ca^{2+} solution was shortly perfused (for about 10 sec long). The removal of extracellular calcium lead to a cease of action potential activity. This effect was found to be reversible in both apical and basal IHCs, as action potential activity recovered after a washout with normal ECS (Figure 25 left).

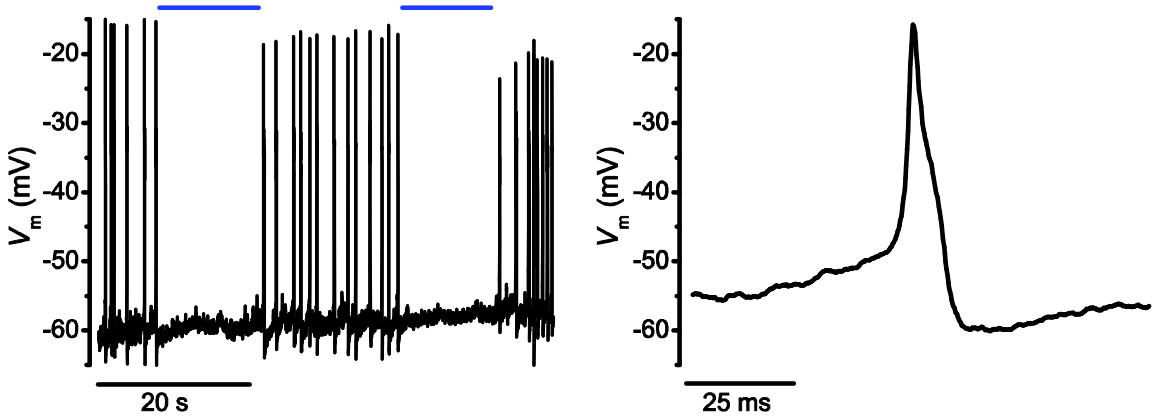

Figure 25: The action potential activity in rats was dependent on calcium in the extracellular solution. When IHCs were superfused with 0-Ca solution the action potential activity reversibly ceased. As soon as the 0-Ca solution was washed out with normal ECS, the action potential activity reappeared in the recording. The recording shown in A was from an IHC at P3, basal coil. The blue bars depict the time ranges, when 0-Ca was perfused. Enlarged view of a single action potential (right) from an IHC, P4 basal coil.

All P2 to P4 apical IHCs and P2 to P5 basal IHCs investigated were found to be spontaneously active. After that time period the overall number of spontaneous IHCs declined and from P9 onwards no spontaneously active cells could be observed (Figure 26).

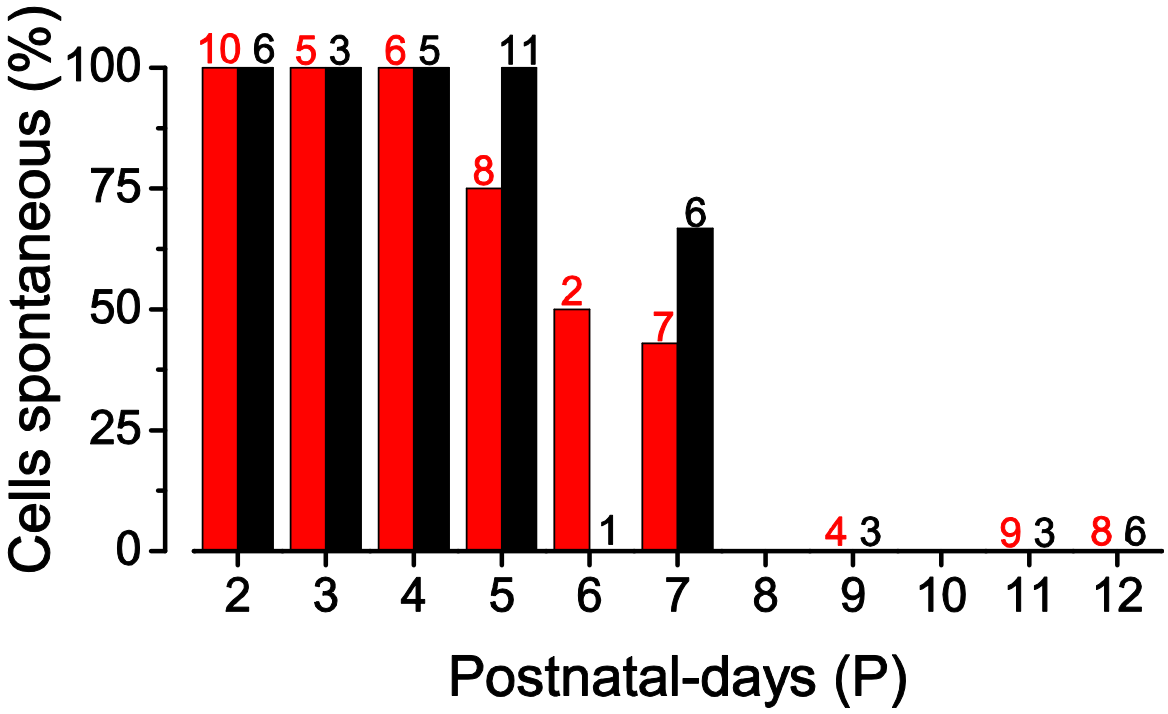

Figure 26: Apical (red) and basal IHCs (black) were found to be spontaneously active. Numbers on top of each column depict the number of IHCs recorded at a certain age. All cells were spontaneously active throughout P2 to P4. From P5 onwards the percentage of spontaneously active cells declined to the point at which no cells with spontaneous activity were found any more.

The resting membrane potential of apical IHCs was similar to that of basal cells (Table 4; two way ANOVA, $F = 0.03$, $df = 1$, $P = 0.86$). However, both in apical and basal IHCs the resting membrane potential became significantly more hyperpolarised with postnatal age (two way ANOVA, $F = 198.23$, $df = 2$, $P < 0.0001$).

Table 4: Resting membrane potential of rat IHCs as a function of age and cochlear position.

		Mean (in mV)	SEM (in mV)	N
P2-4	Apical	-55.2	0.97	8
P2-4	Basal	-55.7	0.41	14
P5-7	Apical	-53.0	1.49	10
P5-7	Basal	-55.7	0.96	18
P9-12	Apical	-77.6	1.88	14
P9-12	Basal	-74.9	1.51	11

3.1.2. Action Potential Activity of Inner Hair Cells depends on their Position along the organ of Corti

Action potentials from apical and basal IHCs were investigated in order to look for possible significant differences in the firing activity such as frequency and patterning. Basal IHCs generated action potentials more regular and with a higher frequency than apical cells. These regional differences were visible in whole cell current clamp recordings as well as in cell attached configuration.

In whole cell current clamp mode the longest and most stable recordings were performed from P4 apical and basal IHCs (Figure 27 A). From both cochlear turns five IHCs each were recorded with an overall recording time of 146.7 s with 186 action potentials in apical cells and 168.9 s with 412 action potentials in basal cells. The mean frequency of action potential activity was significantly different (two tailed t-test: $t = 2.791$, $df = 8$, $P = 0.0235$) with basal (3.5 ± 0.8 Hz, $n = 5$) being higher than apical (1.3 ± 0.2 Hz, $n = 5$). The peak to peak interspike interval (ISI) was 854.8 ± 124.1 ms for the apical and 379.7 ± 118.3 ms for basal IHCs and was found to be significantly different (Figure 27 B - D; two tailed t-test: $t = 2.772$, $df = 8$, $P = 0.0242$). However, the coefficient of variation in apical (0.97 ± 0.15) and basal (0.89 ± 0.11) IHCs did not differ significantly (two tailed t-test: $t = 0.47$, $df = 8$, $P = 0.6509$).

During each experiment current clamp recordings were complemented by voltage clamp measurements in order to test for the possible presence of I_{Na}. Because the main aim of these experiments was to investigate IHCs voltage responses, no channel blockers were used. For this reason the current recorded in voltage clamp mode was a mixture of all currents expressed in immature IHCs and allowed qualitative analysis only. However, the large and fast activation and rapid inactivation of I_{Na} could be easily distinguished from the slower and much smaller inward I_{Ca}. I_{Na} was present in all IHCs between P2 and P9. After P9 the reduced I_{Na} amplitude precluded its detection during this type of recordings (see next chapter for a more comprehensive study of I_{Na} in isolation).

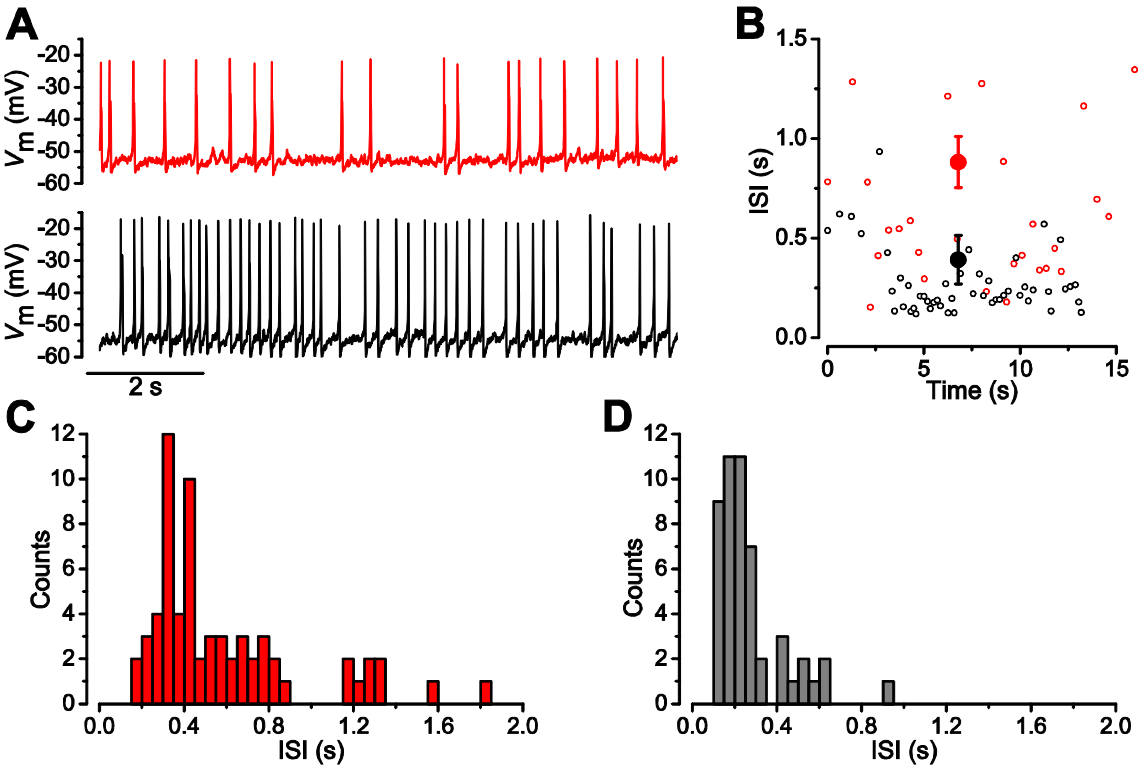

Figure 27: Whole cell current clamp recordings revealed different spike frequency and pattern between apical and basal IHCs. A, Continuous whole cell current clamp recording from apical coil (upper red trace) and basal coil (lower black trace) P4 IHCs. Both panels show a 10 s window out of 38.1 s (apical) and 14 s (basal) that were analysed for frequency and pattern. The apical IHC generated action potentials with a frequency of 1.73 Hz, had a V_m and spike threshold of -52.8 mV. The basal IHC generates action potentials with a frequency of 3.65 Hz. Its V_m and spike threshold is -56.1 mV. Recording conditions were: C_m = 8.9 pF, R_s = 3.28 MΩ, g_{leak} = 4.66 nS for the apical cell and C_m = 8.3 pF, R_s = 1.86 MΩ, g_{leak} = 4.3 nS for the basal cell. Both cells showed a fast activating and inactivating voltage dependent I_{Na}. B, Interspike interval (ISI) for the two recordings shown in A. The mean ISI of all apical (red filled circle with SEM) and basal cells (black filled circle with SEM) at P4 differ significantly with the apical ISI being larger. C and D, Histogram of the ISI from the same cells shown in A. Bin size was 50 ms.

Additionally to current clamp recordings, experiments in cell attached voltage clamp mode were performed. The latter recordings have the advantage that the cell membrane is not ruptured. This leaves the cell cytoplasm in its physiological state without cell dialysis and much longer recordings are possible (longest recording 40 min). Recordings in cell attached voltage clamp mode were performed from 5 apical and 3 basal cells between P1 and P6. During these recordings periodic capacitive currents with a larger negative current phase

followed by a smaller positive current phase were observed (Figure 28 A). These biphasic currents were identified as action potentials since: 1) they ceased when IHCs were perfused with 0-Ca^{2+} solution indicating calcium dependent action potentials; 2) they followed a similar time course as action potentials recorded in current clamp mode; 3) increasing the extracellular potassium concentration increased the frequency, while decreasing the amplitude of biphasic capacitive currents (Johnson *et al.*, 2011b).

Two examples of cell attached recordings are shown below (Figure 28 A and B) and were done from an apical P3 IHC and a basal P1 IHC. Total recording length was 40 min showing 1196 action potentials for the apical IHC and 2 min showing 172 action potentials in the basal IHC. The basal IHC generates action potentials with a frequency of 1.45 Hz, which is about three times higher than in the apical IHC (0.49 Hz). The interspike interval was determined by measuring the time between the occurrences of two action potentials and was plotted as a function of recording time (Figure 28 C and D). The mean apical interspike interval was 2.054 s ± 0.237s (n = 1195) with a coefficient of variance of 3.98. The mean interspike interval of the basal IHC was 0.688 s ± 0.031s (n = 171) with a coefficient of variance of 0.59. These data together with the interspike interval histograms (Figure 28 E and F) show, that the apical IHC generates action potentials burst like with long silent periods (maximum interspike interval: 159.6s) between individual spikes or bursts. On the contrary the basal IHC generates action potentials more regular with on average shorter interspike intervals (longest interspike interval: 2.5 s).

The cells recorded in cell attached mode were published in Johnson *et al*. (2011b), where also a comprehensive statistic analysis on spontaneous action potential activity in dependence of cochlear region was performed.

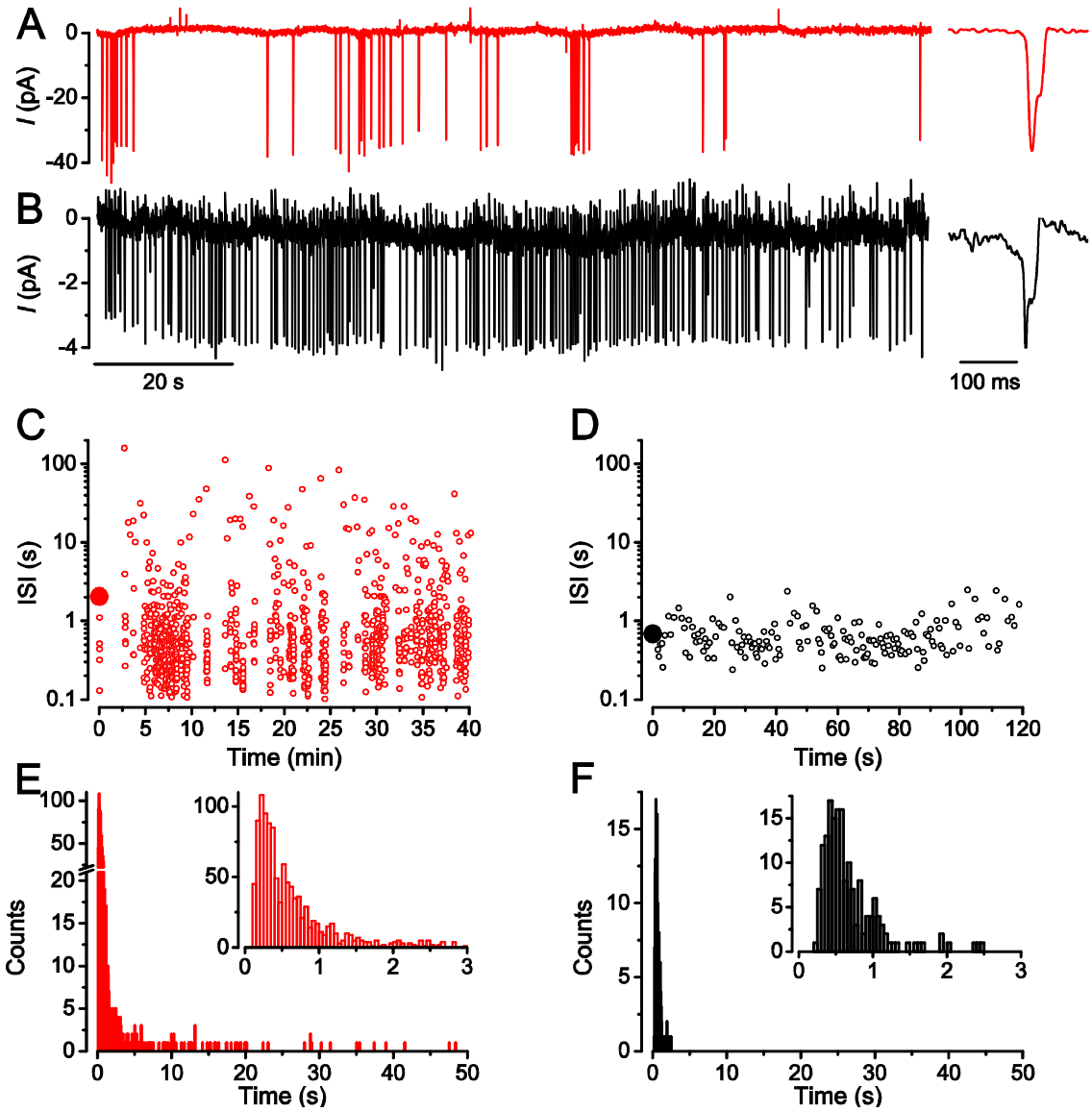

Figure 28: A and B, Example of a cell attached recording from a P3 apical coil (red) and a P1 basal coil (black) IHC. The downward peaks depict capacitive currents that occurred under the patch when a spontaneous action potential changed the membrane potential of the IHC. The insets on the right of each trace depict a scaled up version of a single action potential in cell attached mode. The shown length of the apical (total recording 40 min) and basal (total recording 2 min) traces is 2 min. A total of 1196 action potentials from the apical and 172 from the basal IHC were analysed. C and D, The interspike intervals (ISI) for the same cells as in A and B. The mean ISI (filled circles) was 2.054 s ± 0.237s (n = 1195) for the apical and 0.688 s ± 0.031s (n = 171) for the basal cell. Open circles show individual values. E and F, Histogram of the ISI from the same cells as in A and B. The ISI showed a stronger skewed histogram for the apical IHC as a result of the action potential pattern with longer pauses in action potential activity in between the bursts. Bin size was 50 ms. Insets depict a scaled up window of the first 3 s of the histogram. The maximum ISI was 160 s for the apical cell (not shown for clarity of the histogram) and 2.5 s for the basal cell.

3.1.3. Inner Hair Cells Retain the Ability to Generate Action Potentials throughout the Second Postnatal Week

IHCs that did not exhibit spontaneous activity were tested for their ability to generate action potentials following injection of depolarising currents. Both apical and basal IHCs were able to respond to current injections with repetitive action potentials between P7 and P11 (Figure 29).

A qualitative analysis was made by categorising IHCs depending on their response to current injections (Table 5). In category 1 (repetitive) were all cells that responded to current injections with repetitive action potentials. Category 2 (single action potential) composed of all cells that were no longer able to generate trains of action potentials, but did fire a single action potential at the onset of the current injection. IHCs that were no longer able to generate action potentials, even with 1 nA current injections, were categorised into the third group (no action potentials).

Table 5: Qualitative analysis of induced action potentials. Apical coil IHCs seem to preserve their ability to generate action potentials (APs) slightly longer. Ac = apical IHCs, Bc = basal IHCs. Repetitive: trains of APs could be elicited. Single AP: only an initial single AP could be generated. No AP: even with high current injections of 1 nA no AP was generated by the cell.

Postnatal Day	Apical repetitive	Apical single AP	Apical no AP	Basal repetitive	Basal single AP	Basal no AP
P7	4	0	0	2	0	0
P9	3	1	0	3	0	0
P11	2	5	2	1	2	0
P12	0	4	4	0	0	6

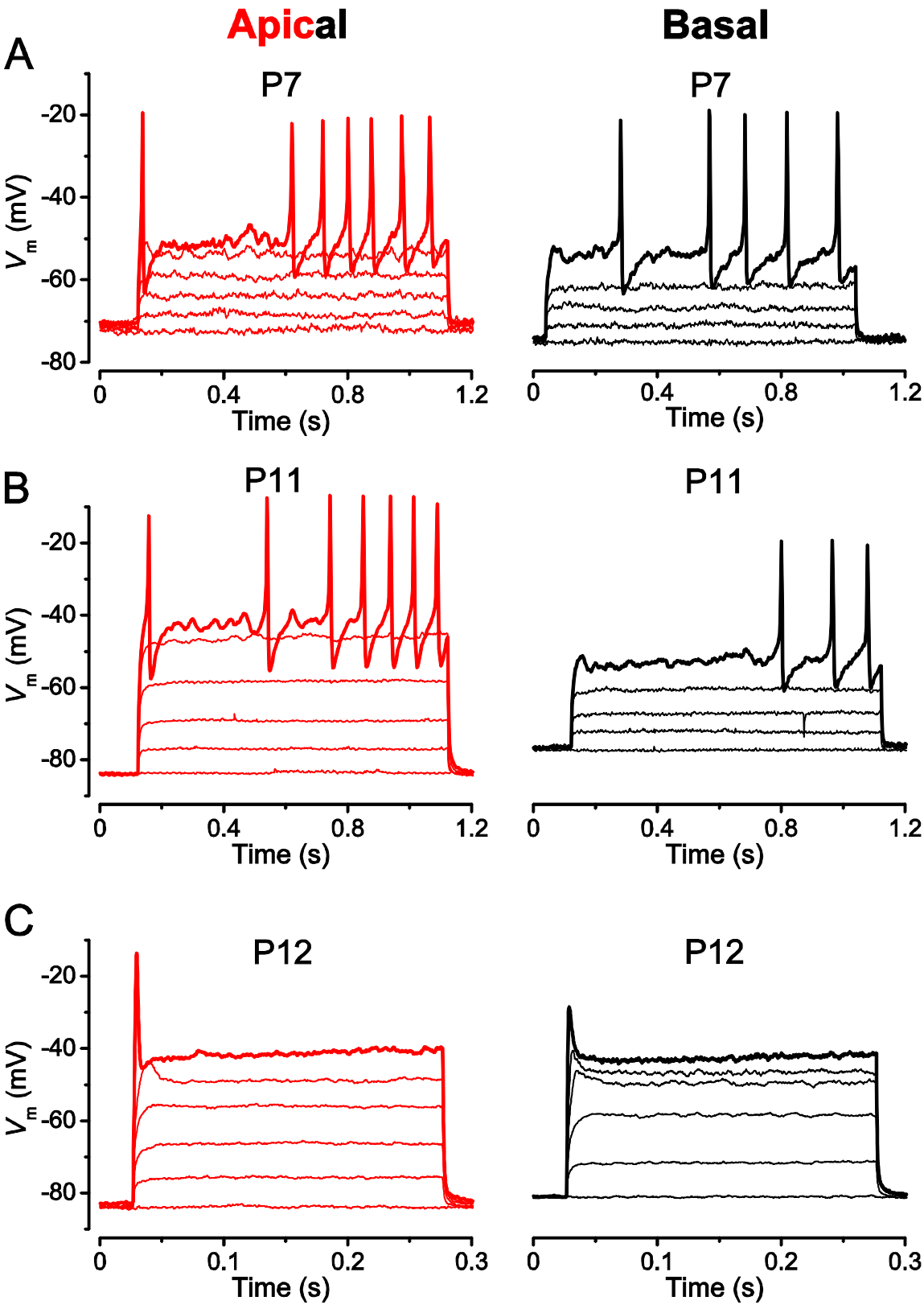
Apical
Basal
A
P7
P7
B
P11
P11
C
P12
P12
-20
-40
-60
-80
V_m (mV)
0
0.4
0.8
1.2
0.1
0.2
0.3
Time (s)

Figure 29: Example of voltage responses during current injections in non spontaneous IHCs at different ages. Red traces are recordings from apical IHCs and black traces from basal IHCs. A, 100 pA (apical) and 80 pA (basal) were needed in these example P7 rat IHCs in order to trigger repetitive action potential activity. The $V_{threshold}$ was -50.9 mV for apical and -54.0 mV for basal IHCs. B, Example of action potentials at P11 during 180 pA current injection in an apical and 160 pA in a basal IHC. $V_{threshold}$ was on average -46.0 mV and -49.9 mV for apical and basal IHCs, respectively. C, None of the cells recorded on P12 were able to generate repetitive action potentials. For clarity only every second trace is shown in A (in pA: 0, 20, 40, 60, 80 in apical and basal IHC and 100 only in the apical IHC) and B (in pA: 0, 40, 80, 120, 160 in both apical and basal IHC and 180 in apical IHC). In C the traces shown for both the apical and basal IHC depict the following current injection in pA: 100, 200, 300, 400 and 800.

At P7 both apical and basal IHCs showed repetitive action potentials during current injections between 20 and 100 pA. At P9 all basal IHCs were still responding with trains of action potentials to current injections between 40 and 160 pA, whereas only three out of four apical cells were categorised as repetitive. At P11 between 80 and 180 pA were needed to trigger action potentials. At this age, two out of nine apical and one out of three basal IHCs showed repetitive action potential activity. Five out of nine apical and the remaining two out of three basal cells only generated a single initial action potential. The remaining two apical IHCs did not show any action potentials to current injections. At P12, around the onset of hearing, none of the basal IHCs responded with action potentials even with 1 nA current injection. Only a small initial depolarising hump, which did not have the characteristic shape of an action potential, could be observed in these cells. Four out of eight apical IHCs showed an initial action potential, but no repetitive spike generation was observed.

3.1.4. Spiking Threshold Depends on the Position of the Inner Hair Cell along the Cochlea

In 44 apical and 46 basal IHCs the membrane potential at which the first train of action potentials was generated was evaluated (Figure 30). IHCs from the basal coil started to generate action potentials from more hyperpolarised membrane potentials than apical IHCs (ANOVA effect of cochlear region: $F = 19.95$, $df = 1$, $P < 0.0001$ and effect of postnatal age: $F = 4.422$, $df = 4$, $P < 0.0042$). The statistical analysis was done only for

spontaneously active cells, because the $V_{threshold}$ could be evaluated with a higher precision. However, when the $V_{threshold}$ was evaluated from current injections in P9 and P11 IHCs, basal cells still generated action potentials at more hyperpolarised membrane potentials than apical cells.

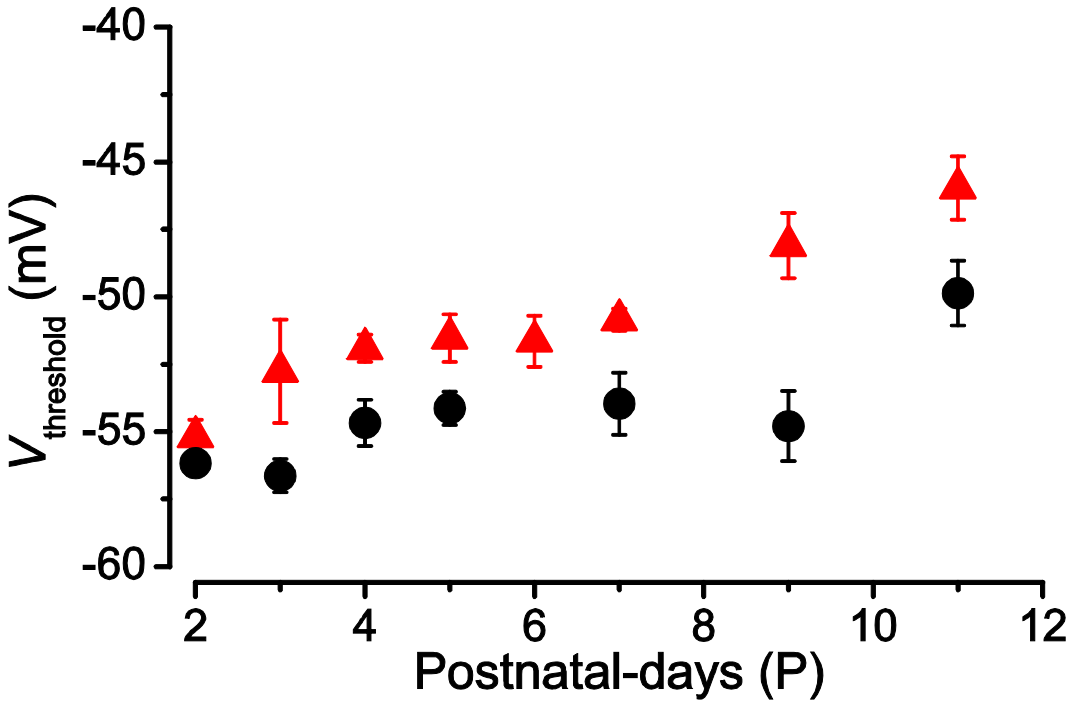

Figure 30: Mean $V_{threshold}$ as a function of age and cochlear region. Basal IHCs (black) started to generate action potentials at more hyperpolarised membrane potentials than apical IHCs (red). On P9 and P11 all IHCs had to be injected with current in order to obtain the $V_{threshold}$. As a result, the $V_{threshold}$ detection was less accurate.

This chapter shows that IHCs were capable to generate spontaneous calcium dependent action potentials throughout the first postnatal week. Frequency and pattern of this spontaneous activity was significantly dependent on cochlear region. After the first postnatal week the membrane potential of the cells became more hyperpolarised and IHCs stopped being spontaneously active. However, the ability to fire repetitive action potentials was preserved until around the onset of hearing.

3.2. Discussion I - Spontaneous Action Potential Activity in Inner Hair Cells

The first aim of this thesis was to characterise the spontaneous action potential activity in immature rat IHCs as a function of age and cochlear position. In order to achieve this, whole cell current clamp recordings were performed on P2 to P12 IHCs. Additionally, recordings were done in cell attached mode between P1 and P6. The results of this study show that IHCs are spontaneously active at P1 and that this spontaneous activity ceases after the first postnatal week. IHCs retain their ability to generate action potentials until just before the onset of hearing at P12. Furthermore, current clamp and cell attached recordings point out a gradient in the pattern and frequency of the spontaneous action potential activity between apical and basal IHCs. Altogether the data presented here are the first comprehensive description of the spontaneous action potential activity in IHCs of the rat. Parts of this study have been included in a recently published paper (Johnson *et al.*, 2011b).

3.2.1. Do IHCs spontaneously generate Action Potentials?

Prior to the start of this study it was hypothesised that IHCs are generally too hyperpolarised to generate action potentials spontaneously (Tritsch *et al.*, 2007). By observing waves of ATP released by supporting cells of the Koelliker's organ, which cause depolarisation of nearby IHCs via the activation of P2X receptors, it was hypothesised that the action potentials in IHCs are caused by ATP. This mechanism was very attractive since it allowed IHCs in close proximity to generate correlated action potentials, similar to calcium waves in the retina. However, Tritsch and colleagues used rather unphysiological solutions, which has been shown to hyperpolarise IHCs in an artefactual way (Johnson *et al.*, 2011b). Under the experimental conditions where a perilymph like extracellular solution and a physiological intracellular solution was used, the IHC resting membrane potential was found to be very close to the spiking threshold (Glowatzki & Fuchs, 2002; Marcotti *et al.*, 2003b; Brandt *et al.*, 2007). Furthermore, in Tritsch *et al.* (2007) a higher

and less physiological calcium buffer concentration of 10 mM EGTA was used to study the action potential activity. This has been shown to uncouple the SK2 channels from the P2X receptors and thus skewing the interpretation of the role of ATP (Johnson *et al.*, 2011b). Therefore IHCs appeared to be only generating action potentials, when sufficiently depolarised by ATP (Tritsch *et al.* 2007). To the contrary, when physiological solutions with low EGTA concentrations (1.3 mM) were used and recordings were performed at body temperature, then IHCs appeared to be spontaneously active (this study; Marcotti *et al*. 2003b, Johnson *et al.* 2011b).

3.2.2. Inner Hair Cells are Spontaneously Active during the First Postnatal Week

Rat IHCs were spontaneously active in animals as young as P1, the earliest time point studied in this work. This finding is comparable to another developmental study, where rat IHCs were electrically active at P3 (Brandt *et al.*, 2007). However, it is very likely that spontaneous action potential activity in rat IHCs is already present from prenatal developmental ages, as indicated from studies in mice, which have a similar developmental time course. Mouse IHCs are spontaneously active as early as E17.5, although at that time action potentials show a wider shape indicating that the functional machinery generating action potentials is not fully developed until about birth (Marcotti *et al.*, 2003a; Marcotti *et al.*, 2003b). After the first postnatal week, the proportion of spontaneously active IHCs declines (Figure 26), which is in line with the literature available on rats, mice and gerbils (Marcotti *et al.*, 2003b; Johnson *et al.*, 2011b). This cessation of spontaneous activity after the first postnatal week is surprising, as the onset of hearing does not occur until about five days later (Figure 29 and Marcotti *et al*., 2003b). A possible explanation for the loss of spontaneous activity is likely to be the resting membrane potential, which becomes successively more hyperpolarised (Table 4, Marcotti *et al*., 2003a) due to the upregulation of both the inward rectifier and the delayed outward rectifier potassium currents (Fuchs & Evans, 1990; Marcotti *et al.*, 1999; Marcotti *et al.*, 2003a).

After the first postnatal week IHCs are no longer spontaneously generating action potentials, thus one could hypothesise that they lose the capability to generate spikes at all. However, rat IHCs retained the capability to generate spikes during the second postnatal week (Figure 29). These experiments consolidate previous findings (Marcotti *et al.*, 2003b; Brandt *et al.*, 2007) indicating that IHCs maintain the ionic currents needed for action potential generation until shortly before the onset of hearing, whereupon the ability to spike is lost (Kros *et al.*, 1998; Marcotti *et al.*, 1999). The most likely explanation for the loss of action potential discharge is a change in the expression pattern of ionic currents with the downregulation of the "transiently expressed" and up regulation of the "late onset" ionic currents.

One important question is: what could be the biological reason for the loss of spontaneous activity about a week before the onset of hearing and not contemporaneously with it? One hypothesis could be that spontaneous action potentials are only essential during a critical period in the first postnatal week. Evidence for this hypothesis is given by morphological studies in which the neuronal loss in the nucleus cochlearis was investigated after deafferentiation by removal of the cochlea or tetrodotoxin block of the eighth nerve. It was found that in the second postnatal week deafferentiation lead to a smaller loss of neurons than in the first week after birth (Tierney *et al.*, 1997; Mostafapour *et al.*, 2000). Moreover, it is not certain that the spontaneous activity ceases *in vivo* at the same time as under the experimental conditions used in this study since during dissection it is impossible to leave the delicate separation of the endolymph and perilymph intact. The immediate effect of this is that stereocilia are bathed in perilymph like solution, which has a much higher calcium concentration. The consequence of this was shown in cochlear hair cells, where the mechanoelectrical transducer current was studied (Johnson *et al.*, 2011a). The unphysiologically high calcium concentration at the stereocilia leads to a reduced mechanoelectrical transducer current (Mammano *et al.*, 2007; Johnson *et al.*, 2011a). Due to the low calcium in the endolymph *in vivo*, more mechanoelectrical transducer channels are open at rest (Beurg *et al.*, 2006) and thereby lead to a larger depolarising influx of cations. This current, which has been previously referred to as a possible “noise source” (Kros *et al.*, 1998), might influence the membrane potential and counteract the hyperpolarising effect of the inward rectifying potassium current. As a result IHCs might

not be as hyperpolarised *in vivo* as under the experimental conditions and thus still be able to produce spontaneous action potentials.

3.2.3. Role of Action Potential Activity in Inner Hair Cell Development

One of the key questions in auditory research to date is: how could spontaneous activity affect the development of IHCs? By perfusion of extracellular solution lacking calcium it was shown that action potentials in mouse IHCs depend on calcium (Marcotti *et al.*, 2003b), which contrasts the sodium driven action potentials in neurons. This study confirms that rat IHCs also show calcium dependent action potentials. The periodic calcium influx, mediated by $Ca_V1.3$ channels (Platzer *et al.*, 2000; Brandt *et al.*, 2003) leads to a transient intracellular rise of the calcium concentration depending on frequency and pattern of the action potential activity. A transient rise of the intracellular calcium concentration was previously reported in several spontaneously active systems during development, such as the retina or dorsal root ganglion cells (Moody & Bosma, 2005). Transient changes in the calcium concentration displays a very potent second messenger function that is known to be involved in changes in gene transcription (Carafoli *et al.*, 2001; Moody & Bosma, 2005). By influencing gene transcription, calcium dependent action potentials could control intrinsic developmental programmes. The second messenger function of calcium can be very complex in nature, encompassing many different signalling pathways and downstream factors (Deisseroth *et al.*, 2003) that transfer the calcium signal to the nucleus. Briefly, one such mechanism of transfer could be initiated by calmodulin, a calcium binding protein that activates kinases. Several kinases translocate the signal to the nucleus were they activate calcium/calmodulin dependent protein kinase IV, which rapidly activates cyclic-AMP-response-element-binding-protein (West *et al.*, 2002; Deisseroth *et al.*, 2003). This transcription factor binds to genes that contain a cyclic-AMP-response-element prior to the genes sequence. Via this pathway it has been shown that both gene activation or inhibition can be facilitated by calcium fluctuations (West *et al.*, 2002).

It has been shown that the way in which the cell responds to an increased intracellular calcium concentration depends on a variety of factors, such as amplitude, frequency and spatiotemporal occurrence of the calcium entry (Buonanno & Fields, 1999; Moody & Bosma, 2005). In IHCs the frequency and pattern of spontaneous activity and therefore also the amplitude and spatiotemporal distribution of calcium entry was shown to depend on cochlear region (Figure 28 and Johnson *et al*., 2011). One could not only hypothesise that gene transcription is modulated by the spontaneous activity, but also that gradients in this modulation are likely to exist along the tonotopic axis of the cochlea. Unfortunately, to date there is no scientific evidence that would prove or disprove such a hypothesis. One experimental approach would probably be to change the action potential activity by modulating or influencing underlying ionic currents other than the calcium current and then investigate possible effects on gene transcription. A feasible way to change action potential activity could involve the insertion of a channel that is usually not present in hair cells and that does not interfere with normal interactions between channels (e.g. calcium influx and SK channel activation; Howorth *et al.*, 2009).

3.2.4. Could the Spontaneous Activity of IHCs have an Effect on the Development of the Auditory Pathway?

In order to be able to affect the auditory system during development, the information contained in the pattern or frequency of the IHC action potentials needs to be transferred to other cells. Action potential activity in immature IHCs causes a rise in the intracellular calcium concentration, which is sufficient to trigger exocytosis of the neurotransmitter glutamate as early as P0 (Beutner & Moser, 2001). This glutamate release is recognised by AMPA receptors in the postsynaptic membrane (Glowatzki & Fuchs, 2002; Ruel *et al.*, 2007). Furthermore, an increase of the extracellular potassium concentration results in a comparable increase in the frequency of IHC action potentials and excitatory postsynaptic currents (EPSCs) at afferent boutons (Glowatzki & Fuchs, 2002). In this study it was further shown that the amplitude of these EPSCs is large enough to trigger action potentials

within the spiral ganglion neurons. Concluding these findings, it seems likely that action potential activity generated by IHCs affects the auditory pathway during development. In fact, it supports the hypothesis that IHCs might have pacemaking capabilities and that the pattern of IHCs spontaneous electric activity is preserved within the auditory pathway. It was indeed shown that the spiking pattern of IHCs shares similar features with the electric activity of spiral ganglion neurons (Tritsch & Bergles, 2010) and neurons from the medial nucleus of the trapezoid body (Tritsch *et al.*, 2010).

The tonotopic organisation of the auditory periphery is preserved throughout the auditory pathway leading to a spatially organised representation and computation of sound stimuli not only in the cochlea, but also in the brain. However, only very little is known about how this magnificent structural organisation is established during maturation (Kandler *et al.*, 2009). Evidence shows that early crude connections between spiral ganglion neurons and their targets in the cochlea and cochlear nucleus undergo an extensive refinement. However, the mechanism by which this reorganisation is controlled remains unknown (Pujol *et al.*, 1998; Rubel & Fritzsch, 2002). In the visual system, the spontaneous electric activity was identified as a mechanism to instruct retinotopic map formation (Penn & Shatz, 1999; Moody & Bosma, 2005). When spontaneous activity was disrupted or modulated, the topographic maps within the brain could not form normally (Penn & Shatz, 1999; Stellwagen & Shatz, 2002; Moody & Bosma, 2005). Therefore, it seems reasonable to consider that the spontaneous activity generated by IHCs controls the pruning of spiral ganglion fibres and instructs the refinement of synaptic connections within brain nuclei.

Whole cell current clamp recordings together with cell attached voltage clamp recordings (carried out in this study together with Johnson *et al.,* 2011b) have revealed that IHCs are able to generate spontaneous action potentials, whose pattern and frequency depends on the cell location along the longitudinal axis of the cochlea. Apical IHCs were found to generate action potentials more burst-like and at a lower frequency than basal IHCs, in which spiking was more sustained (Figure 27 and 28). This defined IHC firing pattern could represent a place-code that is most likely transmitted by the afferent fibres to the developing nuclei of the brain. Thereby spontaneous IHC action potentials could have a

pacemaking effect instructing the reorganisation of neuronal networks and the refinement of tonotopic maps.

3.2.5. Spontaneous Action Potential Activity is modulated by several Mechanisms

The aim of this paragraph is to discuss the physiological mechanisms that underlie the significant differences in spiking behaviour between apical and basal IHCs. Therefore, it seems important to look at the ionic machinery that drives and modulates action potential activity in IHCs. The major ionic current that drives spontaneous action potential activity in IHCs is carried by $Ca_V1.3$ Ca^{2+} channels (Figure 25; Platzer *et al.*, 2000; Marcotti *et al.*, 2003b). The calcium current shows a steep voltage dependence and it seems likely that even small changes of the resting membrane potential have a strong influence on action potential activity. Indeed, it could be shown that the frequency of action potentials increases when injecting depolarising currents (Brandt *et al.*, 2007; Johnson *et al.*, 2011b). These findings suggest that patterning of spontaneous action potential activity is influenced by channels or molecules that are able to modulate the resting membrane potential. Over the past years, ATP and actelycholine (ACh) have been identified as possible modulators of the IHCs resting membrane potential (Figure 31; Glowatzki & Fuchs, 2000; Tritsch *et al.*, 2007; Johnson *et al.*, 2011b).

ACh exerts its action on IHCs through efferent nerve fibres originating from the superior olivary nucleus that transiently contact IHCs during immaturity (Simmons, 2002). They release ACh, thereby activating α9α10 heteromeric nicotinic acetylcholine receptors in the basolateral membrane of the IHCs (Elgoyhen *et al.*, 1994; Elgoyhen *et al.*, 2001). First synaptic events were found in P1 IHCs indicating that efferents make contact to IHCs soon after birth (Roux *et al.*, 2011).

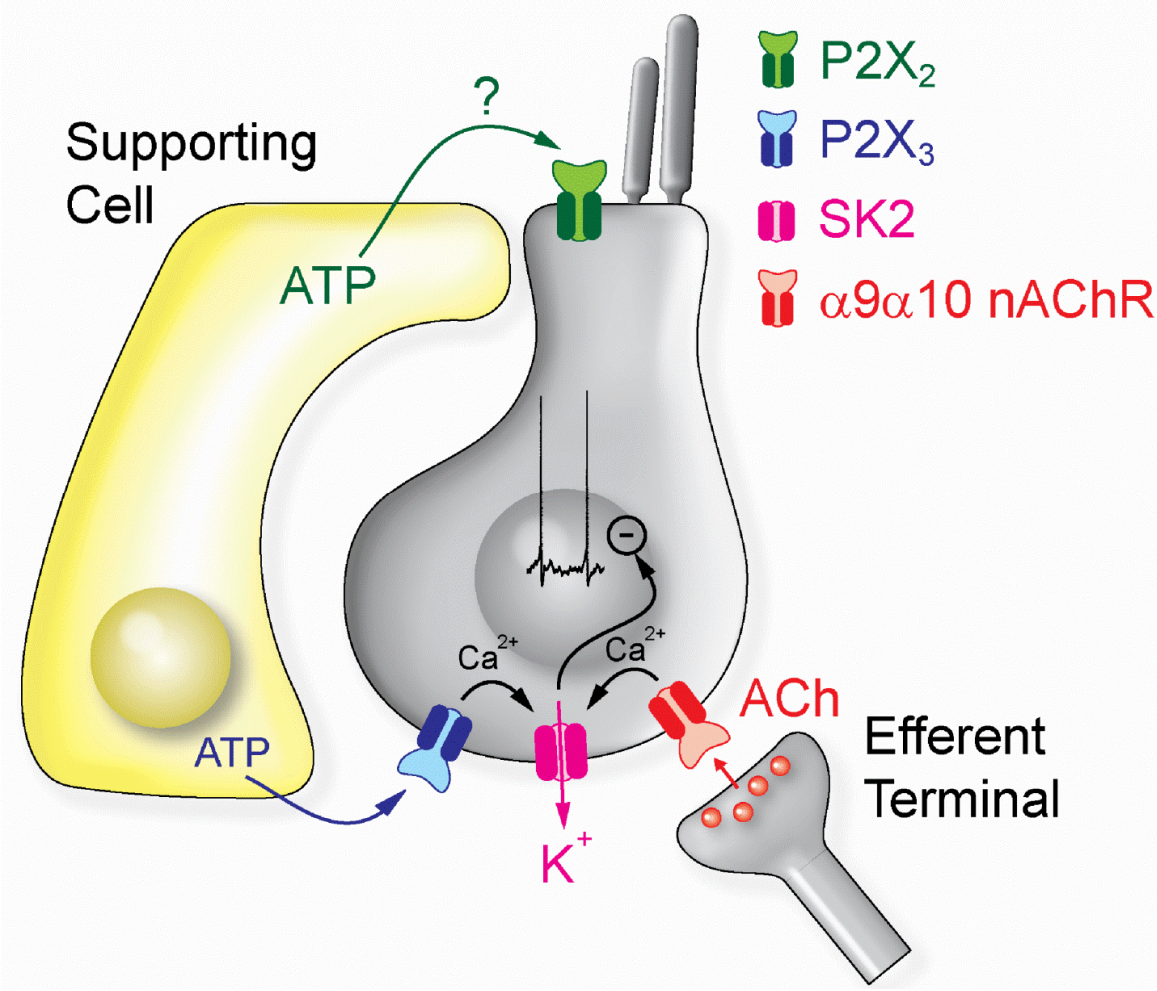

Figure 31: Modulation of IHC spiking behaviour via ATP and ACh. Efferent release of ACh activates α9α10 nicotinic acetylcholine receptors (nAChR), which leads to the hyperpolarisation of the IHCs membrane potential through calcium influx and activation of colocalised SK2 channels. ATP is released by supporting cells forming the Koelliker's Organ. Depending on ATP concentration this de- or hyperpolarises the IHCs (see text for details; Picture with courtesy from Johnson *et al*. 2011b).

The immediate effect of ACh is an influx of cations such as calcium through nicotinic acetylcholine receptors (Weisstaub *et al.*, 2002; Gomez-Casati *et al.*, 2005). This ACh mediated calcium influx leads to the activation of SK2 channels (Glowatzki & Fuchs, 2000), which are clustered with the acetylcholine receptors (Roux *et al.*, 2011) ultimately leading to a hyperpolarisation (Liegeois *et al.*, 2003). Superfusion of apical IHCs with strychnine, a specific blocker of α9α10 nicotinic acetylcholine receptors leads to a slight depolarisation due to cessation of SK2 channel activity, which results in a change of the

spiking behaviour from burst like, to more sustained higher firing frequency resembling the activity of basal IHCs (Johnson *et al.*, 2011b). In that study, the effect of strychnine was more pronounced in apical than in basal IHCs, and it was shown that it is most likely related to a higher ACh release by the efferent system in the apical coil, rather than a higher amount of ACh receptors or SK2 channels. However, the magnitude and temporal properties of efferent ACh release *in vivo* remain unclear; is it for example a continuous release or does it appear in waves and how is it controlled?

ATP responses are mediated via P2X receptors in the spontaneously active IHCs (Housley *et al.*, 2006). As described in the introduction, the action of ATP mediated responses in IHCs displays a more complex behaviour as it can be both depolarising as well as hyperpolarising (Johnson *et al.*, 2011b). These two antagonising effects are likely to be caused by two different P2X receptor isoforms, which express different sensitivities to ATP (North & Surprenant, 2000; Johnson *et al.*, 2011b). Low concentrations of ATP in the nanomolar range are likely to trigger the activation of $P2X_3$ receptors that are colocalised with SK2 channels. The calcium influx through these receptors causes a slight hyperpolarisation, via the activation of SK2 channels, very much like the effect of ACh described above (Johnson *et al.*, 2011b). Higher concentrations of ATP in the micromolar range are likely to activate $P2X_2$ receptors that are thought to be localised towards the apex of IHCs (Housley *et al.*, 2006). These receptors mediate a larger inward cation current, possibly due to their sheer number, that cause IHC depolarisation (Tritsch *et al.*, 2007).

Furthermore, the data presented in this thesis show that basal IHCs were able to generate action potentials at more hyperpolarised potentials than apical IHCs (Figure 30). On average, this difference in the spiking threshold showed that in order to generate action potentials apical IHCs had to be more depolarised than basal IHCs. Although only one Ca^{2+} channel α subunit isoform ($Ca_V1.3$) was found in IHCs (Platzer *et al*. 2000), different slice variances or a different composition of auxiliary subunits could be present along the tonotopic axis. This could cause differences in the voltage dependence of activation

resulting in a difference in action potential generation. However, scientific evidence for a difference in voltage dependent calcium current activation between different cochlear regions is to date not found, although calcium currents activate significantly faster in apical than in basal IHCs (Johnson & Marcotti, 2008).

Another IHC action potential modulator is the transiently expressed sodium current, which has been shown to speed up the depolarising phase of action potentials (Marcotti *et al.*, 2003b). However, a profound description of its biophysical properties as a function of age and cochlear region was to date missing, but is going to be addressed in the next chapter.

4. Biophysical Properties and Molecular Identity of the Na^+ Channel in Rat Immature Inner Hair Cells

Chapter four of this thesis is about the biophysical properties and the molecular identity of the Na^+ channel found in rat IHCs. First the results are presented, after which they are discussed in context with the current literature.

4.1. Results II - Biophysics of the sodium current

The aim of chapter four is to describe the biophysical properties of the sodium current (I_{Na}) expressed in P0 to P12 rat IHCs as a function of temperature and cell position along the tonotopic axis of the cochlea. The expression of I_{Na} seems to correlate with the presence of spontaneous action potential activity in immature IHCs. The results in this chapter further highlight a potential role for I_{Na} in the modulation of the spontaneous action potential activity.

4.1.1. IHCs Express a Fast Activating and Inactivating Voltage Dependent Sodium Current

During whole cell voltage clamp recordings using depolarising voltage steps a transient inward current with an amplitude of several nanoampere was observed in immature IHCs (Figure 32). Two approaches were undertaken in order to verify the type of channel responsible to carry the inward current. The first approach involved exchanging sodium

with the Na^+ channel impermeable ion $NMDG^+$ (Figure 32 A; Wooltorton *et al.*, 2007) and the second, the application of the common Na^+ channel blocker tetrodotoxin (Figure 32 B; Catterall *et al.*, 2005). Under both conditions the major inward current was abolished and only a small current of a few hundred pA persisted, which most likely was the calcium current through $Ca_V1.3$ Ca^{2+} channels.

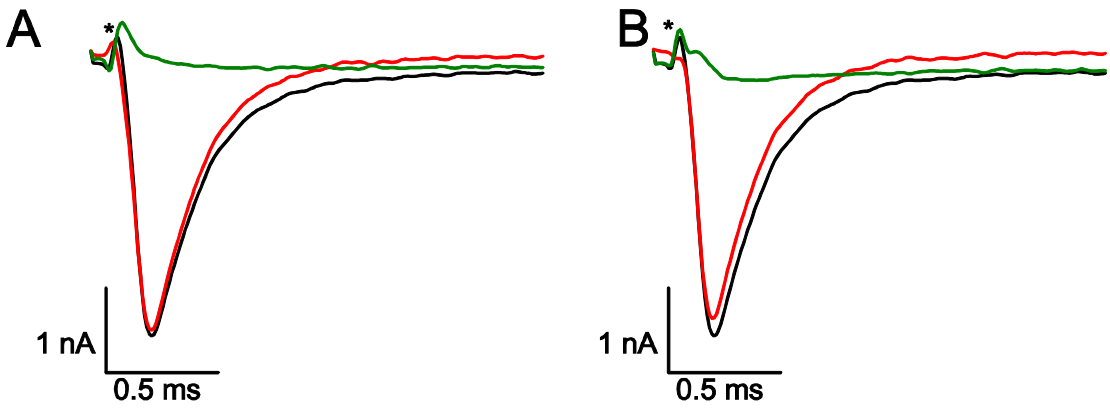

Figure 32: Current responses from a P2 apical IHC under control (black trace), NMDG (A; green trace) or TTX (B; green trace) perfusion. The red trace depicts the isolated sodium current. Under both conditions the fast activating and inactivating current was abolished. The small residual current of 200 to 300 pA was most likely an inward calcium current, as cesium in the pipette filling solution abolished all potassium currents. The recording conditions were R_s = 0.7 MΩ, C_m = 7.7 pF, g_{leak} = 1.6 nS, τ_{clamp} = 10 µs, the tetrodotoxin concentration was 1000 nM. The asterisks depict a small residual uncompensated R_s artifact. For clarity only one voltage step to a cell membrane potential of -22.5 mV using the Nacvc-voltage clamp protocol is shown.

Both tetrodotoxin and $NMDG^+$ current isolation procedures showed similar results. Under both conditions I_{Na} was fully abolished indicated by the large reduction of the inward current (Figure 32). By plotting the peak I_{Na} as a function of corresponding membrane potential, current to voltage relations were created (Figure 33). For further experiments mainly $NMDG^+$ was used as it allowed full recovery of the sodium current after washout and thus made recording from more than one IHC per preparation possible, whereas the effect of tetrodotoxin was less reversible (not shown).

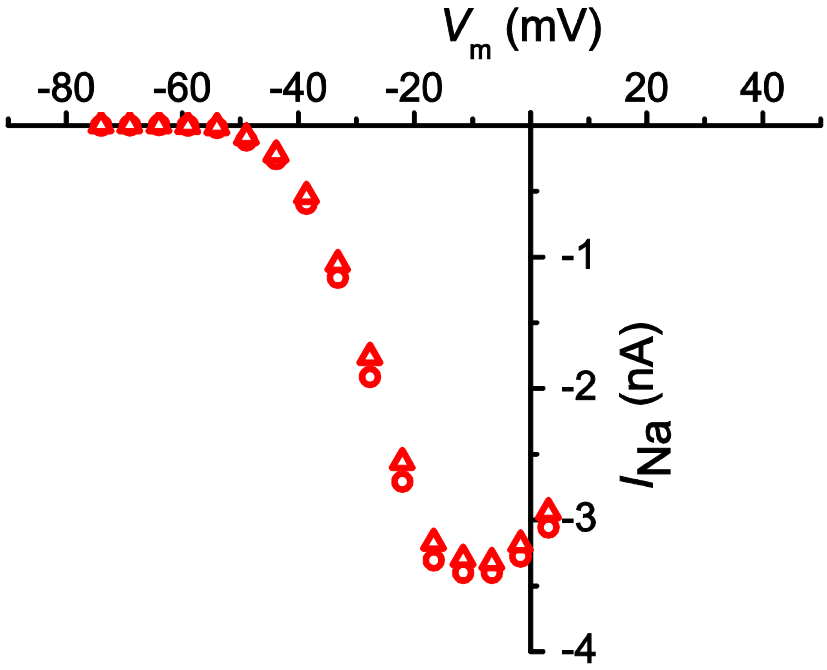

Figure 33: Peak sodium current to voltage relation of the two cells in Figure 32 obtained from I_{Na} isolation using TTX (open triangle) or NMDG (open circle). Under both conditions the current to voltage response follows the same course with activation from -60 mV towards positive voltages with a peak current amplitude between -20 and -10 mV.

4.1.2. Kinetics and Peak Amplitude of the Voltage Dependent Sodium Current in Inner Hair Cells are Temperature Dependent

Most of the available electrophysiological recordings from mammalian cochlear hair cells are performed at room temperature, disobeying that their physiological temperature is around 37˚C. In order to understand possible consequences associated with performing experiments using unphysiological temperature conditions, the biophysical properties of I_{Na} recorded from apical IHCs at room temperature were compared to those from apical IHCs near body temperature. Room temperature was defined as the temperature within the experimental chamber with the heating systems switched off, and was on average 24.9˚C ± 0.2 (n = 7). With the heating switched on, temperatures between 34 to 37˚C were achieved and defined as body temperature.

In order to elicit I_{Na}, a voltage step protocol ("Nacvc") was used. From a potential of -110 mV, IHCs were depolarised to potentials between -81 mV and 0 mV using 10 ms voltage steps with a nominal increment of 5 mV (Figure 34). I_{Na} isolation was done offline by subtracting the current in presence of NMDG from the total current (see also methods: pg. 70).

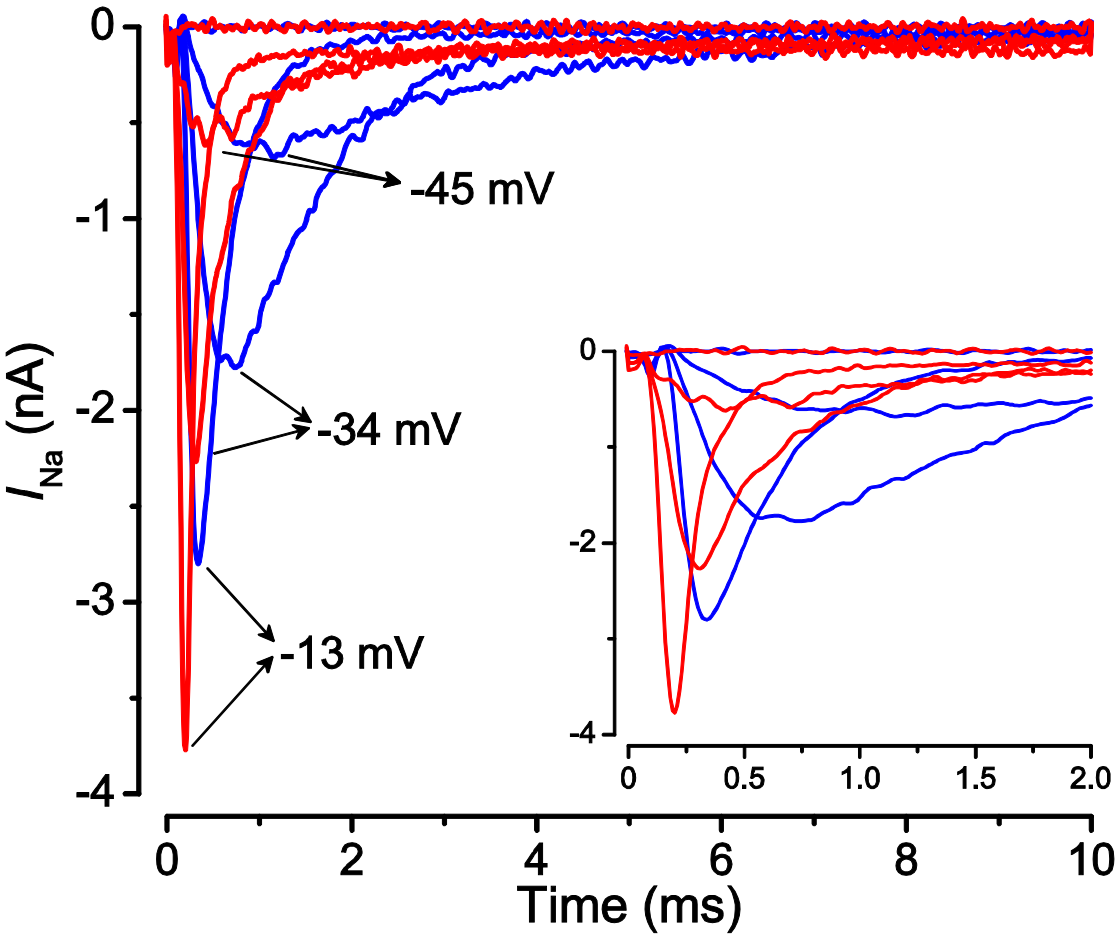

Figure 34: Isolated sodium currents from P4 apical IHCs at room (blue) and body temperature (red) elicited by a voltage step protocol. Note the difference in current amplitude and time to peak. The recording conditions for the cell at body temperature were: R_s = 0.84 MΩ, C_m = 10.2 pF, g_{leak} = 2.23 nS, τ_{clamp} = 10 µs and those of the cell at room temperature: R_s = 1.14 MΩ, C_m = 8.6 pF, g_{leak} = 1.28 nS, τ_{clamp} = 10 µs. The small inset depicts for clarity the first 2 ms of the 10 ms voltage step, only.

Increasing the temperature from room temperature to body temperature caused a significant (t-test: t = 8.496, df = 10, P < 0.0001) increase of I_{Na} peak amplitude from 2.1 nA ± 0.1 nA (n = 7) to 3.8 nA ± 0.2 nA (n = 5; Figure 35). The temperature coefficient Q_{10} for this increase is 1.8 and was calculated using the following equation:

$$\text{Equation 2:} \quad Q_{10} = (I_2/I_1) \exp(10/(T_2-T_1))$$

where I_1 and I_2 are the peak current amplitude at body and room temperature respectively, T_1 is room and T_2 body temperature, for which an average of 35.5˚C was used.

By plotting the peak I_{Na} at different voltage steps against the corresponding membrane potential, current to voltage relations were created from seven P4 IHCs at room and five P3 to P4 cells at body temperature (Figure 35 A). The isolated I_{Na} activated at potentials more positive than -60 mV, peaked at -14 mV at body and -16 mV at room temperature. The reversal potential (V_{rev}) was calculated from the Nernst equation using the intra and extracellular sodium concentrations and was -42.2 mV for body and 40.5 mV for room temperature. Current to voltage curves were fitted with the following equation with a fixed V_{rev}:

$$\text{Equation 3:} \quad I = (g_{max}(V-V_{rev})) / (1 + \exp((V_{half}-V)/dx))$$

where V is the membrane potential, V_{rev} the reversal potential and V_{half} is the membrane potential at which half maximal activation occurs. g_{max} represents the maximal chord conductance and dx is the slope of the current to voltage curve negative from the peak I_{Na}, which represents the voltage sensitivity of activation. The fitting parameters were for g_{max} significantly different (t-test: t = 7.031, df = 10, P < 0.0001) with 49.3 nS ± 2.0 nS (n = 5) for body and 35.8 nS ± 0.8 nS (n = 7) for room temperature. However, the voltage sensitivity of I_{Na} activation, reflected by the slope, was similar between body and room temperature (t-test: t = 0.1700, df = 10, P = 0.8684). Likewise, V_{half} did not change significantly (t-test: t = 1.267, df = 10, P = 0.2340) when increasing the temperature by 10˚C (Figure 35 B).

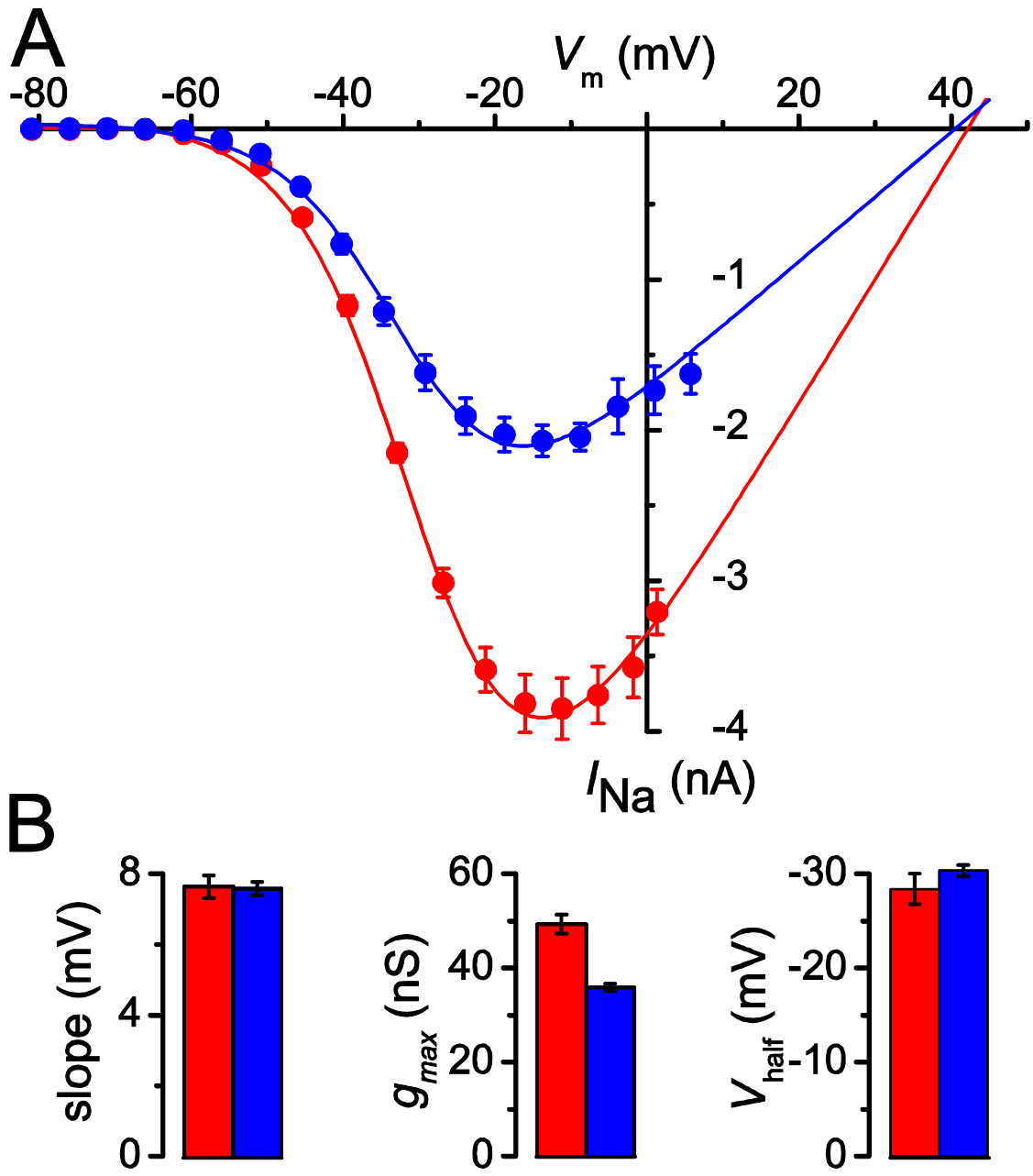

Figure 35: Temperature dependence of averaged current to voltage responses. A) Mean peak current with fit from 5 cells at body temperature (red) and 7 cells at room temperature (blue) from apical IHCs. I_{Na} opened from -60 mV towards positive membrane potentials. Peak I_{Na} was at -14 mV for body temperature and -16 mV for room temperature. Reversal potential was at -42 mV. The Q_{10} of the peak current amplitude was found to be 1.8. B) Values derived from the current to voltage fit. At body temperature, g_{max} was significantly higher than at room temperature.

The inactivation time constant ($\tau_{inactivation}$) was evaluated by fitting the decay after the peak of the current elicited by the Nacvc protocol using a single exponential function (see also Methods: pg. 70, 71 and Figure 21). The $\tau_{inactivation}$ significantly changed as a function of temperature and membrane potential (Figure 36, two way ANOVA with effect of temperature: $F = 198.2$, $df = 1$, $P < 0.0001$ and effect of membrane potential: $F = 53.69$, $df = 7$, $P < 0.0001$), with I_{Na} inactivating faster at body temperature and at more depolarised membrane potentials. At -15 mV, the membrane potential where the peak I_{Na} occurs, $\tau_{inactivation}$ was about 2.5 fold smaller at body temperature compared to room temperature.

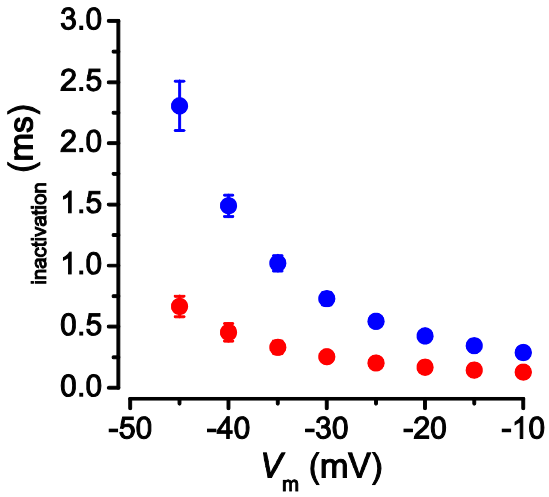

Figure 36: Temperature dependence of the time constant of I_{Na} inactivation at body temperature (red) and room temperature (blue) as a function of membrane potential. Inactivation was significantly faster at body temperature and with more depolarising voltage steps.

The time course of I_{Na} activation was measured as time to half maximal current amplitude ($t_{50\%\ peak}$) and time to peak current (t_{peak}), where $t = 0$ corresponds to the start of the voltage step (Nacvc). Both t_{peak} (two way ANOVA effect of temperature: $F = 501.9$, $df = 1$, $P < 0.0001$ and effect of membrane potential: $F = 68.28$, $df = 7$, $P < 0.0001$) and $t_{50\%\ peak}$ (two way ANOVA for effect of temperature: $F = 177.0$, $df = 1$, $P < 0.0001$ and effect of membrane potential: $F = 13.25$, $df = 7$, $P < 0.0001$) were significantly lower at body temperature. On average the $t_{50\%\ peak}$ and t_{peak} at -15 mV and -20 mV became 1.3 to 1.5 fold higher at room temperature (Figure 37).

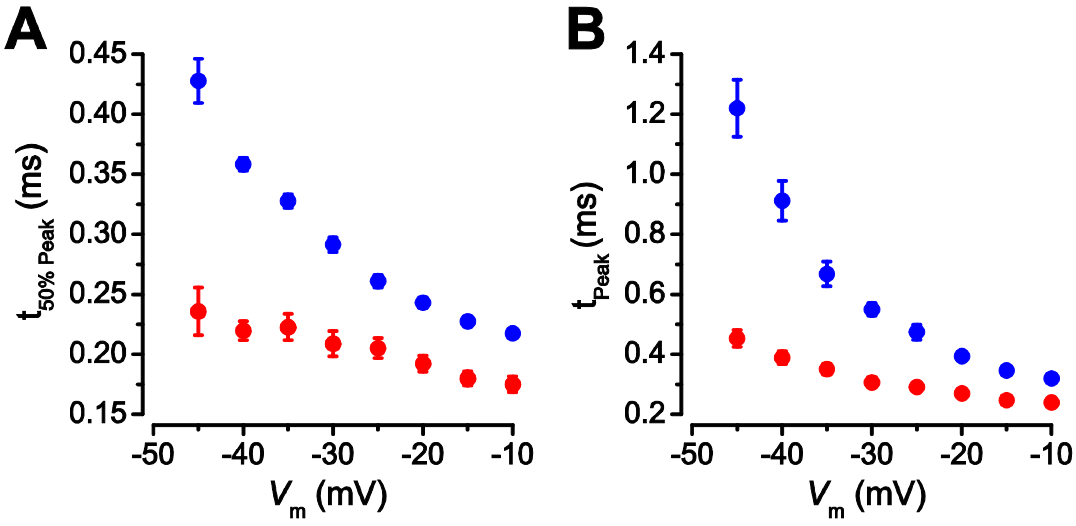

Figure 37: Temperature dependence of activation kinetics. $t_{50\%\ peak}$ (left) and t_{peak} (right) were significantly lower at body temperature (red) compared to room temperature (blue). The activation became also faster with increasing voltage step.

Steady state inactivation curves for I_{Na} were obtained from six P4 IHCs at room temperature and six P3 to P4 cells at body temperature by measuring the peak I_{Na} during a 10 ms depolarising step to -21 mV following a conditioning pre-step of 50 ms to different potentials ranging between -131 mV to -1 mV, with an increment of 5 mV (see methods: pg. 67 – "Inactivation" protocol); V_{hold} was -81 mV. The current was normalised and plotted against the membrane potential of the conditioning steps (Figure 38 A, B). Data points were fitted with a first order Boltzmann function:

$$\text{Equation 4:} \quad I = I_{max} / (1 + \exp((V\text{-}V_{half})/dx))$$

where I is the peak current of the voltage step, I_{max} is the maximal peak current. V and V_{half} are the membrane potentials of the voltage step and of half maximal activation. dx is the slope of the Boltzmann fit representing the voltage sensitivity of the Na^+ channel inactivation. V_{half} inactivation was significantly different between room and body temperature (t-test: t = 3.067, df = 10, P = 0.0119) with body temperature being shifted by 2.7 mV to depolarised membrane potentials. The voltage sensitivity was not significantly affected by a change in temperature (t-test: t = 0. 0.8755, df = 10, P = 0.4019).

The activation curve was obtained from normalising the chord conductance from five P4 IHCs, at room and five P3 to P4 cells at body temperature. Data points were fit using the following first order Boltzmann function:

$$\text{Equation 5:} \quad g = g_{max} / (1 + \exp((V_{half}-V)/dx)$$

where g is the chord conductance at different membrane potentials and g_{max} is the maximal chord conductance. The other parameters are the same as in the equation 4, for the steady state inactivation (see previous page 113). There was no significant effect of temperature found in either V_{half} (t-test: t = 7509, df = 8, P = 0.4742) or the voltage sensitivity (t-test: t = 0.4782, df = 8, P = 0.6453).

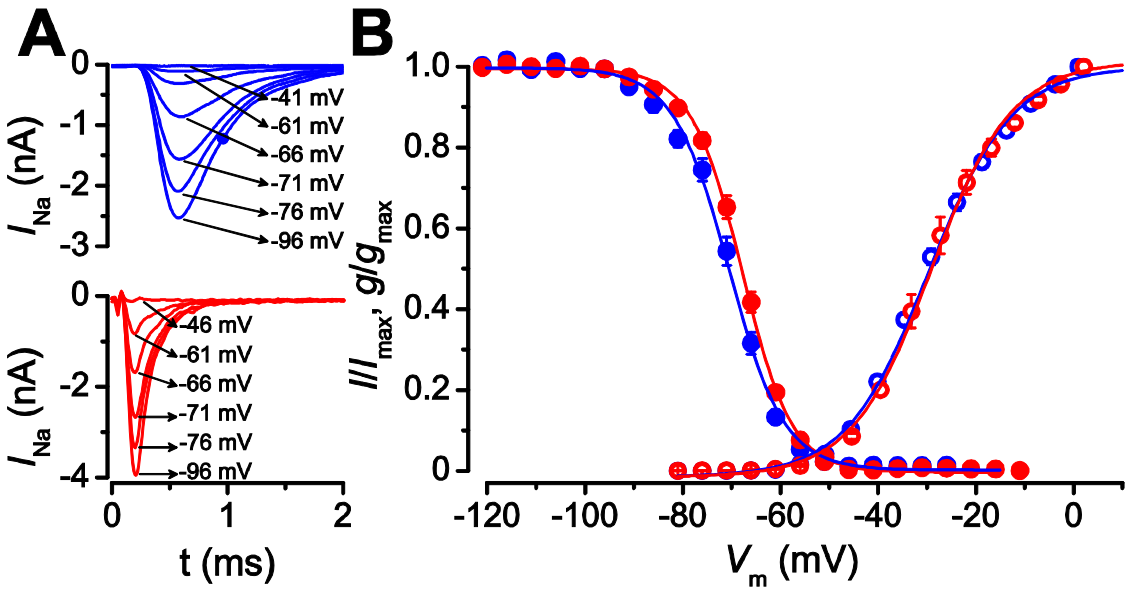

Figure 38: Sodium current activation and inactivation. A, Peak I_{Na} at -21 mV following a conditioning step of potentials between -131 and -1 mV in 5 mV increments. Recording conditions were R_s = 1.14 MΩ, C_m = 7.5 pF, g_{leak} = 1.73 nS, τ_{clamp} = 10 µs for the cell at room temperature (blue traces) and R_s = 0.84 MΩ, C_m = 10.2 pF, g_{leak} = 2.23 nS, τ_{clamp} = 10 µs at body temperature (red traces). Membrane potentials tested are shown next to the recordings. For clarity only the first 2 ms of the voltage step and only a few voltage steps are shown. B, Average steady state inactivation (filled circles) generated from averaging the normalised peak current (from recordings like in Panel A) obtained from 6 cells at body and room temperature each. Lines depict the fit from the first order Boltzmann curve with the following fitting parameters: V_{half} -70.6 mV, slope 5.6 mV for room temperature and V_{half} -67.9 mV, slope 5.2 mV for body temperature. The normalised activation (open symbols) was evaluated from the normalised chord conductance obtained with the Nacvc protocol. Lines depict the first order Boltzmann fit with the following fitting parameters: V_{half} -29.6 mV, slope 8.4 mV for room and V_{half} -29.1 mV, slope 8.22 mV for body temperature.

Recovery from inactivation was obtained from measuring the peak I_{Na} of two voltage steps in sequence (see methods for more details: pg. 68). Both steps were performed from a holding potential of -131 mV, were 10 ms long and 110 mV in amplitude. The time in between the two voltage steps was gradually increased from 0.1 ms to 50 ms. Data recorded from nine P4 cells at room temperature and eight P4 cells at body temperature were fitted with a two exponential equation (Figure 39):

$$\text{Equation 6:} \quad I = y0 + A_{fast} \exp(-x/\tau_{fast}) + A_{slow} \exp(-x/\tau_{slow})$$

where τ_{fast} and τ_{slow} represent the two time constants, A_{fast} and A_{slow} the corresponding amplitudes and y0 the offset of the function, which is the fully recovered I_{Na} normalised (Figure 39). The two time constants τ_{fast} and τ_{slow} were 0.14 ms ± 0.01 ms (n = 8) and 2.29 ms ± 0.46 ms (n = 8) at body temperature and 0.58 ms ± 0.03 ms (n = 9) and 8.77 ms ± 2.77 ms (n = 9) at room temperature. The temperature had a highly significant effect on the recovery from inactivation (two way ANOVA: $P < 0.0001$) with the I_{Na} recovering faster at body temperature compared to room-temperature.

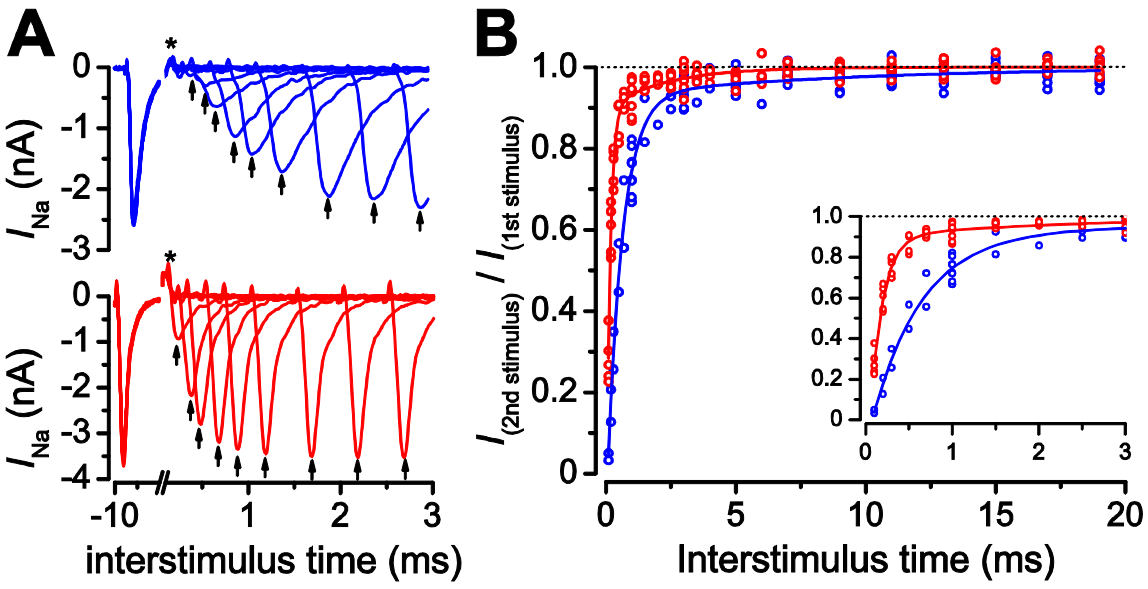

Figure 39: Recovery from inactivation was highly temperature dependent. A, Recovery from inactivation at room (blue) and body temperature (red): I_{Na} recovers significantly faster from inactivation at body temperature. The break in the x-axis between -9 ms and 0.1 ms is for clarity. Only the first few traces up to 3 sec are shown (interstimulus times in ms for both room and body temperature: 0.1, 0.2, 0.3, 0.5, 0.7, 1, 1.5,

2, 2.5). 0 on the x axis depicts the time when the first stimulus ended. The arrows indicate the peak I_{Na} and the asterisks depict a small uncompensated R_s artifact. Recording conditions were for room temperature: R_s = 1.14 MΩ, C_m = 8.6 pF, g_{leak} = 1.28 nS, τ_{clamp} = 10 µs and for body temperature: R_s = 0.84 MΩ, C_m = 10.2 pF, g_{leak} = 2.23 nS, τ_{clamp} = 10 µs. B, Two exponential fit of individual interstimulus times (open circles) from nine cells recorded at room temperature (blue) and eight cells at body temperature (red). The small inlet shows a scaled up version of the first 3 seconds.

All together these data highlight that with increasing the temperature I_{Na} not only becomes larger in amplitude, its response to membrane potential changes becomes also significantly faster.

4.1.3. Expression of the Sodium Current in Inner Hair Cells correlates with Spontaneous Action Potential Generation

One aspect of this study was to look for a possible correlation between spontaneous spiking activity and expression of I_{Na} in immature IHCs. For this purpose, the possible presence of I_{Na} was investigated throughout postnatal development from P0 until the onset of hearing at P12.

Both apical (n = 48) and basal (n = 33) IHCs were recorded in order to measure the peak I_{Na} amplitude (Figure 40). A peak I_{Na} in the range of nanoamperes was found in all cells between P0 to P9. The largest currents for both apical and basal IHCs were found during the same developmental time, when the cells showed spontaneous activity. The largest current amplitudes of -9.16 nA for apical IHCs and -5.47 nA for basal IHCs were both recorded at P2. From P5 onwards I_{Na} amplitude declined and from P10 in basal and P11 in apical IHCs, respectively, no current could be detected any longer. Overall, apical IHCs had a significantly larger I_{Na} than basal cells (two way ANOVA, effect of cochlear region: F = 10.14, df = 1, P = 0.0032).

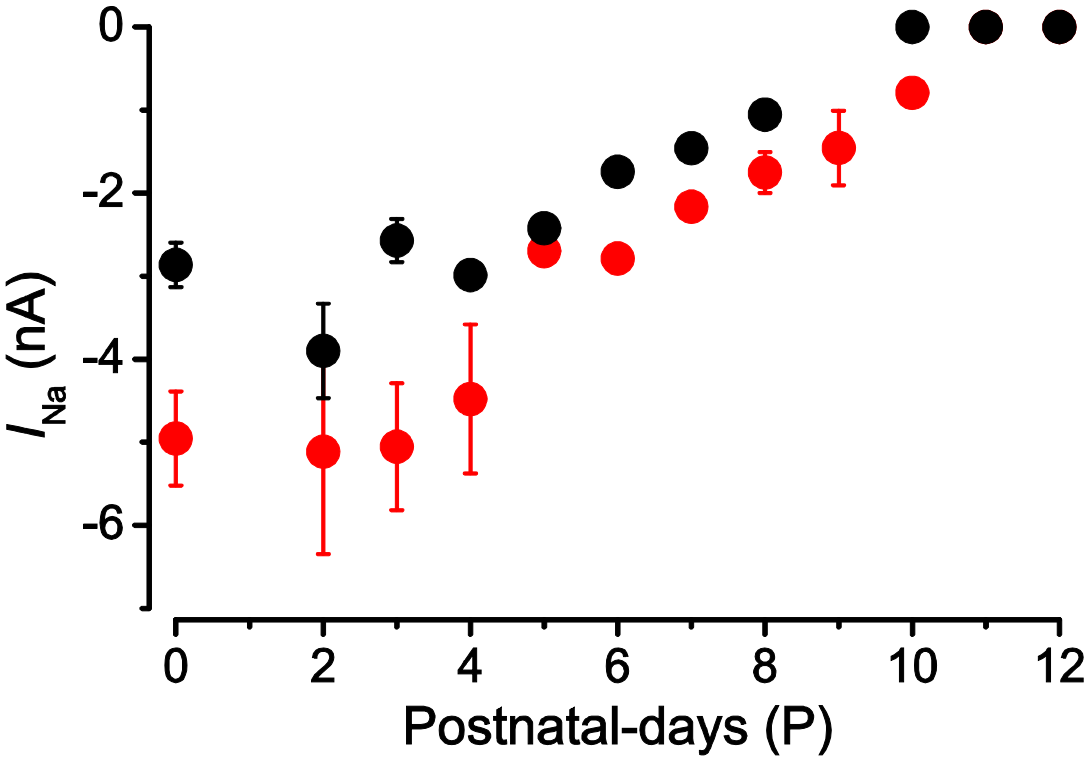

Figure 40: Development of the peak I_{Na} during the first two postnatal weeks until the onset of hearing at P12. Apical IHCs (red) show a significantly larger current than basal IHCs (black) on all days measured. During the time window where all IHCs generate spontaneous action potentials (P0-P4) I_{Na} was largest in both apical and basal cells. Recordings were made from 3 – 6 cells unless otherwise indicated (apical: P1 = 0, P7 = 1, P10 = 1; basal: P1 = 0, P5 = 2, P6 = 1, P7 = 1, P9 = 0, P12 = 0)

4.1.4. Biophysical Properties of the Sodium Current in IHCs as a Function of Cochlear Region

The sodium current was elicited from apical and basal IHCs by running the same voltage step protocol used for the temperature dependence ("Nacvc"; see also Methods pg. 66). Briefly, from a potential of -110 mV 10 ms depolarising voltage steps in 5 mV increments were applied and I_{Na} was isolated offline by subtraction (Figure 41).

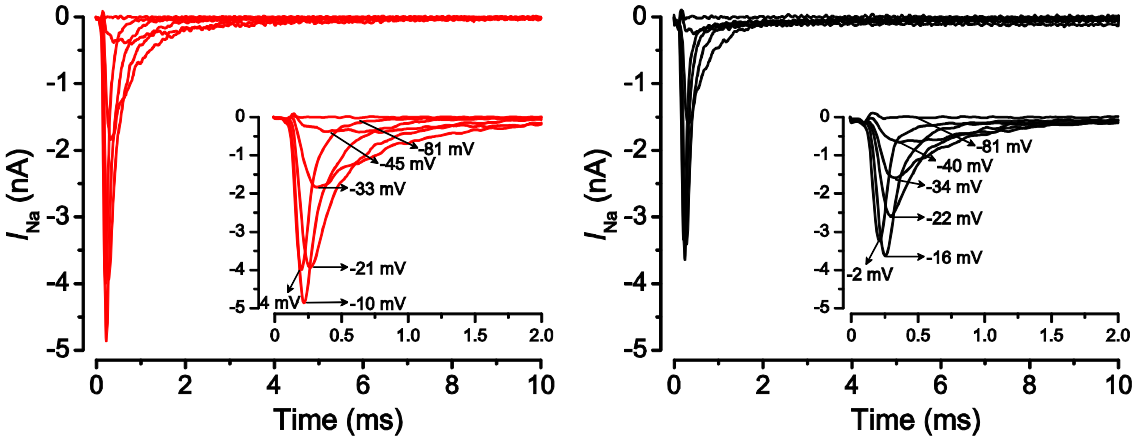

Figure 41: Isolated I_{Na} from P0 apical (left) and basal (right) IHCs. Apical IHCs show larger current amplitudes than basal cells. For clarity not all current traces are shown. Inset depicts a closer view on the first 2 ms of the 10 ms voltage step. Numbers aside the current traces depict the membrane potential corrected for R_s. Recording conditions were R_s = 1.16 MΩ, C_m = 4.5 pF, g_{leak} = 0.58 nS, τ_{clamp} = 10 µs for the apical cell and R_s = 1.1 MΩ, C_m = 7.1 pF, g_{leak} = 2.59 nS, τ_{clamp} = 10 µs for the basal cell.

Current to voltage curves were created from 14 apical and 12 basal cells between P0-P4 (Figure 42). By using equation 3 (see pg. 110), current to voltage responses were fit with the following fitting parameters g_{max} 48.7 nS, slope 7.1 mV and V_{half} -28.0 mV for apical and g_{max} 40.6 nS, slope 6.8 mV and V_{half} -31.5 mV for basal IHCs. The slope representing the voltage sensitivity of the Na^+ channel was not significantly different between the apical and basal coil (t-test: t = 1.048, df = 24, P = 0.3053). However, the membrane potential of half maximal activation differed highly significantly between both cochlear regions (t-test: t = 3.739, df = 24, P = 0.0010). Furthermore, apical IHCs showed a significantly larger I_{Na} than basal IHCs (t-test: t = 16.13, df = 24, P < 0.0001).

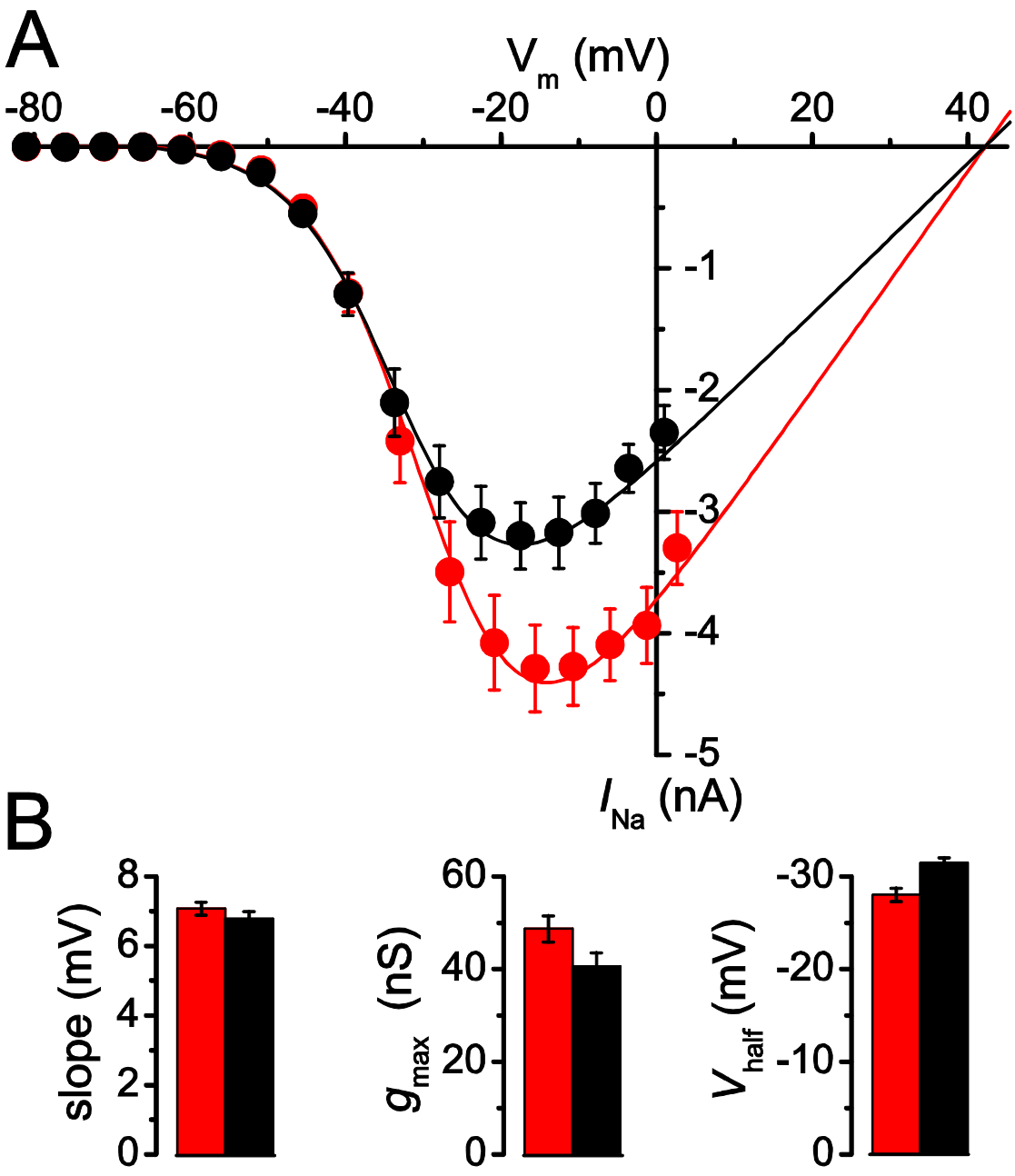

Figure 42: A) Average current to voltage relation for apical (red) and basal (black) IHCs from P0 to P4. For both apical and basal IHCs the current activated at potentials positive to -60 mV. The line shows the fit with the following fitting parameters (shown in B): g_{max} 48.7 nS, slope 7.1 mV and V_{half} -28.0 mV for apical and g_{max} 40.6 nS, slope 6.8 mV and V_{half} -31.5 mV for basal. V_{rev} was fixed for both apical and basal IHCs at the calculated potential of 42.16 mV. The peak of the current to voltage relation obtained by the fit was -14.2 mV in apical and -17.6 mV in basal IHCs.

From the current to voltage relation the chord conductance g_{chord} was calculated with the following equation:

$$\text{Equation 7:} \quad g_{chord} = I_{peak} / (V\text{-}V_{rev})$$

where I_{peak} was the peak I_{Na} of the voltage step, V was the membrane potential reached by the voltage step, and V_{rev} was the reversal potential fixed to 42.16 mV. The chord conductance was normalised, plotted against the membrane potentials (Figure 44 A) and fitted with the same Boltzmann function for activation as in equation 5 (see pg. 114). Mean fitting parameters were the following for apical: V_{half} -28 mV, slope 7.57 mV and for basal: V_{half} -30.5 mV, slope 7.38 mV (Figure 44 B). V_{half} was found to be significantly shifted towards more depolarised values in apical IHCs (t-test: t = 2.773, df = 24, P = 0.0103), the slope was not significantly different (t-test: t = 0.6874, df = 24, P = 0.4982).

Steady state inactivation curves were obtained from 12 cells from the apical coil and 10 cells from the basal coil at P0-P4 by measuring the peak I_{Na} during a 10 ms depolarising step to -21 mV following a conditioning pre-step of 50 ms to different potentials ranging between -131 mV and -1 mV, with an increment of 5 mV. V_{hold} was -81mV (example recordings Figure 43).

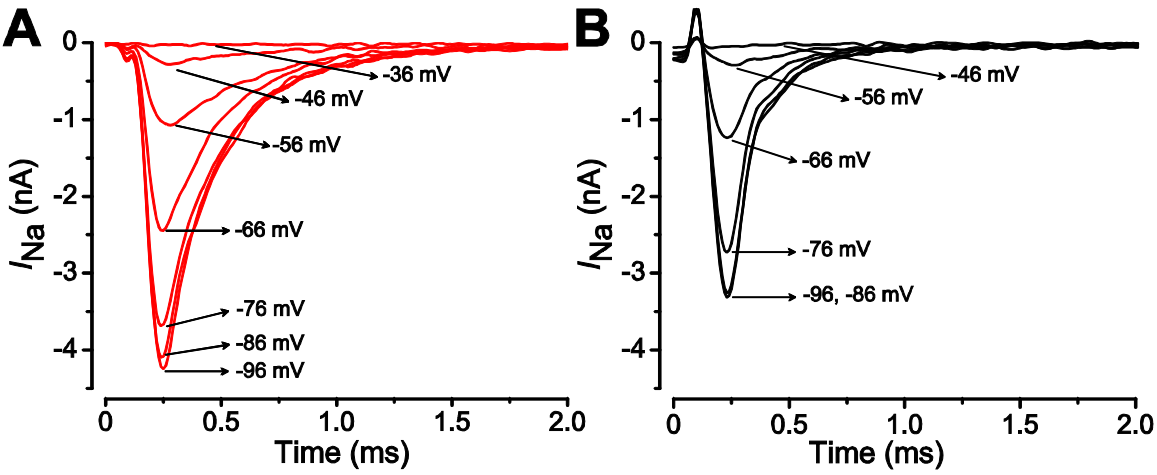

Figure 43: A and B) Isolated I_{Na} after a 50 ms conditioning step to varying membrane potentials (numbers aside traces) in an exemplary apical (A), and a basal IHC (B) both recorded at P0. For clarity not all traces of the measurement are shown. Recording conditions for the apical cell were: R_s = 1.16 MΩ, C_m = 4.5 pF, g_{leak} = 0.58 nS, τ_{clamp} = 10 µs and for the basal cell : R_s = 1.1 MΩ, C_m = 7.1 pF, g_{leak} = 2.59 nS, τ_{clamp} = 10 µs.

The peak I_{Na} obtained from these recordings was normalised and fitted using a first order Boltzmann function (Figure 44 C). Mean fitting parameters were for apical IHCs V_{half} -66.9 mV, slope 5.33 mV and for basal IHCs V_{half} -68.8 mV, slope 4.79 mV. Cells from the two cochlear regions were significantly different in their V_{half} (t-test: t = 2.204, df = 20, P = 0.0394). But not in the slope (t-test: t = 1.878, df = 20, P = 0.0750).

Altogether, the similar slope of both, activation and inactivation between the two cochlear regions indicates the same sensitivity of the channel towards voltage changes. However, the potential of half maximal activation and inactivation was significantly different, as were the current amplitudes.

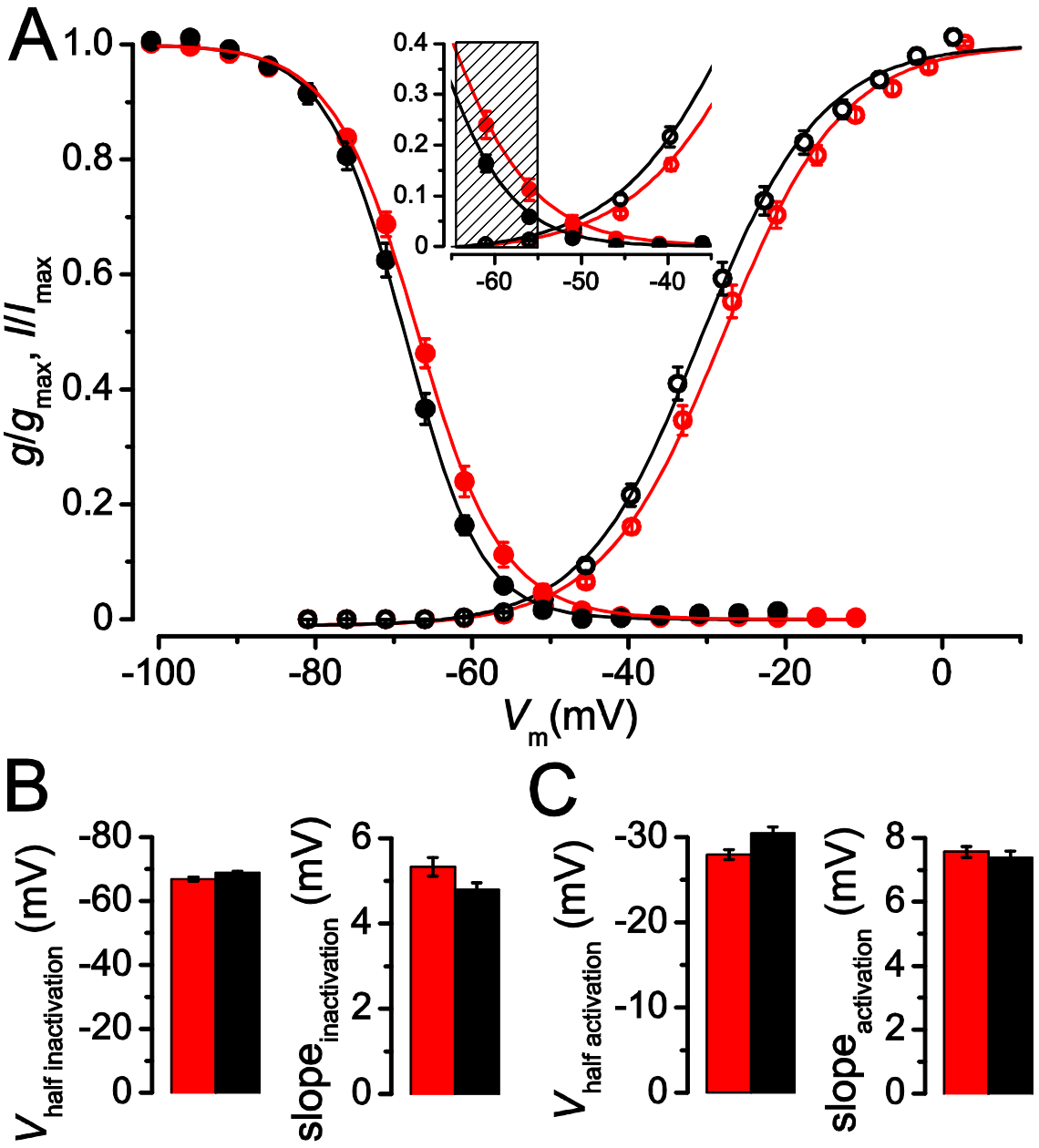

Figure 44: Steady state inactivation of the sodium current. A) The steady state inactivation (filled symbols) was averaged from 12 apical (red) and 10 basal (black) rat IHCs between P0 and P4 and fitted with a first order Boltzmann function (line) with the following parameters (B): apical V_{half} -66.9 mV, I_{max} 4.341 nA, slope 5.33 mV; basal V_{half} -68.8 mV, I_{max} 2.687 nA, slope 4.79 mV. For the activation curves (open symbols) 14 apical (red) and 13 basal IHCs (black) from P0 to P4 rats were used. Values were obtained by normalising the chord conductance from Nacvc recordings. Parameters for the activation fit (C) were for the apical IHCs: V_{half} -28.0 mV, slope 7.57 mV and for the basal IHCs: V_{half} -30.5 mV, slope 7.38 mV. The small inlet in A shows the steady state inactivation and activation enlarged for clarity. The shaded rectangle depicts physiological membrane potentials close to the resting membrane potential. B and C, Fitting parameters of the first order Boltzmann fit of the steady state inactivation and activation (lower bar charts). The difference between apical and basal coil is significant for V_{half} for both activation and inactivation, but not for the slope.

The time constant of inactivation ($\tau_{inactivation}$) was obtained from fitting the decaying current with a single exponential fit after I_{Na} peak was reached (Figure 45). On average 6 membrane voltage steps could be fitted per cell and by interpolation 6 values were taken from fixed membrane potentials for statistical comparison (see also Methods – pg. 71 and 72). IHCs from the apical coil at P0 (n = 3), P2 (n = 5) and P4 (n = 4) and four cells from the basal coil at each of the three postnatal days were analysed. $\tau_{inactivation}$ was significantly dependent on the membrane potential at all ages and on the cochlear region at P0 and P2 (two way ANOVA effect of membrane potential at P0: F = 70.42, df = 5, P < 0.0001; at P2: F = 172.3, df = 5, P < 0.0001 and at P4: F = 37.52, df = 5, P < 0.0001. Effect of cochlear region at P0: F = 33.88, df = 1, P < 0.0001 and P2: F = 50.46, df = 1, P < 0.0001). On P4 the cochlear region did no longer have a significant effect on $\tau_{inactivation}$ (two way ANOVA: F = 0.5362, df = 1, P < 0.4687).

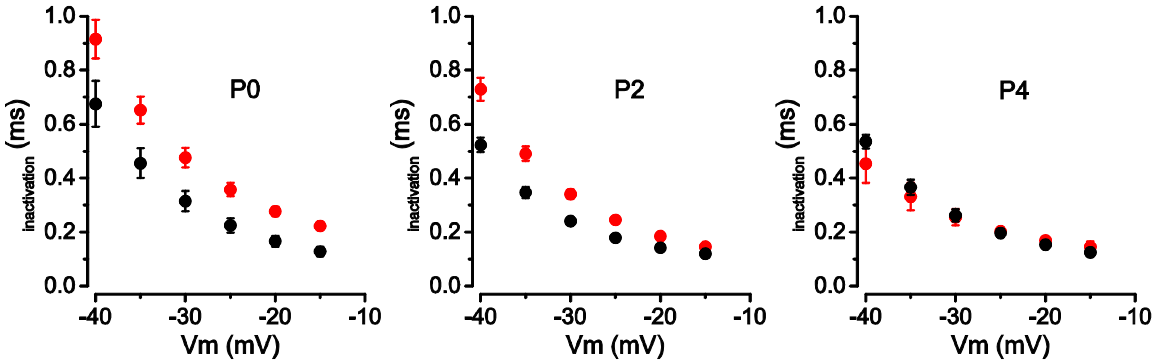

Figure 45: $\tau_{inactivation}$ of I_{Na} was obtained from a single exponential fit at three different ages: P0 (left), P2 (middle) and P4 (right). Time constants were corrected for membrane potential by fitting them for each cell and comparing the apical with the basal fit at fixed membrane potentials. $\tau_{inactivation}$ was significantly dependent on the membrane potential, as the current inactivated faster with increasing depolarisation from V_{hold} (-81 mV). At P0 and P2 IHCs from the basal coil (black) inactivate significantly faster than those from the apical coil (red). On P4 there is no significant difference between apical and basal $\tau_{inactivation}$.

To evaluate the speed of I_{Na} activation, the time from the onset of the voltage step to the peak and to 50 % peak was measured (Figure 46). 16 apical and 14 basal IHCs were analysed for voltage steps between -10 and -45 mV. Values were grouped for membrane potential (bin size 5 mV ± 2.5 mV) and compared with a two way ANOVA. No significant difference was found between apical and basal IHCs for $t_{50\%\ peak}$ ($F = 2.593$, $df = 1$, $P = 0.1090$), but the peak I_{Na} amplitude was reached significantly faster in basal IHCs ($F = 10.56$, $df = 1$, $P = 0.0014$). For both $t_{50\%\ peak}$ and t_{peak} the size of the voltage step significantly changed the speed of activation (two way ANOVA $t_{50\%\ peak}$: $F = 13.20$, $df = 7$, $P < 0.0001$ and t_{peak}: $F = 45.80$, $df = 7$, $P < 0.0001$).

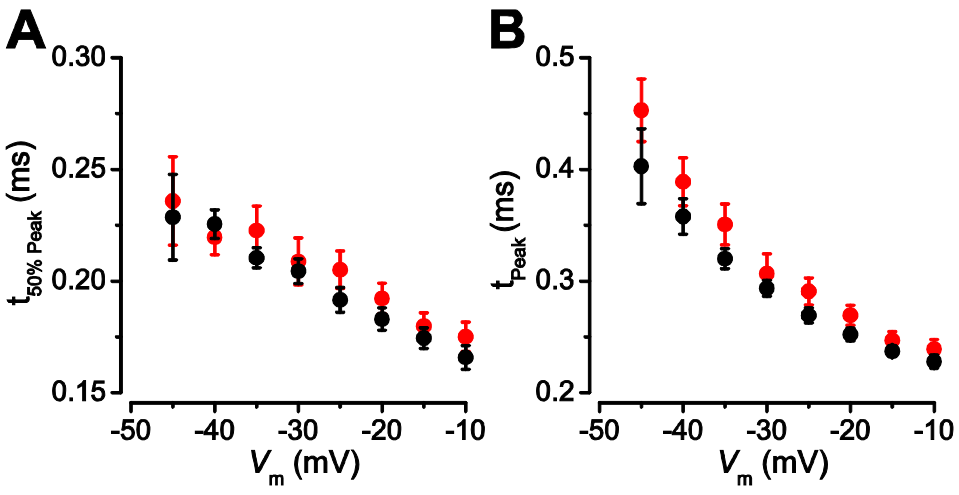

Figure 46: A, Average time to reach half peak I_{Na} is not significantly different ($P = 0.1090$) between apical (red) and basal (black) IHCs. At -15 mV, $t_{50\%\ peak}$ was 0.180 ms for apical IHCs and 0.174 ms for basal IHCs. B, Average time to peak at -15 mV is significantly shorter by 0.01 ms in basal IHC than in apical IHCs ($P = 0.0014$). 16 apical and 14 basal IHC were analysed. Because of differences in I_{Na} amplitude and R_s between the measurements, the membrane potentials were grouped (bin size 5 ± 2.5 mV).

One key question is how I_{Na} is able to modulate action potentials. To test whether the proportion of I_{Na} available at rest is able to influence the shape of action potentials, the waveform of an action potential was applied to IHCs in the presence and absence of I_{Na}. In order to create this protocol, action potentials were initially recorded in current clamp mode, averaged and computed into a voltage clamp protocol. This protocol was used to elicit voltage gated currents in four P2-P3 apical IHCs. Using tetrodotoxin subtraction a sodium current could be isolated from the total current (Figure 47) at a V_{hold} of -60 mV. The mean I_{Na} amplitude was -200.3 pA ± 32.5 pA (n = 4) and occurred 0.28 ms ± 0.04 ms (n = 4) before the peak of the protocol of the action potential waveform.

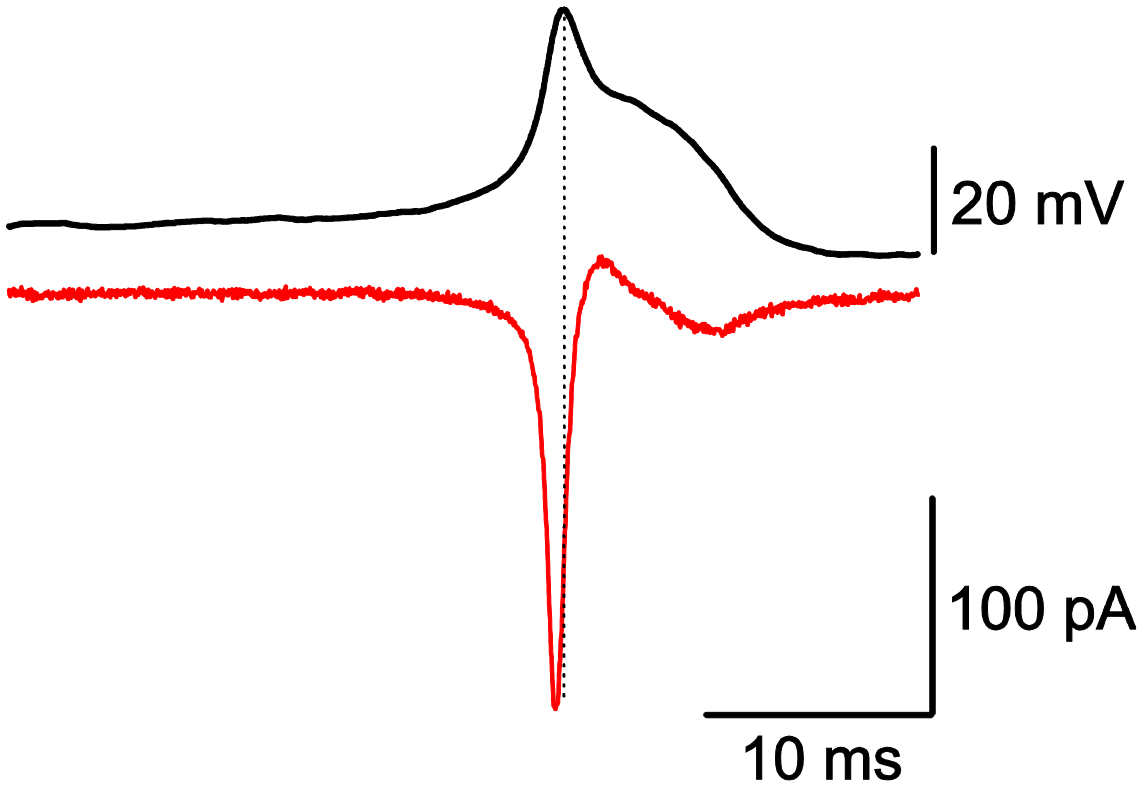

Figure 47: Average isolated I_{Na} during an action potential voltage clamp protocol. Top trace (black trace) displays the action potential waveform used as a voltage command protocol. V_{hold} was -60 mV. The spike protocol amplitude was 43.6 mV. The averaged ionic current (red trace) shows the isolated I_{Na} current. The peak I_{Na} was 200.3 pA and occurred on average 0.28 ms before the peak of the voltage protocol (highlighted by the vertical dotted line).

4.2. Results III - Molecular Identity of the Na^+ Channel

The molecular identity of the transiently expressed I_{Na} in immature IHCs is to date unknown. In order to identify which α subunits are expressed in IHCs, *in situ* hybridisation experiments on cross sections of the immature cochlea of the rat were performed. *In situ* hybridisation experiments using RNA probes against $Na_V1.6$ were complemented with RNA probes against myelin basic protein (MBP) to test whether the material and methods did work. These probes were provided by the Hearing Research Center Tübingen (Molecular Physiology of Hearing, Lab Prof. M. Knipper) and were used as general positive controls for both the protocols and materials used in order to perform *in situ* hybridisation.

MBP antisense and sense RNA probes were used for *in situ* hybridisation experiments on cross sections of the immature P3 rat cochlea. While no staining was seen with the sense probe, the antisense probe produced a clear and strong staining in the neurons of the facial nerve adjacent to the cochlea. The comparison between antisense and sense probe indicated the presence of a specific labelling with a very high signal to noise ratio (Figure 48). This *in situ* hybridisation experiment was complemented with $Na_V1.6$ sense and antisense RNA probes on additional cross sections from the same cochlea. The result (Figure 49) showed a very weak signal to noise ratio between antisense and control RNA probe. Even after several *in situ* hybridisation trials during which iteratively hybridisation temperature and RNA probe dilution was altered it was not possible to improve the signal to noise ratio. However these results showed possibly a weak specific stain in the facial nerve.

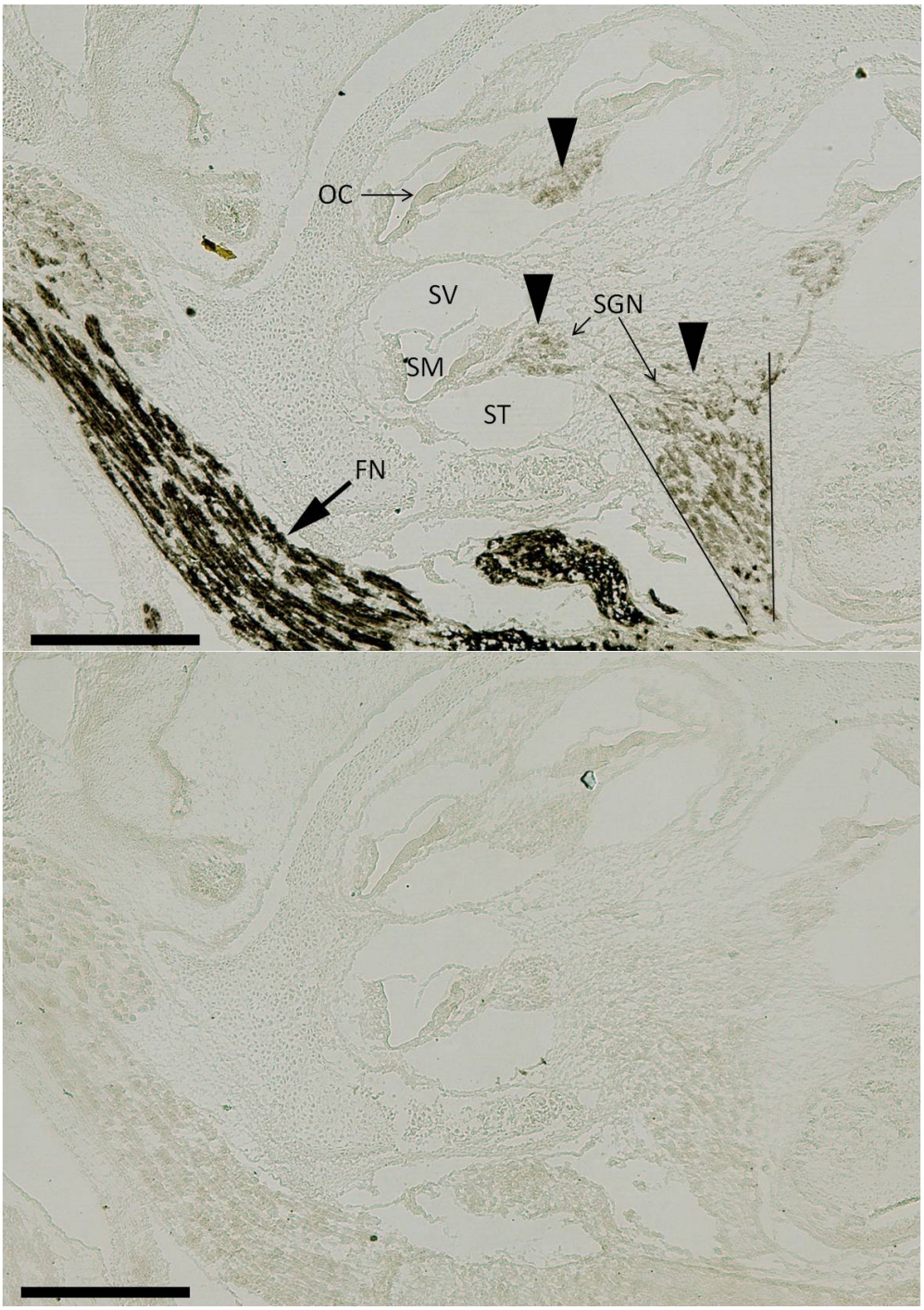

Figure 48: Cross section of the rat cochlea, P3, 50x magnification. *In situ* hybridisation with the antisense (above) RNA probe and sense (below) against MBP, a myelin sheath marker. Strong specific staining can be seen in facial nerve (indicated by the arrow) as well as a slighter specific stain in the spiral ganglia of the cochlea (arrowheads and between the drawn line), the picture below shows staining with the sense RNA probe. Staining in this picture depicts unspecific stain and shows that stain with the antisense probe is specific. Scale bar is 500 µm. OC = organ of Corti; SV = scala vestibuli; ST = scala tympani; SM = scala media; FN = facial nerve; SGN = spiral ganglion neurons.

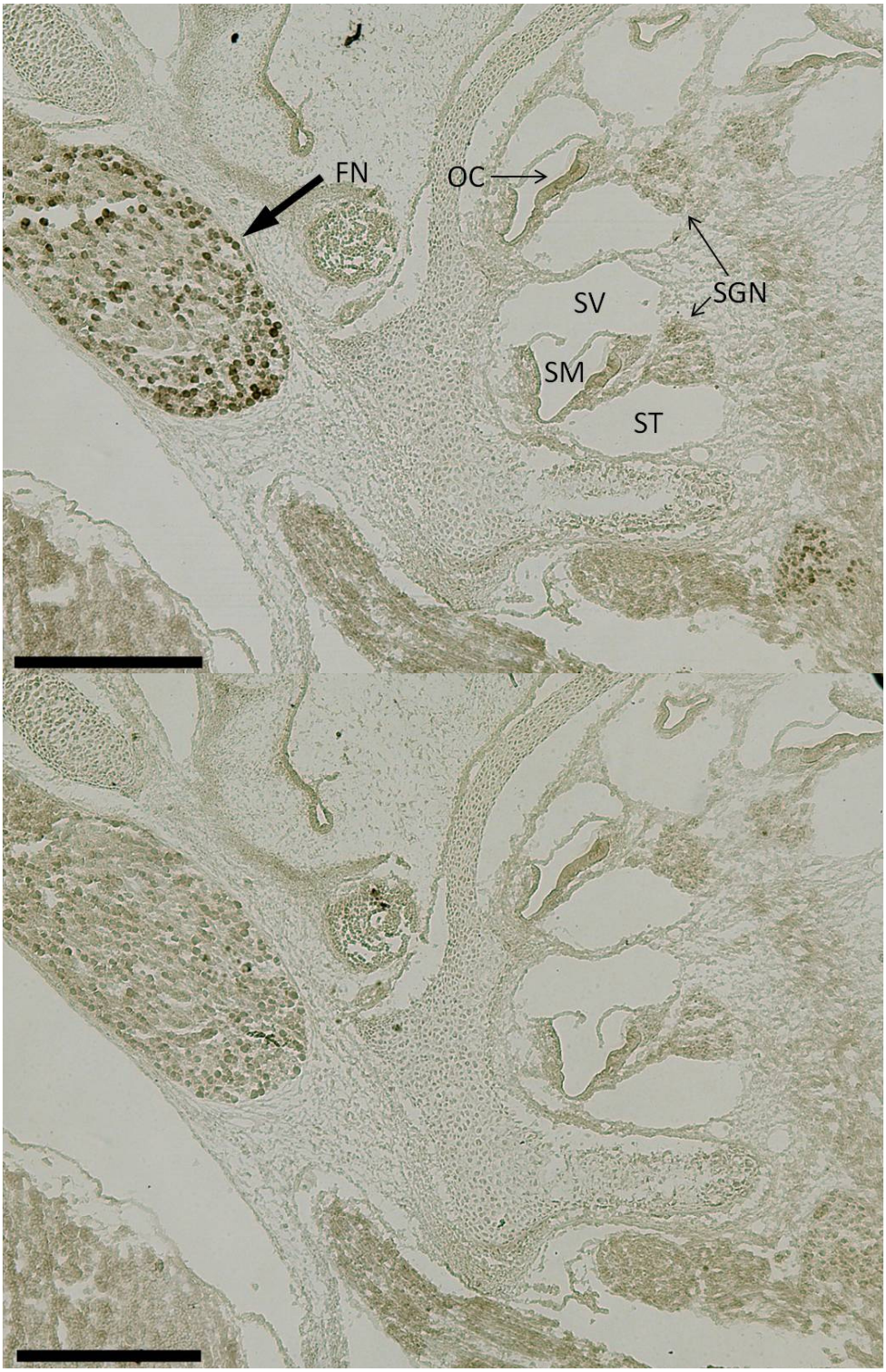

Figure 49: Cross section of the rat cochlea, P3, 50x magnification. *In situ* hybridisation with the antisense (above) RNA probe and sense (below) against $Na_V1.6$. Comparing both sense and antisense staining reveals a very low signal to noise ratio with a possible specific staining in the facial nerve and spiral ganglion neurons. Scale bar is 500 µm. OC = organ of Corti; SV = scala vestibuli; ST = scala tympani; SM = scala media; FN = facial nerve; SGN = spiral ganglion neurons.

4.3. Discussion II - Biophysical Properties and Molecular Identity of the Inner Hair Cell Na^+ Channel

Voltage gated Na^+ channels are widely expressed across the animal kingdom and are crucial for the transmission of neuronal signals since they carry a depolarising current that is required for generating action potentials (Goldin, 2001). One of the main aims of this study was to characterise the biophysical properties of the rat IHC sodium current as a function of development and cochlear region. The results of this thesis are the first comprehensive description of the biophysical properties of the sodium current in mammalian IHCs and can be summarised as follows: 1) Immature IHCs display a voltage dependent transiently activating sodium current. 2) This sodium current activates and inactivates with very fast kinetics. 3) Current amplitude is largest within the first few postnatal days. From P5 onwards the current amplitude declines steadily until the current is no longer detectable at around the onset of hearing. 4) The amplitude and voltage dependent activation and inactivation of the sodium current seems to change progressively along the tonotopic axis of the cochlea. 5) The amplitude and kinetics are highly temperature dependent. 6) The functional role of the sodium current in IHCs seems to shape the action potential waveform by exerting its action during the upstroke of the action potential, thus likely speeding up the depolarisation phase. Therefore, the sodium current is likely to contribute to both frequency and pattern of action potential activity, which might alter the development of IHCs or the auditory system.

4.3.1. Biophysics of the rat Inner Hair Cell Sodium Current

This thesis shows that immature rat IHCs express a voltage dependent sodium current (Figure 32). In order to determine which Na^+ channel α subunit carries the sodium currents of rat IHCs, their biophysical properties were compared with Na^+ currents described in cochlear and vestibular hair cells as well as sodium currents from α subunit isoforms in expression systems (Table 6).

Briefly, the voltage clamp recordings of this study revealed a transient, sodium selective conductance with very fast activation and inactivation kinetics. The membrane potential at which half maximal inactivation occurred was -71 mV at room temperature and -68 mV at body temperature. Half maximal activation occurred at membrane potentials around -30 mV. Recovery from inactivation was very fast and highly dependent on temperature. However, to match the sodium current of rat IHCs with a single α subunit isoform seems to be a very challenging task, as both the cells background in which the current is expressed (Smith *et al.*, 1998; Cummins *et al.*, 2001) as well as the experimental conditions (Hille, 2001) have shown to significantly influence current properties. Furthermore, it was shown that the expression of accessory β subunits essentially changes current properties (Smith *et al.*, 1998; Smith & Goldin, 1998).

The sodium current expressed by IHCs is most likely limited to tetrodotoxin sensitive isoforms (see also introduction pg. 51; $Na_V1.1$ to $Na_V1.4$, $Na_V1.6$ and $Na_V1.7$). It was previously shown that mouse IHCs express a sodium current with a half maximal inhibitory concentration of 5 nM, which is fully abolished at concentrations above 100 nM (Marcotti *et al.*, 2003b). Due to the close physiological relation between mice and rats, the exact tetrodotoxin sensitivity of the sodium current was not investigated in rat IHCs. However, in the course of the experiments it was shown that 1 μM tetrodotoxin was sufficient to fully abolish the sodium current (Figure 32). Therefore, it seems very unlikely that IHCs express a tetrodotoxin resistant isoform since their half maximal inhibitory concentrations are in the range of at least one micromolar (Goldin, 2001; Catterall *et al.*, 2005).

When the potential of half maximal activation and inactivation (see also Table 6, below for a summary) between the single Na^+ channel isoforms were compared it became apparent that the results of this study fit very well with all neuronal tetrodotoxin sensitive isoforms. However, it is unlikely that the α subunit $Na_V1.4$, which is predominantly found in the skeletal muscle is expressed in IHCs, as half maximal inactivation occurs at more depolarised voltages (about 10 mV; Chahine *et al.*, 1994; Catterall *et al.*, 2005). Taking the kinetics of inactivation and recovery from inactivation into account, it seems possible to further narrow down the subunits that might potentially be expressed in IHCs. The sodium current of rat IHCs both inactivates and recovers from inactivation with a remarkable

speed, suggesting $Na_V1.1$ could be expressed in IHCs. The time constant of this channel subunit are the closest match to those found for the sodium current of IHCs.

Table 6: Comparison of biophysical properties of sodium currents recorded from rat IHCs (line 1-3) with those recorded from α subunit isoforms in expression systems (line 4-9) or from other vertebrate hair cells (line 10-14). Abbreviations are: BT = body temperature; RT = room temperature; V_{half} = membrane potential of half maximal activation and inactivation; inact = inactivation; act = activation; recov = recovery from inactivation; τ_s and τ_f = slow and fast time constant; TTX-R = tetrodotoxin resistant; TTX-S = tetrodotoxin sensitive; HC = hair cell

	V_{half} inact. (in mV)	V_{half} act. (in mV)	$\tau_{inact.}$ at -10 mV (in ms)	τ_{recov} (in ms)
Apical BT	-66.9	-28.0	0.13	τ_f 0.14 / τ_s 2.29
Basal BT	-68.8	-30.5	0.10	
Apical RT	-70.6	-29.6	0.29	τ_f 0.58 / τ_s 8.77
$Na_V1.1$	-35[14] / -41[14] /-72[1]	-15[14] / -19[14] / -33[1]	0.67[1]	τ_f 1.4[14] / τ_s 13[14]
$Na_V1.2$	-42[14] / -57[14] / -63[1]	-18[14] / -22[14] / -24[1]	0.78[1,2]	τ_f 2.2[14] / τ_s 47[14]
$Na_V1.3$	-47[3] / -65[2] to -69[1,2]	-12[3] / -23[1,2] to -26[2]	0.81[1,2,3] to 1.5[2,13]	2.5[3] / <5[13]
$Na_V1.4$	-50[15] / -56[2]	-26[2] to -30[2]	0.8[12]	<10[12]
$Na_V1.6$	-51[14] / -55[14] / -55[2] / -72[1] / -98[2]	-9[2,14] /-17[14] / -29[1] / -38[2]	1.08[1]	3.8[14]
$Na_V1.7$	-40[2] to -80[2]	-31[2] to -45[2]	1[12]	<10[12]
IHCs, mouse[4]	-71.4	-30.5	0.1	
OHC, rat[5] and guinea pig[7]	-84.8[5] (BT) or -92.6[5] (RT) / -82[7]	-45.0[5] / -37[7]		
Utricular HC	-104[8] / -80.1[9] / -80[10]	-39.0[9,10]	About 0.4[9]	
Semicircular type I HC	rat: -84.7[11] gerbil: -102[11] chick: -95.7[6]		chick 0.5[6] / rat 0.25[11]	3.9[6]
Utricular HC[16]	TTX-R[16]: -94 TTX-S[16]: -72	TTX-R[16]: -38 TTX-S[16]: -31	0.2[16]	TTX-R[16]: 0.91 TTX-S[16]: τ_f 0.35 /τ_s 23

1 = Clare *et al.*, (2000); 2 = Catterall *et al.*, (2005); 3 = Meadows *et al.*, (2002); 4 = Marcotti *et al.*, (2003b); 5 = Oliver *et al.*, (1997); 6 = Masetto *et al.*, (2003); 7 = Witt *et al.*, (1994); 8 = Rusch and Eatock (1997); 9 = Chabbert *et al.*, (2003); 10 = Mechaly *et al.*, (2005); 11 = Li *et al.*, (2010); 12 = Cummins *et al.*, (1998), 13 = Cummins *et al.*, (2001); 14 = Smith *et al.*, (1998); 15 = Chahine *et al.*, (1994); 16 = Wooltorton *et al.*, (2007)

4.3.2. Molecular Identity of the rat IHC Sodium Channel

In order to further investigate which Na^+ channel isoform is expressed in rat IHCs, the electrophysiological recordings were complemented with *in situ* hybridisation experiments. Although the materials and methods were successfully tested on MBP (Figure 48) it was not possible to obtain a sufficient signal to noise ratio for most of the target Na^+ channel isoforms. The strongest result was obtained with the RNA probe against $Na_V1.6$, which showed a faint staining within the nervus facialis and possibly spiral ganglion neurons (Figure 49). This stain is probably specific, as the expression of $Na_V1.6$ was previously reported in spiral ganglion neurons (Hossain *et al.*, 2005; Fryatt *et al.*, 2009) and generally at nodes of Ranvier (Boiko *et al.*, 2001). The neurons of the facial nerve, which is located very close to the cochlea (Erixon *et al.*, 2009) are myelinated (Lee *et al.*, 2008), thus a positive stain by RNA probes against $Na_V1.6$ at their Ranvier nodes seems very likely. In contrast, probes failed to specifically stain cochlear hair cells. Possible explanations for a lack of staining could be: 1) cochlear hair cells express splice variants of Na^+ channel isoforms that the RNA probes do not recognise since they were originally designed from dorsal root ganglion neurons (Fukuoka *et al.*, 2008) and are due to that not specific enough; 2) the target mRNA was below detection threshold. It was previously shown that 10 to 20 mRNA copies are needed to specifically stain a cell via digoxigenin labelled RNA probes (Komminoth & Werner, 1997). An accurate assessment of Na^+ channel isoform mRNA expression in rat IHCs using *in situ* hybridisation experiments will probably require the generation of new RNA probes from cochlear tissue in order to maximise the probe specificity. Due to a lack of time this approach could not be undertaken within the scope of this thesis, but could be the content of future work.

Altogether, the electrophysiological data of this study suggest $Na_V1.1$ being functionally expressed in IHCs. The *in situ* hybridisation experiments could not further narrow down, which α subunits are expressed in rat IHCs. Therefore, in order to deepen our knowledge about Na^+ channel α subunit expression in IHCs it was decided to "outsource" the molecular approach and test the expression of Na^+ channel α subunit expression at the protein level via immune histology.

These data were obtained by the Hearing Research Center Tübingen (Molecular Physiology of Hearing, Lab Prof. M. Knipper) and highlight the expression of $Na_V1.1$ and $Na_V1.6$ but not $Na_V1.7$ in cochlear hair cells. $Na_V1.2$ awaits further testing and several antibodies from different companies against $Na_V1.3$ were not working for unknown reasons (unpublished data from our collaborator Prof. M. Knipper, University of Tübingen, Germany - Eckrich *et al*., in preparation).

4.3.3. Comparison with Sodium Currents Expressed in Vertebrate Hair Cells

Previous studies on vertebrate hair cells have investigated sodium currents of OHCs in rat and guinea pigs (Witt *et al.*, 1994; Oliver *et al.*, 1997), vestibular hair cells of mice (Rusch & Eatock, 1997; Chabbert *et al.*, 2003; Wooltorton *et al.*, 2007), vestibular hair cells of birds (Masetto *et al.*, 2003) hair cells of the alligator cochlea (Evans & Fuchs, 1987) or mouse IHCs (Marcotti *et al.*, 2003b). Altogether, the biophysical properties found in this study closely match the results of Marcotti *et al*. (2003) with only small differences in membrane potential of half activation and inactivation. Both studies used very similar experimental conditions such as body temperature as well as solutions designed to mimic perilymph. Hence, a plausible explanation for small differences in the half maximal steady state inactivation and activation is probably found in the different animal model in which currents where studied. Another difference that could account for changes in biophysical properties is the cochlear region from which IHCs were patched. Apical IHCs in this study correspond to a characteristic frequency in the adult animal of 1.5 to 5 kHz (von Bekesy, 1960; Mueller, 1991), in contrast to Marcotti *et al*. (2003) where IHCs were recorded from a region that encodes sound frequencies of 3 to 6 kHz in the adult animal. Moreover, both steady state inactivation and activation were shown to be dependent on the cochlear region in rat IHCs. Therefore, it seems likely that differences between this study and Marcotti *et* al. (2003) are related to slight differences in the cochlear region from which IHCs were patched. Interestingly sodium currents of IHCs express significant differences to most of the sodium currents recorded from other types of hair cells in the inner ear. For example

OHCs and most studies on vestibular hair cells display a current, which inactivates at much more hyperpolarised membrane potentials (shift by up to 30 mV, see Table 6). Also the membrane potential of half maximal activation is shifted by 7 to 15 mV to more positive voltages in IHCs. These results highlight major differences in the current properties that possibly allow the hypothesis that IHCs might express different Na^+ channel isoforms than OHCs. This hypothesis is backed up by a recent study, which describes two different populations of sodium currents in immature utricular hair cells (Wooltorton *et al.*, 2007). The first one is tetrodotoxin resistant and displays properties that are very close to those of the sodium current in OHCs and vestibular hair cells, whereas the second sodium current is tetrodotoxin sensitive and closely matches the sodium current found in IHCs.

4.3.4. The Sodium Current of IHCs is Physiologically Active

When investigating a potential function of the sodium current in IHCs it is essential to know if this current is active in physiological conditions. This becomes especially important, considering many previous studies that have concluded from the very negative steady state inactivation that sodium currents of vertebrate hair cells are likely to be silent at physiological membrane potentials (Witt *et al.*, 1994; Oliver *et al.*, 1997; Rusch & Eatock, 1997; Chabbert *et al.*, 2003; Masetto *et al.*, 2003). On the contrary, IHCs seem to express a different sodium current, which is available at physiological conditions. In order to discuss availability under physiological conditions it is essential to know at which physiological membrane potentials IHCs operate. Estimates can be drawn from the long lasting current clamp experiments of this study. These highlight that at the postnatal age at which the sodium current expression peaks, the resting membrane potential appears to be around -55 mV. This is close to resting membrane potentials described in immature IHCs (Glowatzki & Fuchs, 2002; Marcotti *et al.*, 2003a; Johnson *et al.*, 2011a; Johnson *et al.*, 2011b). Several different mechanisms and events can change this membrane potential. These can be depolarising, such as spontaneous action potentials, which have been shown to reach membrane potentials of -10 to -20 mV at their peak (Figure 24, 25 andFigure 29;

Glowatzki and Fuchs, 2002; Brandt *et al*. 2007; Johnson *et al*. 2011). Or they can be hyperpolarising, such as the afterhyperpolarising phase of an action potential or inhibitory postsynaptic potentials elicited through the hyperpolarising action of ACh released from the efferent system. These inhibitory events have shown to hyperpolarise the IHCs membrane potential to values of below -65 mV (Figure 50 and Goutman *et al*., 2005). This means that rat IHCs could potentially recruit between 5 and 50 % of the Na^+ channels close to physiological conditions during the first postnatal week. During the second week, where the resting membrane potential becomes more hyperpolarised the fraction of available Na^+ channels could be even higher. These data suggest that the sodium current found in immature IHCs is physiologically not silent.

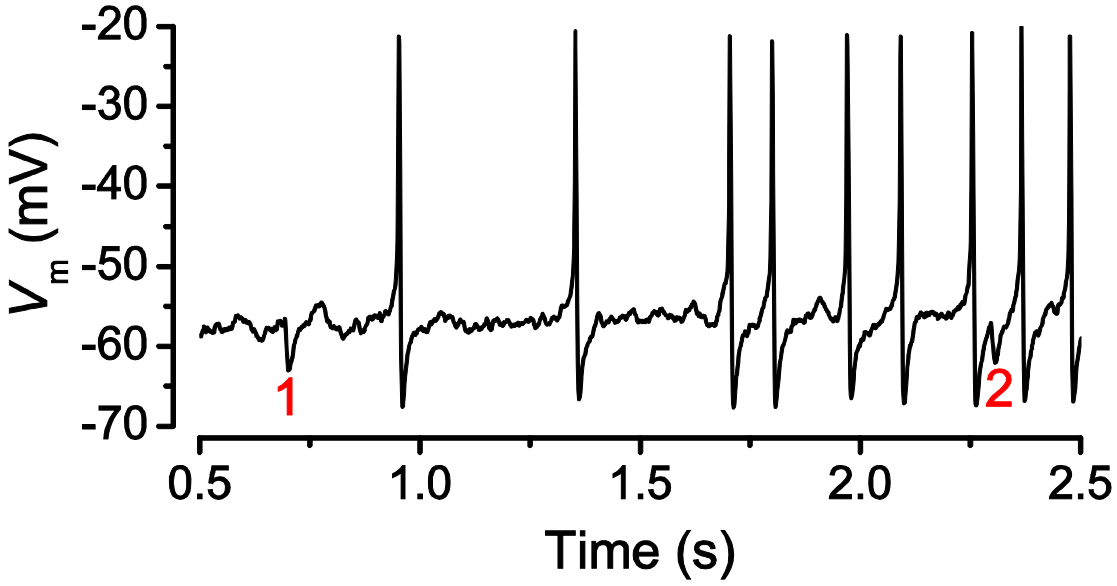

Figure 50: Whole cell current Clamp recording of a rat P2 basal IHC. Resting membrane potential and the threshold potential from which action potentials were triggered was -57.1 mV. The voltage range of this cell was between -68 mV to -17 mV. Considering the steady state inactivation this would correspond to 8 to 47 % of Na^+ channels being available at rest or at membrane potentials occurring during the afterhyperpolarisation phase or inhibitory postsynaptic potentials (two examples of the latter are indicated by numbers 1 and 2) prior to an action potential depolarisation.

4.3.5. Is the Sodium Current involved in Action Potential Generation?

One of the key questions that still remains open for discussion, is why IHCs transiently express a sodium current during immature development. The expression pattern shows that the peak sodium current amplitude is maximal during the first postnatal week (Figure 40) and is then down regulated during the second postnatal week. By the onset of hearing the sodium current is no longer detectable. This transient expression limited to immature development was previously reported for vertebrate hair cells and strongly suggests that sodium currents might play a key role in hair cell maturation (Chabbert *et al.*, 2003; Marcotti *et al.*, 2003b; Wooltorton *et al.*, 2007). The expression pattern of Na^+ channels in rat IHCs over postnatal development is congruent with the generation of spontaneous action potential activity (Figure 26). Therefore, it seems very likely that sodium currents are significantly involved in shaping the action potentials. To back up this hypothesis an action potential protocol was applied in voltage clamp (Figure 47). Results show a peak sodium current of up to -300 pA (mean -200.3 pA ± 32.5 pA, n = 4) occurring just before the peak of the action potential itself, indicating that sodium currents in IHCs seems to have a classical role in speeding up the upstroke of action potentials (Hille, 2001). Previously this was shown by tetrodotoxin application under which the action potential waveform significantly widens (Marcotti *et al.*, 2003b).

4.3.5. Does the Sodium Current modulate the Frequency or Pattern of the Spontaneous Action Potential Activity?

As stated above, one of the findings of this study was the significant difference in the membrane potential at which first action potentials are generated (spike threshold) depending on cochlear region (Figure 30). Apical IHCs start to generate action potentials at more depolarised membrane potentials, which indicates that possible differences in the action potential generation between IHCs of the apical and basal coil exist. The lower spike threshold of basal IHCs could for example be explained by a current that activates from

more hyperpolarised membrane potentials. Likely candidates could be the calcium or sodium current as they are directly involved in action potential generation. To date no differences in the membrane potential of activation of the calcium channel have been found as a function of cochlear region (Figure 42 and Figure 44; Johnson & Marcotti, 2008). However, a significant difference in the membrane potential of half maximal activation and inactivation of the sodium current was found in this thesis, although it remains elusive how this could influence the spike threshold. It would be interesting to quantify the expression level of α and β subunits of the Na^+ channel as a function of cochlear region since these are known to modulate the voltage dependencies of the current. Possibly a molecular approach could highlight subtle differences in the channel composition (Smith *et al.*, 1998; Royeck *et al.*, 2008; Chahine & O'Leary, 2011).

4.3.6. Role of Sodium Currents in Inner Hair Cell Development

Spontaneous action potentials facilitate periodic calcium influx that is thought to orchestrate developmental changes in gene expression (Johnson *et al.*, 2011b). Changes in gene expression have been shown to be dependent on the amplitude, temporal pattern and frequency of the calcium influx (Buonanno & Fields, 1999; Fields *et al.*, 2005; Moody & Bosma, 2005). As stated above, the sodium current is directly involved in shaping the action potential, thus it seems very likely that it also takes part in shaping the calcium influx. Assuming that calcium influx changes gene expression in IHCs, the sodium currents would be indirectly involved in this mechanism as well.

4.3.7. Role of Sodium Currents in the Development of the Auditory Pathway

The role of the sodium current in development might not be limited to the IHC level. Another potential mechanism could exist by which sodium currents of IHCs modulate auditory development. It was shown that the pattern and frequency of spontaneous action potential activity differs as a function of cochlear region. Several results such as the availability at rest and activation of the sodium current during an action potential highlight its involvement in action potential generation. Furthermore, several biophysical properties of the sodium current, such as amplitude, voltage dependent activation and steady state inactivation depend on cochlear region and might influence the pattern of action potential activity. Therefore, it is possible that the sodium current contributes to tonotopic differences in IHC spiking activity. Should the spontaneous activity lead to the refinement of synaptic connections, such as the tonotopic organisation in the auditory pathway, then it seems very likely that sodium currents are needed for normal development. Furthermore, under the condition that the frequency and pattern of spontaneous action potential activity instructs developmental roles, such as the tonotopic organisation of the auditory pathway, it seems very plausible that the sodium current takes an active part in the developmental program through shaping the pattern of electric activity.

4.3.8. Could the Sodium Current support Spontaneous Action Potential Activity?

The action potential activity described here and in other rodent IHCs (Johnson *et al.*, 2011b) seems to appear at a higher frequency than in other spontaneous systems such as the retina (Moody & Bosma, 2005). It is unknown, which strains are put on an individual IHC in order to maintain frequent spiking. However, one could imagine that an increased amount of energy is needed in order to recycle calcium not only to avoid "overloading" the cell with calcium, but also in order to maintain the extracellular calcium concentration at optimum levels. It was reported that the external calcium concentration has a direct effect

on the voltage dependent activation of voltage gated ion channels in the following manner: lowering the extracellular calcium concentration shifts the activation curve of sodium currents towards hyperpolarised membrane potentials (Hille, 2001). It has been further shown that action potentials can lower the extracellular calcium concentration, which again lowers the amplitude of calcium currents (Borst & Sakmann, 1999). This could lead to an increased sodium current, which could potentially support action potential generation in IHCs when extracellular calcium concentrations are lowered. However, further experiments with altered extracellular calcium concentrations would be needed to prove or disprove a possible interplay between calcium concentration and sodium current activation in IHCs.

5. Conclusion

The aims of this thesis were to characterise both spontaneous electric activity and the sodium current as a function of postnatal development and frequency position along the cochlea. The data provided here show that IHCs do not generate intrinsic spontaneous activity randomly. The difference in spiking pattern along the cochlea provides strong evidence for the hypothesis that spontaneous activity instructs tonotopic maps within the auditory pathway. Furthermore, the calcium dependent action potentials are likely to orchestrate differences in gene expression.

The biophysical properties of the Na^+ channel provide evidence that the sodium current is involved in the mechanism that generates spontaneous activity. Therefore, it is likely that the sodium current is involved in IHC development, especially considering its transient expression during immature stages. However, some ideas provided in this thesis need further investigation. For example, we still know very little about the role and function of spontaneous action potential activity itself. By increasing this knowledge, the functional role of the sodium current could be further highlighted. Therefore, it might be a fruitful venture to further study the spontaneous action potential activity by, for example, altering it *in vivo* and monitoring on the physiological consequences in the normal development and function of the cochlea. However, modulating the spontaneous activity is a very challenging task, as one would probably have to design a genetically altered animal model with aberrant spontaneous action potential activity, but without additional side effects. One way of modulating spontaneous action potential activity could for instance be, to knock out one of the channels involved in action potential generation. Rather than knocking out channels that are also needed for mature function, like the $Ca_V1.3$ Ca^{2+} channel it seems interesting to target one of the channels that are only transiently expressed. The Na^+ channel would be a suited candidate, as it has been shown in a previous study that under TTX perfusion, mouse IHCs are still able to generate calcium action potentials, but with an altered shape and frequency (Marcotti *et al.*, 2003b). This thesis provides novel data that the sodium current in IHCs is likely to be carried by the Na^+ channel isoform $Na_V1.1$. In addition with the collaborative work performed by the Hearing Research Center Tübingen

(Molecular Physiology of Hearing, Lab Prof. M. Knipper) $Na_V1.6$ was positively stained via immunolabeling. A knock out of one of these isoforms or a double knock out could be therefore an interesting target for a conditional knockout. Another possible future study could also involve molecular approaches in order to reveal the β subunits of the Na^+ channel that are expressed in IHCs, as these are directly modulating the sodium current (Smith & Goldin, 1998; Smith *et al.*, 1998).

6. Reference List

Akopian AN, Souslova V, England S, Okuse K, Ogata N, Ure J, Smith A, Kerr BJ, McMahon SB, Boyce S, Hill R, Stanfa LC, Dickenson AH, & Wood JN (1999). The tetrodotoxin-resistant sodium channel SNS has a specialized function in pain pathways. *Nat Neurosci* **2**, 541-548.

Anniko M & Wroblewski R (1986). Ionic environment of cochlear hair cells. *Hear Res* **22**, 279-293.

Armstrong CM (1981). Sodium channels and gating currents. *Physiol Rev* **61**, 644-683.

Beckh S (1990). Differential expression of sodium channel mRNAs in rat peripheral nervous system and innervated tissues. *FEBS Lett* **262**, 317-322.

Beckh S, Noda M, Lubbert H, & Numa S (1989). Differential regulation of three sodium channel messenger RNAs in the rat central nervous system during development. *EMBO J* **8**, 3611-3616.

Beneski DA & Catterall WA (1980). Covalent labeling of protein components of the sodium channel with a photoactivable derivative of scorpion toxin. *Proc Natl Acad Sci U S A* **77**, 639-643.

Beurg M, Evans MG, Hackney CM, & Fettiplace R (2006). A large-conductance calcium-selective mechanotransducer channel in mammalian cochlear hair cells. *J Neurosci* **26**, 10992-11000.

Beurg M, Fettiplace R, Nam JH, & Ricci AJ (2009). Localization of inner hair cell mechanotransducer channels using high-speed calcium imaging. *Nat Neurosci* **12**, 553-558.

Beutner D & Moser T (2001). The presynaptic function of mouse cochlear inner hair cells during development of hearing. *J Neurosci* **21**, 4593-4599.

Beutner D, Voets T, Neher E, & Moser T (2001). Calcium dependence of exocytosis and endocytosis at the cochlear inner hair cell afferent synapse. *Neuron* **29**, 681-690.

Blankenship AG & Feller MB (2010). Mechanisms underlying spontaneous patterned activity in developing neural circuits. *Nat Rev Neurosci* **11**, 18-29.

Blatchley BJ, Cooper WA, & Coleman JR (1987). Development of auditory brainstem response to tone pip stimuli in the rat. *Brain Res* **429**, 75-84.

Boiko T, Rasband MN, Levinson SR, Caldwell JH, Mandel G, Trimmer JS, & Matthews G (2001). Compact myelin dictates the differential targeting of two sodium channel isoforms in the same axon. *Neuron* **30**, 91-104.

Bok J, Chang W, & Wu DK (2007). Patterning and morphogenesis of the vertebrate inner ear. *Int J Dev Biol* **51**, 521-533.

Borst JG & Sakmann B (1999). Depletion of calcium in the synaptic cleft of a calyx-type synapse in the rat brainstem. *J Physiol* **521 Pt 1**, 123-133.

Bosher SK & Warren RL (1971). A study of the electrochemistry and osmotic relationships of the cochlear fluids in the neonatal rat at the time of the development of the endocochlear potential. *J Physiol* **212**, 739-761.

Brackenbury WJ & Isom LL (2011). Na Channel beta Subunits: Overachievers of the Ion Channel Family. *Front Pharmacol* **2**, 53.

Brandt A, Khimich D, & Moser T (2005). Few CaV1.3 channels regulate the exocytosis of a synaptic vesicle at the hair cell ribbon synapse. *J Neurosci* **25**, 11577-11585.

Brandt A, Striessnig J, & Moser T (2003). CaV1.3 channels are essential for development and presynaptic activity of cochlear inner hair cells. *J Neurosci* **23**, 10832-10840.

Brandt N, Kuhn S, Munkner S, Braig C, Winter H, Blin N, Vonthein R, Knipper M, & Engel J (2007). Thyroid hormone deficiency affects postnatal spiking activity and expression of Ca2+ and K+ channels in rodent inner hair cells. *J Neurosci* **27**, 3174-3186.

Brownell WE, Bader CR, Bertrand D, & de Ribaupierre Y (1985). Evoked mechanical responses of isolated cochlear outer hair cells. *Science* **227**, 194-196.

Buonanno A & Fields RD (1999). Gene regulation by patterned electrical activity during neural and skeletal muscle development. *Curr Opin Neurobiol* **9**, 110-120.

Carafoli E, Santella L, Branca D, & Brini M (2001). Generation, control, and processing of cellular calcium signals. *Crit Rev Biochem Mol Biol* **36**, 107-260.

Catterall WA (1980). Neurotoxins that act on voltage-sensitive sodium channels in excitable membranes. *Annu Rev Pharmacol Toxicol* **20**, 15-43.

Catterall WA (1986). Voltage-dependent gating of sodium channels: correlating structure and function. *Trends Neurosci* **9**, 10.

Catterall WA (1992). Cellular and molecular biology of voltage-gated sodium channels. *Physiol Rev* **72**, S15-S48.

Catterall WA (2000). From ionic currents to molecular mechanisms: the structure and function of voltage-gated sodium channels. *Neuron* **26**, 13-25.

Catterall WA, Goldin AL, & Waxman SG (2003). International Union of Pharmacology. XXXIX. Compendium of voltage-gated ion channels: sodium channels. *Pharmacol Rev* **55**, 575-578.

Catterall WA, Goldin AL, & Waxman SG (2005). International Union of Pharmacology. XLVII. Nomenclature and structure-function relationships of voltage-gated sodium channels. *Pharmacol Rev* **57**, 397-409.

Chabbert C, Mechaly I, Sieso V, Giraud P, Brugeaud A, Lehouelleur J, Couraud F, Valmier J, & Sans A (2003). Voltage-gated Na+ channel activation induces both action potentials in utricular hair cells and brain-derived neurotrophic factor release in the rat utricle during a restricted period of development. *J Physiol* **553**, 113-123.

Chahine M, Bennett PB, George AL, Jr., & Horn R (1994). Functional expression and properties of the human skeletal muscle sodium channel. *Pflugers Arch* **427**, 136-142.

Chahine M & O'Leary ME (2011). Regulatory Role of Voltage-Gated Na Channel beta Subunits in Sensory Neurons. *Front Pharmacol* **2**, 70.

Chatterjee S, Kraus P, & Lufkin T (2010). A symphony of inner ear developmental control genes. *BMC Genet* **11**, 68.

Chen C, Bharucha V, Chen Y, Westenbroek RE, Brown A, Malhotra JD, Jones D, Avery C, Gillespie PJ, III, Kazen-Gillespie KA, Kazarinova-Noyes K, Shrager P, Saunders TL, Macdonald RL, Ransom BR, Scheuer T, Catterall WA, & Isom LL (2002a). Reduced sodium channel density, altered voltage dependence of inactivation, and increased susceptibility to seizures in mice lacking sodium channel beta 2-subunits. *Proc Natl Acad Sci U S A* **99**, 17072-17077.

Chen P, Johnson JE, Zoghbi HY, & Segil N (2002b). The role of Math1 in inner ear development: Uncoupling the establishment of the sensory primordium from hair cell fate determination. *Development* **129**, 2495-2505.

Chen P & Segil N (1999). p27(Kip1) links cell proliferation to morphogenesis in the developing organ of Corti. *Development* **126**, 1581-1590.

Chioni AM, Brackenbury WJ, Calhoun JD, Isom LL, & Djamgoz MB (2009). A novel adhesion molecule in human breast cancer cells: voltage-gated Na+ channel beta1 subunit. *Int J Biochem Cell Biol* **41**, 1216-1227.

Clare JJ, Tate SN, Nobbs M, & Romanos MA (2000). Voltage-gated sodium channels as therapeutic targets. *Drug Discov Today* **5**, 506-520.

Corwin JT (1992). Regeneration in the auditory system. *Exp Neurol* **115**, 7-12.

Cummins TR, Aglieco F, Renganathan M, Herzog RI, Dib-Hajj SD, & Waxman SG (2001). Nav1.3 sodium channels: rapid repriming and slow closed-state inactivation display quantitative differences after expression in a mammalian cell line and in spinal sensory neurons. *J Neurosci* **21**, 5952-5961.

Cummins TR, Howe JR, & Waxman SG (1998). Slow closed-state inactivation: a novel mechanism underlying ramp currents in cells expressing the hNE/PN1 sodium channel. *J Neurosci* **18**, 9607-9619.

Dallos P & Fakler B (2002). Prestin, a new type of motor protein. *Nat Rev Mol Cell Biol* **3**, 104-111.

Dallos P, Zheng J, & Cheatham MA (2006). Prestin and the cochlear amplifier. *J Physiol* **576**, 37-42.

Dannhof BJ & Bruns V (1993). The innervation of the organ of Corti in the rat. *Hear Res* **66**, 8-22.

Deisseroth K, Mermelstein PG, Xia H, & Tsien RW (2003). Signaling from synapse to nucleus: the logic behind the mechanisms. *Curr Opin Neurobiol* **13**, 354-365.

Dietrich PS, McGivern JG, Delgado SG, Koch BD, Eglen RM, Hunter JC, & Sangameswaran L (1998). Functional analysis of a voltage-gated sodium channel and its splice variant from rat dorsal root ganglia. *J Neurochem* **70**, 2262-2272.

Driver EC & Kelley MW (2009). Specification of cell fate in the mammalian cochlea. *Birth Defects Res C Embryo Today* **87**, 212-221.

Eatock RA, Corey DP, & Hudspeth AJ (1987). Adaptation of mechanoelectrical transduction in hair cells of the bullfrog's sacculus. *J Neurosci* **7**, 2821-2836.

Eatock RA & Hurley KM (2003). Functional development of hair cells. *Curr Top Dev Biol* **57**, 389-448.

Ehret G (1977). Postnatal development in the acoustic system of the house mouse in the light of developing masked thresholds. *J Acoust Soc Am* **62**, 143-148.

Elgoyhen AB, Johnson DS, Boulter J, Vetter DE, & Heinemann S (1994). Alpha 9: an acetylcholine receptor with novel pharmacological properties expressed in rat cochlear hair cells. *Cell* **79**, 705-715.

Elgoyhen AB, Vetter DE, Katz E, Rothlin CV, Heinemann SF, & Boulter J (2001). alpha10: a determinant of nicotinic cholinergic receptor function in mammalian vestibular and cochlear mechanosensory hair cells. *Proc Natl Acad Sci U S A* **98**, 3501-3506.

Engel J, Braig C, Ruttiger L, Kuhn S, Zimmermann U, Blin N, Sausbier M, Kalbacher H, Munkner S, Rohbock K, Ruth P, Winter H, & Knipper M (2006). Two classes of outer hair cells along the tonotopic axis of the cochlea. *Neuroscience* **143**, 837-849.

Erixon E, Hogstorp H, Wadin K, & Rask-Andersen H (2009). Variational anatomy of the human cochlea: implications for cochlear implantation. *Otol Neurotol* **30**, 14-22.

Evans MG & Fuchs PA (1987). Tetrodotoxin-sensitive, voltage-dependent sodium currents in hair cells from the alligator cochlea. *Biophys J* **52**, 649-652.

Fekete DM & Wu DK (2002). Revisiting cell fate specification in the inner ear. *Curr Opin Neurobiol* **12**, 35-42.

Felts PA, Yokoyama S, Dib-Hajj S, Black JA, & Waxman SG (1997). Sodium channel alpha-subunit mRNAs I, II, III, NaG, Na6 and hNE (PN1): different expression patterns in developing rat nervous system. *Brain Res Mol Brain Res* **45**, 71-82.

Fettiplace R (2006). Active hair bundle movements in auditory hair cells. *J Physiol* **576**, 29-36.

Fields RD, Lee PR, & Cohen JE (2005). Temporal integration of intracellular Ca2+ signaling networks in regulating gene expression by action potentials. *Cell Calcium* **37**, 433-442.

Firth SI, Wang CT, & Feller MB (2005). Retinal waves: mechanisms and function in visual system development. *Cell Calcium* **37**, 425-432.

Forsythe ID (2007). Hearing: a fantasia on Kolliker's organ. *Nature* **450**, 43-44.

Fozzard HA & Lipkind GM (2010). The tetrodotoxin binding site is within the outer vestibule of the sodium channel. *Mar Drugs* **8**, 219-234.

Fryatt AG, Vial C, Mulheran M, Gunthorpe MJ, & Grubb BD (2009). Voltage-gated sodium channel expression in rat spiral ganglion neurons. *Mol Cell Neurosci* **42**, 399-407.

Fuchs PA & Evans MG (1990). Potassium currents in hair cells isolated from the cochlea of the chick. *J Physiol* **429**, 529-551.

Fuchs PA, Glowatzki E, & Moser T (2003). The afferent synapse of cochlear hair cells. *Curr Opin Neurobiol* **13**, 452-458.

Fukuoka T, Kobayashi K, Yamanaka H, Obata K, Dai Y, & Noguchi K (2008). Comparative study of the distribution of the alpha-subunits of voltage-gated sodium channels in normal and axotomized rat dorsal root ganglion neurons. *J Comp Neurol* **510**, 188-206.

Furness DN, Hackney CM, & Evans MG (2010). Localisation of the mechanotransducer channels in mammalian cochlear hair cells provides clues to their gating. *J Physiol* **588**, 765-772.

Garstang M (2004). Long-distance, low-frequency elephant communication. *J Comp Physiol A Neuroethol Sens Neural Behav Physiol* **190**, 791-805.

Geal-Dor M, Freeman S, Li G, & Sohmer H (1993). Development of hearing in neonatal rats: air and bone conducted ABR thresholds. *Hear Res* **69**, 236-242.

Geisler CD (1998). *From Sound to Synapse* Oxford University Press, New York.

Glowatzki E & Fuchs PA (2000). Cholinergic synaptic inhibition of inner hair cells in the neonatal mammalian cochlea. *Science* **288**, 2366-2368.

Glowatzki E & Fuchs PA (2002). Transmitter release at the hair cell ribbon synapse. *Nat Neurosci* **5**, 147-154.

Gnuegge L, Schmid S, & Neuhauss SC (2001). Analysis of the activity-deprived zebrafish mutant macho reveals an essential requirement of neuronal activity for the development of a fine-grained visuotopic map. *J Neurosci* **21**, 3542-3548.

Goldin AL (1999). Diversity of mammalian voltage-gated sodium channels. *Ann N Y Acad Sci* **868**, 38-50.

Goldin AL (2001). Resurgence of sodium channel research. *Annu Rev Physiol* **63**, 871-894.

Goldin AL (2002). Evolution of voltage-gated Na(+) channels. *J Exp Biol* **205**, 575-584.

Goldin AL, Barchi RL, Caldwell JH, Hofmann F, Howe JR, Hunter JC, Kallen RG, Mandel G, Meisler MH, Netter YB, Noda M, Tamkun MM, Waxman SG, Wood JN, & Catterall WA (2000). Nomenclature of voltage-gated sodium channels. *Neuron* **28**, 365-368.

Gomez-Casati ME, Fuchs PA, Elgoyhen AB, & Katz E (2005). Biophysical and pharmacological characterization of nicotinic cholinergic receptors in rat cochlear inner hair cells. *J Physiol* **566**, 103-118.

Goutman JD, Fuchs PA, Glowatzki E (2005). Facilitating efferent inhibition of inner hair cells in the cochlea of the neonatal rat. *J Physiol* **566**, 49-59.

Grubb MS & Thompson ID (2004). The influence of early experience on the development of sensory systems. *Curr Opin Neurobiol* **14**, 503-512.

Hafidi A, Beurg M, & Dulon D (2005). Localization and developmental expression of BK channels in mammalian cochlear hair cells. *Neuroscience* **130**, 475-484.

Hall JW, III (2000). Development of the ear and hearing. *J Perinatol* **20**, S12-S20.

Halliwell JV, Plant TD, & Standen NB (1994). Voltage clamp techniques. In *Microelectrode Techniques - The Plymouth Workshop Handbook*, ed. Ogden D, pp. 17-35. The Company of Biologists Limited, Cambridge.

Hanlon MR & Wallace BA (2002). Structure and function of voltage-dependent ion channel regulatory beta subunits. *Biochemistry* **41**, 2886-2894.

Hanson MG & Landmesser LT (2004). Normal patterns of spontaneous activity are required for correct motor axon guidance and the expression of specific guidance molecules. *Neuron* **43**, 687-701.

Heinemann SH, Terlau H, Stuhmer W, Imoto K, & Numa S (1992). Calcium channel characteristics conferred on the sodium channel by single mutations. *Nature* **356**, 441-443.

Heldmaier G & Neuweiler G (2003). Vergleichende Tierphysiologie Vol 1: Neuro- und Sinnesphysiologie. *Springer Verlag*.

Hibino H, Nin F, Tsuzuki C, & Kurachi Y (2010). How is the highly positive endocochlear potential formed? The specific architecture of the stria vascularis and the roles of the ion-transport apparatus. *Pflugers Arch* **459**, 521-533.

Hille B (1992). *Ionic Channels of Excitable Membranes*, second ed. Sinauer Associates Inc., Sunderland, Massachusetts.

Hille B (2001). *Ion Channels of Excitable Membranes*, Third ed. Sinauer Associates, Inc., Sunderland, Massachusetts U.S.A.

Hodgkin AL, Huxley AF, & Katz B (1952). Measurement of current-voltage relations in the membrane of the giant axon of Loligo. *J Physiol* **116**, 424-448.

Holley MC (2005). Keynote review: The auditory system, hearing loss and potential targets for drug development. *Drug Discov Today* **10**, 1269-1282.

Hossain WA, Antic SD, Yang Y, Rasband MN, & Morest DK (2005). Where is the spike generator of the cochlear nerve? Voltage-gated sodium channels in the mouse cochlea. *J Neurosci* **25**, 6857-6868.

Housley GD, Marcotti W, Navaratnam D, & Yamoah EN (2006). Hair cells--beyond the transducer. *J Membr Biol* **209**, 89-118.

Howard J & Hudspeth AJ (1987). Mechanical relaxation of the hair bundle mediates adaptation in mechanoelectrical transduction by the bullfrog's saccular hair cell. *Proc Natl Acad Sci U S A* **84**, 3064-3068.

Howorth PW, Thornton SR, O'Brien V, Smith WD, Nikiforova N, Teschemacher AG, & Pickering AE (2009). Retrograde viral vector-mediated inhibition of pontospinal noradrenergic neurons causes hyperalgesia in rats. *J Neurosci* **29**, 12855-12864.

Huang LC, Ryan AF, Cockayne DA, & Housley GD (2006). Developmentally regulated expression of the P2X3 receptor in the mouse cochlea. *Histochem Cell Biol* **125**, 681-692.

Huang LC, Thorne PR, Housley GD, & Montgomery JM (2007). Spatiotemporal definition of neurite outgrowth, refinement and retraction in the developing mouse cochlea. *Development* **134**, 2925-2933.

Huangfu M & Saunders JC (1983). Auditory development in the mouse: structural maturation of the middle ear. *J Morphol* **176**, 249-259.

Hudspeth AJ (1989). How the ear's works work. *Nature* **341**, 397-404.

Hudspeth AJ (1997). How hearing happens. *Neuron* **19**, 947-950.

Isom LL, De Jongh KS, & Catterall WA (1994). Auxiliary subunits of voltage-gated ion channels. *Neuron* **12**, 1183-1194.

Isom LL, Ragsdale DS, De Jongh KS, Westenbroek RE, Reber BF, Scheuer T, & Catterall WA (1995). Structure and function of the beta 2 subunit of brain sodium channels, a transmembrane glycoprotein with a CAM motif. *Cell* **83**, 433-442.

Ito K & Dulon D (2010). Purinergic signaling in cochleovestibular hair cells and afferent neurons. *Purinergic Signal* **6**, 201-209.

Jaffe LA & Cross NL (1986). Electrical regulation of sperm-egg fusion. *Annu Rev Physiol* **48**, 191-200.

Jia S, Dallos P, & He DZ (2007). Mechanoelectric transduction of adult inner hair cells. *J Neurosci* **27**, 1006-1014.

Johnson SL, Adelman JP, & Marcotti W (2007). Genetic deletion of SK2 channels in mouse inner hair cells prevents the developmental linearization in the Ca2+ dependence of exocytosis. *J Physiol* **583**, 631-646.

Johnson SL, Beurg M, Marcotti W, & Fettiplace R (2011a). Prestin-driven cochlear amplification is not limited by the outer hair cell membrane time constant. *Neuron* **70**, 1143-1154.

Johnson SL, Eckrich T, Kuhn S, Zampini V, Franz C, Ranatunga KM, Roberts TP, Masetto S, Knipper M, Kros CJ, & Marcotti W (2011b). Position-dependent patterning of spontaneous action potentials in immature cochlear inner hair cells. *Nat Neurosci* **14**, 711-717.

Johnson SL, Forge A, Knipper M, Munkner S, & Marcotti W (2008). Tonotopic variation in the calcium dependence of neurotransmitter release and vesicle pool replenishment at mammalian auditory ribbon synapses. *J Neurosci* **28**, 7670-7678.

Johnson SL & Marcotti W (2008). Biophysical properties of CaV1.3 calcium channels in gerbil inner hair cells. *J Physiol* **586**, 1029-1042.

Johnson SL, Marcotti W, & Kros CJ (2005). Increase in efficiency and reduction in Ca2+ dependence of exocytosis during development of mouse inner hair cells. *J Physiol* **563**, 177-191.

Jorgensen MB & Kanneworff M (1998). Middle ear transmission in the grass frog, Rana temporaria. *J Comp Physiol A* **182**, 59-64.

Kallen RG, Sheng ZH, Yang J, Chen LQ, Rogart RB, & Barchi RL (1990). Primary structure and expression of a sodium channel characteristic of denervated and immature rat skeletal muscle. *Neuron* **4**, 233-242.

Kandler K, Clause A, & Noh J (2009). Tonotopic reorganization of developing auditory brainstem circuits. *Nat Neurosci* **12**, 711-717.

Katz LC & Shatz CJ (1996). Synaptic activity and the construction of cortical circuits. *Science* **274**, 1133-1138.

Kennedy HJ, Crawford AC, & Fettiplace R (2005). Force generation by mammalian hair bundles supports a role in cochlear amplification. *Nature* **433**, 880-883.

Kennedy HJ, Evans MG, Crawford AC, & Fettiplace R (2006). Depolarization of cochlear outer hair cells evokes active hair bundle motion by two mechanisms. *J Neurosci* **26**, 2757-2766.

Knirsch M, Brandt N, Braig C, Kuhn S, Hirt B, Munkner S, Knipper M, & Engel J (2007). Persistence of Ca(v)1.3 Ca2+ channels in mature outer hair cells supports outer hair cell afferent signaling. *J Neurosci* **27**, 6442-6451.

Komminoth P & Werner M (1997). Target and signal amplification: approaches to increase the sensitivity of in situ hybridization. *Histochem Cell Biol* **108**, 325-333.

Kros CJ (2007). How to build an inner hair cell: challenges for regeneration. *Hear Res* **227**, 3-10.

Kros CJ & Crawford AC (1990). Potassium currents in inner hair cells isolated from the guinea-pig cochlea. *J Physiol* **421**, 263-291.

Kros CJ, Ruppersberg JP, & Rusch A (1998). Expression of a potassium current in inner hair cells during development of hearing in mice. *Nature* **394**, 281-284.

Kubisch C, Schroeder BC, Friedrich T, Lutjohann B, El-Amraoui A, Marlin S, Petit C, & Jentsch TJ (1999). KCNQ4, a novel potassium channel expressed in sensory outer hair cells, is mutated in dominant deafness. *Cell* **96**, 437-446.

Land MF & Fernald RD (1992). The evolution of eyes. *Annu Rev Neurosci* **15**, 1-29.

Lee SJ, Lim AY, Lim IJ, Lim TC, & Pho RW (2008). Innervation of the Face Studied Using Modifications to Sihler's Technique in a Primate Model. *Plast Reconstr Surg* **121**, 1188-1205.

Lee YS, Liu F, & Segil N (2006). A morphogenetic wave of p27Kip1 transcription directs cell cycle exit during organ of Corti development. *Development* **133**, 2817-2826.

Lenoir M, Puel JL, & Pujol R (1987). Stereocilia and tectorial membrane development in the rat cochlea. A SEM study. *Anat Embryol (Berl)* **175**, 477-487.

Li GQ, Meredith FL, & Rennie KJ (2010). Development of K(+) and Na(+) conductances in rodent postnatal semicircular canal type I hair cells. *Am J Physiol Regul Integr Comp Physiol* **298**, R351-R358.

Liberman MC (1980). Morphological differences among radial afferent fibers in the cat cochlea: an electron-microscopic study of serial sections. *Hear Res* **3**, 45-63.

Liberman MC, Dodds LW, & Pierce S (1990). Afferent and efferent innervation of the cat cochlea: quantitative analysis with light and electron microscopy. *J Comp Neurol* **301**, 443-460.

Liberman MC, Gao J, He DZ, Wu X, Jia S, & Zuo J (2002). Prestin is required for electromotility of the outer hair cell and for the cochlear amplifier. *Nature* **419**, 300-304.

Liegeois JF, Mercier F, Graulich A, Graulich-Lorge F, Scuvee-Moreau J, & Seutin V (2003). Modulation of small conductance calcium-activated potassium (SK) channels: a new challenge in medicinal chemistry. *Curr Med Chem* **10**, 625-647.

Lukashkin AN, Richardson GP, & Russell IJ (2010). Multiple roles for the tectorial membrane in the active cochlea. *Hear Res* **266**, 26-35.

Maffei L & Galli-Resta L (1990). Correlation in the discharges of neighboring rat retinal ganglion cells during prenatal life. *Proc Natl Acad Sci U S A* **87**, 2861-2864.

Maison SF & Liberman MC (2000). Predicting vulnerability to acoustic injury with a noninvasive assay of olivocochlear reflex strength. *J Neurosci* **20**, 4701-4707.

Maison SF, Luebke AE, Liberman MC, & Zuo J (2002). Efferent protection from acoustic injury is mediated via alpha9 nicotinic acetylcholine receptors on outer hair cells. *J Neurosci* **22**, 10838-10846.

Mammano F, Bortolozzi M, Ortolano S, & Anselmi F (2007). Ca2+ signaling in the inner ear. *Physiology (Bethesda)* **22**, 131-144.

Mann ZF & Kelley MW (2011). Development of tonotopy in the auditory periphery. *Hear Res* **276**, 2-15.

Marcotti W (2012). 2011 Sharpey-Schafer Lecture: Functional assembly of mammalian cochlear hair cells. *J Physiol* epub. ahead of print.

Marcotti W, Geleoc GS, Lennan GW, & Kros CJ (1999). Transient expression of an inwardly rectifying potassium conductance in developing inner and outer hair cells along the mouse cochlea. *Pflugers Arch* **439**, 113-122.

Marcotti W, Johnson SL, Holley MC, & Kros CJ (2003a). Developmental changes in the expression of potassium currents of embryonic, neonatal and mature mouse inner hair cells. *J Physiol* **548**, 383-400.

Marcotti W, Johnson SL, Rusch A, & Kros CJ (2003b). Sodium and calcium currents shape action potentials in immature mouse inner hair cells. *J Physiol* **552**, 743-761.

Marcotti W, Johnson SL, & Kros CJ (2004). A transiently expressed SK current sustains and modulates action potential activity in immature mouse inner hair cells. *J Physiol* **560**, 691-708.

Marinkovic S, Stankovic P, Strbac M, Tomic I, & Cetkovic M (2011). Cochlea and other spiral forms in nature and art. *Am J Otolaryngol*.

Marston JH & Chang MC (1965). The breeding, management and reproductive physiology of the mongolian gerbil (Meriones unguiculatus). *Lab Anim Care* **15**, 34-48.

Masetto S, Bosica M, Correia MJ, Ottersen OP, Zucca G, Perin P, & Valli P (2003). Na+ currents in vestibular type I and type II hair cells of the embryo and adult chicken. *J Neurophysiol* **90**, 1266-1278.

McClatchey AI, Van den Bergh P, Pericak-Vance MA, Raskind W, Verellen C, McKenna-Yasek D, Rao K, Haines JL, Bird T, Brown RH, Jr., & . (1992). Temperature-sensitive mutations in the III-IV cytoplasmic loop region of the skeletal muscle sodium channel gene in paramyotonia congenita. *Cell* **68**, 769-774.

McLaughlin T, Torborg CL, Feller MB, & O'Leary DD (2003). Retinotopic map refinement requires spontaneous retinal waves during a brief critical period of development. *Neuron* **40**, 1147-1160.

Meadows LS, Chen YH, Powell AJ, Clare JJ, & Ragsdale DS (2002). Functional modulation of human brain Nav1.3 sodium channels, expressed in mammalian cells, by auxiliary beta 1, beta 2 and beta 3 subunits. *Neuroscience* **114**, 745-753.

Mechaly I, Scamps F, Chabbert C, Sans A, & Valmier J (2005). Molecular diversity of voltage-gated sodium channel alpha subunits expressed in neuronal and non-neuronal excitable cells. *Neuroscience* **130**, 389-396.

Meister M, Wong RO, Baylor DA, & Shatz CJ (1991). Synchronous bursts of action potentials in ganglion cells of the developing mammalian retina. *Science* **252**, 939-943.

Meyer RL (1983). Tetrodotoxin inhibits the formation of refined retinotopography in goldfish. *Brain Res* **282**, 293-298.

Moody WJ (1998) Control of spontaneous activity during development. *J Neurobiol* **37**, 97-109

Moody WJ & Bosma MM (2005). Ion channel development, spontaneous activity, and activity-dependent development in nerve and muscle cells. *Physiol Rev* **85**, 883-941.

Morsli H, Choo D, Ryan A, Johnson R, & Wu DK (1998). Development of the mouse inner ear and origin of its sensory organs. *J Neurosci* **18**, 3327-3335.

Moser T, Brandt A, & Lysakowski A (2006). Hair cell ribbon synapses. *Cell Tissue Res* **326**, 347-359.

Mostafapour SP, Cochran SL, Del Puerto NM, & Rubel EW (2000). Patterns of cell death in mouse anteroventral cochlear nucleus neurons after unilateral cochlea removal. *J Comp Neurol* **426**, 561-571.

Mülhardt C, (2008). Der Experimentator: Molekularbiologie / Genomics. *Spektrum Akademischer Verlag*, 6. Aufl.

Mueller M (1991). Developmental changes of frequency representation in the rat cochlea. *Hear Res* **56**, 1-7.

Nayak GD, Ratnayaka HS, Goodyear RJ, & Richardson GP (2007). Development of the hair bundle and mechanotransduction. *Int J Dev Biol* **51**, 597-608.

Neher E (1992). Correction for liquid junction potentials in patch clamp experiments. *Methods Enzymol* **207**, 123-131.

Nikolic P, Housley GD, & Thorne PR (2003). Expression of the P2X7 receptor subunit of the adenosine 5'-triphosphate-gated ion channel in the developing and adult rat cochlea. *Audiol Neurootol* **8**, 28-37.

North RA & Surprenant A (2000). Pharmacology of cloned P2X receptors. *Annu Rev Pharmacol Toxicol* **40**, 563-580.

Nouvian R, Beutner D, Parsons TD, & Moser T (2006). Structure and function of the hair cell ribbon synapse. *J Membr Biol* **209**, 153-165.

Numberger N & Draguhn A (1996). Patch-Clamp-Technik. *Spektrum Akademischer Verlag GmbH, Heidelberg Berlin Oxford.*

Oliver D, Knipper M, Derst C, & Fakler B (2003). Resting potential and submembrane calcium concentration of inner hair cells in the isolated mouse cochlea are set by KCNQ-type potassium channels. *J Neurosci* **23**, 2141-2149.

Oliver D, Plinkert P, Zenner HP, & Ruppersberg JP (1997). Sodium current expression during postnatal development of rat outer hair cells. *Pflugers Arch* **434**, 772-778.

Patino GA & Isom LL (2010). Electrophysiology and beyond: multiple roles of Na+ channel beta subunits in development and disease. *Neurosci Lett* **486**, 53-59.

Patuzzi R & Sellick PM (1983). A comparison between basilar membrane and inner hair cell receptor potential input-output functions in the guinea pig cochlea. *J Acoust Soc Am* **74**, 1734-1741.

Payandeh J, Scheuer T, Zheng N, & Catterall WA (2011). The crystal structure of a voltage-gated sodium channel. *Nature* **475**, 353-358.

Payne RS (1971). Acoustic location of prey by barn owls (Tyto alba). *J Exp Biol* **54**, 535-573.

Penn AA & Shatz CJ (1999). Brain waves and brain wiring: the role of endogenous and sensory-driven neural activity in development. *Pediatr Res* **45**, 447-458.

Pickles JO, Comis SD, & Osborne MP (1984). Cross-links between stereocilia in the guinea pig organ of Corti, and their possible relation to sensory transduction. *Hear Res* **15**, 103-112.

Platzer J, Engel J, Schrott-Fischer A, Stephan K, Bova S, Chen H, Zheng H, & Striessnig J (2000). Congenital deafness and sinoatrial node dysfunction in mice lacking class D L-type Ca2+ channels. *Cell* **102**, 89-97.

Ptacek LJ, George AL, Jr., Griggs RC, Tawil R, Kallen RG, Barchi RL, Robertson M, & Leppert MF (1991). Identification of a mutation in the gene causing hyperkalemic periodic paralysis. *Cell* **67**, 1021-1027.

Pujol R, Lavigne-Rebillard M, & Lenoir M (1998). Development of sensory and neural structures in the mammalian cochlea. In *Development of the Auditory System*, ed. Rubel EW, Popper AN & Fay RR. *Springer, New York* 146-192.

Raphael Y & Altschuler RA (2003). Structure and innervation of the cochlea. *Brain Res Bull* **60**, 397-422.

Richter CP, Emadi G, Getnick G, Quesnel A, & Dallos P (2007). Tectorial membrane stiffness gradients. *Biophys J* **93**, 2265-2276.

Romand R, Romand MR, Mulle C, & Marty R (1980). Early stages of myelination in the spiral ganglion cells of the kitten during development. *Acta Otolaryngol* **90**, 391-397.

Roth B & Bruns V (1992a). Postnatal development of the rat organ of Corti. I. General morphology, basilar membrane, tectorial membrane and border cells. *Anat Embryol (Berl)* **185**, 559-569.

Roth B & Bruns V (1992b). Postnatal development of the rat organ of Corti. II. Hair cell receptors and their supporting elements. *Anat Embryol (Berl)* **185**, 571-581.

Roux I, Wersinger E, McIntosh JM, Fuchs PA, & Glowatzki E (2011). Onset of cholinergic efferent synaptic function in sensory hair cells of the rat cochlea. *J Neurosci* **31**, 15092-15101.

Royeck M, Horstmann MT, Remy S, Reitze M, Yaari Y, & Beck H (2008). Role of axonal NaV1.6 sodium channels in action potential initiation of CA1 pyramidal neurons. *J Neurophysiol* **100**, 2361-2380.

Rubel EW & Fritzsch B (2002). Auditory system development: primary auditory neurons and their targets. *Annu Rev Neurosci* **25**, 51-101.

Ruben RJ (1967). Development of the inner ear of the mouse: a radioautographic study of terminal mitoses. *Acta Otolaryngol* Suppl-44.

Ruel J, Wang J, Rebillard G, Eybalin M, Lloyd R, Pujol R, & Puel JL (2007). Physiology, pharmacology and plasticity at the inner hair cell synaptic complex. *Hear Res* **227**, 19-27.

Rusch A & Eatock RA (1997). Sodium Currents in Hair Cells of the Mouse Utricle. In *Diversity in Auditory Mechanics*, eds. Lewis ER, Long GR, Lyon RF, Steele CR, Narins PM, & Hecht-Poinar E, pp. 549-555. World Scientific, Singapore.

Ryugo DK (1992). The auditory nerve: Peripheral innervation, cell body morphology, and central projections. In: Mammmalian Auditory Pathway: Neuroanatomy, (eds. D.B. Webster et al.). *Springer-Verlag, New York, NY* 22-65.

Sato C, Ueno Y, Asai K, Takahashi K, Sato M, Engel A, & Fujiyoshi Y (2001). The voltage-sensitive sodium channel is a bell-shaped molecule with several cavities. *Nature* **409**, 1047-1051.

Schlief T, Schonherr R, Imoto K, & Heinemann SH (1996). Pore properties of rat brain II sodium channels mutated in the selectivity filter domain. *Eur Biophys J* **25**, 75-91.

Schmidt JT & Buzzard M (1993). Activity-driven sharpening of the retinotectal projection in goldfish: development under stroboscopic illumination prevents sharpening. *J Neurobiol* **24**, 384-399.

Schwander M, Kachar B, & Muller U (2010). Review series: The cell biology of hearing. *J Cell Biol* **190**, 9-20.

Schwartz AM, Parakkal M, & Gulley RL (1983). Postnatal development of spiral ganglion cells in the rat. *Am J Anat* **167**, 33-41.

Sengpiel F & Kind PC (2002). The role of activity in development of the visual system. *Curr Biol* **12**, R818-R826.

Sernagor E, Eglen SJ, & Wong RO (2001). Development of retinal ganglion cell structure and function. *Prog Retin Eye Res* **20**, 139-174.

Shatz CJ & Stryker MP (1988). Prenatal tetrodotoxin infusion blocks segregation of retinogeniculate afferents. *Science* **242**, 87-89.

Simmons DD (2002). Development of the inner ear efferent system across vertebrate species. *J Neurobiol* **53**, 228-250.

Smith CA, Lowry OH, & Wu ML (1954). The electrolytes of the labyrinthine fluids. *Laryngoscope* **64**, 141-153.

Smith MR, Smith RD, Plummer NW, Meisler MH, & Goldin AL (1998). Functional analysis of the mouse Scn8a sodium channel. *J Neurosci* **18**, 6093-6102.

Smith RD & Goldin AL (1998). Functional analysis of the rat I sodium channel in xenopus oocytes. *J Neurosci* **18**, 811-820.

Sobkowicz HM, Rose JE, Scott GE, & Slapnick SM (1982). Ribbon synapses in the developing intact and cultured organ of Corti in the mouse. *J Neurosci* **2**, 942-957.

Spitzer NC (2002). Activity-dependent neuronal differentiation prior to synapse formation: the functions of calcium transients. *J Physiol Paris* **96**, 73-80.

Spitzer NC (2006). Electrical activity in early neuronal development. *Nature* **444**, 707-712.

Standen NB, Davies NW, & Langton PD (1994). Separation and analysis of macroscopic currents. In *Microelectrode Techniques: The Plymouth Workshop Handbook*, ed. Ogden D, pp. 37-52. The Company of Biologists Limited, Cambridge.

Stellwagen D & Shatz CJ (2002). An instructive role for retinal waves in the development of retinogeniculate connectivity. *Neuron* **33**, 357-367.

Sterling P & Matthews G (2005). Structure and function of ribbon synapses. *Trends Neurosci* **28**, 20-29.

Stuhmer W, Conti F, Suzuki H, Wang XD, Noda M, Yahagi N, Kubo H, & Numa S (1989). Structural parts involved in activation and inactivation of the sodium channel. *Nature* **339**, 597-603.

Terlau H & Stuhmer W (1998). Structure and function of voltage-gated ion channels. *Naturwissenschaften* **85**, 437-444.

Tierney TS, Russell FA, & Moore DR (1997). Susceptibility of developing cochlear nucleus neurons to deafferentation-induced death abruptly ends just before the onset of hearing. *J Comp Neurol* **378**, 295-306.

Toledo-Aral JJ, Moss BL, He ZJ, Koszowski AG, Whisenand T, Levinson SR, Wolf JJ, Silos-Santiago I, Halegoua S, & Mandel G (1997). Identification of PN1, a predominant voltage-dependent sodium channel expressed principally in peripheral neurons. *Proc Natl Acad Sci U S A* **94**, 1527-1532.

tom Dieck S & Brandstätter JH (2006). Ribbon synapses of the retina. *Cell Tissue Res* **326**, 339-346.

Tritsch NX & Bergles DE (2010). Developmental regulation of spontaneous activity in the Mammalian cochlea. *J Neurosci* **30**, 1539-1550.

Tritsch NX, Rodriguez-Contreras A, Crins TT, Wang HC, Borst JG, & Bergles DE (2010). Calcium action potentials in hair cells pattern auditory neuron activity before hearing onset. *Nat Neurosci* **13**, 1050-1052.

Tritsch NX, Yi E, Gale JE, Glowatzki E, & Bergles DE (2007). The origin of spontaneous activity in the developing auditory system. *Nature* **450**, 50-55.

Turner RG, Muraski AA, & Nielsen DW (1981). Cilium length: influence on neural tonotopic organization. *Science* **213**, 1519-1521.

Vassilev PM, Scheuer T, & Catterall WA (1988). Identification of an intracellular peptide segment involved in sodium channel inactivation. *Science* **241**, 1658-1661.

Vater M & Kössl M (2010). Comparative aspects of cochlear functional organization in mammals. *Hear Res*.

von Bekesy G (1960). *Experiments in Hearing* McGraw-Hill Book Co., New York.

Waguespack J, Salles FT, Kachar B, & Ricci AJ (2007). Stepwise morphological and functional maturation of mechanotransduction in rat outer hair cells. *J Neurosci* **27**, 13890-13902.

Wangemann P (2002). K+ cycling and the endocochlear potential. *Hear Res* **165**, 1-9.

Weisstaub N, Vetter DE, Elgoyhen AB, & Katz E (2002). The alpha9alpha10 nicotinic acetylcholine receptor is permeable to and is modulated by divalent cations. *Hear Res* **167**, 122-135.

West AE, Griffith EC, & Greenberg ME (2002). Regulation of transcription factors by neuronal activity. *Nat Rev Neurosci* **3**, 921-931.

Witt CM, Hu HY, Brownell WE, & Bertrand D (1994). Physiologically silent sodium channels in mammalian outer hair cells. *J Neurophysiol* **72**, 1037-1040.

Wolfe JM, Kluender KR, Levi DM, Bartoshuk LM, Herz RS, Klatzky RL, Lederman SJ, & Merfeld DM (2008). *Sensation and Perception*, second ed. Sinauer Associates, Inc, Sunderland, MA.

Wood JN & Baker M (2001). Voltage-gated sodium channels. *Curr Opin Pharmacol* **1**, 17-21.

Wooltorton JR, Gaboyard S, Hurley KM, Price SD, Garcia JL, Zhong M, Lysakowski A, & Eatock RA (2007). Developmental changes in two voltage-dependent sodium currents in utricular hair cells. *J Neurophysiol* **97**, 1684-1704.

Yang N, George AL, Jr., & Horn R (1996). Molecular basis of charge movement in voltage-gated sodium channels. *Neuron* **16**, 113-122.

Yu FH & Catterall WA (2003). Overview of the voltage-gated sodium channel family. *Genome Biol* **4**, 207.

Yu FH, Yarov-Yarovoy V, Gutman GA, & Catterall WA (2005). Overview of molecular relationships in the voltage-gated ion channel superfamily. *Pharmacol Rev* **57**, 387-395.

Zhang LI & Poo MM (2001). Electrical activity and development of neural circuits. *Nat Neurosci* **4 Suppl**, 1207-1214.

Zheng J, Shen W, He DZ, Long KB, Madison LD, & Dallos P (2000). Prestin is the motor protein of cochlear outer hair cells. *Nature* **405**, 149-155.

Zimmer WM, Rosin DF, & Saunders JC (1994). Middle-ear development. VI: Structural maturation of the rat conducting apparatus. *Anat Rec* **239**, 475-484.